12-2017

Brain Energy Homeostasis and the Regulation of N-acetyl-aspartate Metabolism in Development and Disease

Samantha Zaroff
PhD

BRAIN ENERGY HOMEOSTASIS AND THE REGULATION OF N-ACETYL-ASPARTATE METABOLISM IN DEVELOPMENT AND DISEASE

Samantha Zaroff, B.S.

A Dissertation submitted to the Graduate School of Biomedical Sciences, Rowan University in partial fulfillment of the requirements for the Ph.D. Degree.

Stratford, New Jersey 08084

December 2017

Table of Contents

Acknowledgments

Undertaking such an extraordinary and demanding thesis project would not have been possible without the continuous guidance of my mentor, Jeremy Francis, Ph.D. Throughout my time at UMDNJ/Rowan SOM I have faced numerous blockades which could have limited my success as a Ph.D. candidate, however, Dr. Francis maintained a level of compassion and professionalism that allowed me the ability to successfully complete my thesis project as well as publish a first author manuscript. Within this section, I would like to acknowledge the extreme amount of effort and attention that he placed, on not only completing my thesis work but also assisting me in my future career path. I would also like to acknowledge the members of my thesis committee for their continued assistance in all scientific concerns I had throughout my thesis work, as well as their numerous experimental suggestions. Particularly, the chair of my committee Paola Leone, Ph.D., has truly been an inspiration and a key ally throughout my 4.5 years. She has helped me not only on a scientific level, but a personal one as well, and I will forever be grateful for her kindhearted words of encouragement. It is also important to me that I acknowledge my lab mates, Vladimir Markov, MD and Dawid Wojas, MS, as they have taught me many laboratory techniques and had the patience to ensure that I understood, and was able to carry out every experiment correctly and independently. Also, my thesis work, although taking place in the laboratory, would not have been possible without the never-ending support of my immediate and Rowan-SOM family.

Lastly, this project was supported by an NIH/NIA STTR grant (Grant # 1R41G044890-01A1), the Boye Foundation Inc. (NJ), Canavan Research (IL), the

Silver Foundation (IL), Bamboo Therapeutics (15-0190 to PL) and partially by the NIH (STTR#R41G044890-01A1 to JS and NS088763-01A1 to PL) with additional support from the Ralph & Lois Silver Foundation, and Jacob's Cure.

Abstract

N-acetylaspartate (NAA) is a non-invasive clinical marker of neuronal metabolic integrity because of its strong proton magnetic resonance spectroscopy (H-MRS) peak and direct correlation with energetic integrity. Specifically, NAA is used to track the progression of neurodegenerative diseases due to the characteristic reduction of whole brain levels of NAA which occur simultaneously with reduced glucose utilization and mitochondrial dysfunction, but prior to the onset of disease specific pathology. However, NAA will also significantly increase simultaneously with energetic integrity during periods of recovery or remission in applicable disorders, such as traumatic brain injuries. Unfortunately, it remains enigmatic exactly why NAA is so tightly linked to overall neuronal integrity and why its levels seem to decrease prior to disease pathology. In order to shed some light on this unknown, we undertook an analysis of NAA metabolism in two distinct contexts, neurodegenerative disease progression and post-natal development.

We first analyzed possible controlling mechanisms behind the characteristic drop in whole brain levels of NAA during neurodegenerative disease progression using the 5xFAD mouse model of Familial Alzheimer's Disease. During 5XFAD disease progression, the reduction of NAA could not be accounted for by neuronal loss, mitochondrial loss, or the reduction of substrate-providing mechanisms. However, our results revealed that *Nat8L*, the gene encoding the NAA synthetic enzyme, was significantly down-regulated simultaneously with reduced levels of NAA as well as reduced mitochondrial integrity. We also show that both reductions are preceded by a significant up-regulation of the gene encoding oligodendrocytic

aspartoacylase (ASPA); the sole known NAA-catabolizing enzyme. Therefore, we hypothesized that NAA is reduced during 5XFAD progression due the active down-regulation of *Nat8L* and up-regulation of *ASPA* in response to reduced energetic integrity.

We then analyzed the expression of *Nat8L* during the first 4-weeks of postnatal development of ASPA null (Nur7) mice. Our results revealed that *Nat8l* was up-regulated during a period of early postnatal development normally punctuated by low *Nat8L* expression and the transcriptional up-regulation of *ASPA*. Taken together, the results from our 5XFAD and Nur7 experiments indicate ASPA as a possible negative regulator of *Nat8L* in response to energetic crisis. The results also predict the presence of signaling mechanisms involving cross talk between neurons and oligodendrocytes which control NAA metabolism during both postnatal development and neurodegenerative disease progression.

Introduction

NAA is the second most concentrated amino acid derivative in the mammalian brain (10 mM) (1-2), secondary only to glutamate. The only experimentally proven role of NAA is to supply oligodendrocytes with acetyl groups for production of myelin fatty acids during early postnatal development (3-4). However, concentrations of NAA remain relatively high throughout adult life (5), despite not having a truly defined role within the adult brain. The only inclination as to NAA's function in the adult brain is that reductions of whole brain levels of NAA coincide with reduced neuronal energetic integrity, specifically during periods of stress or direct trauma to the brain. Therefore, by investigating NAA metabolism during early stage neurodegenerative disease, we believed that we might be able to elucidate a role of NAA in the adult brain.

NAA is drastically reduced from normal biological levels of 5-10 mM during early stage neurodegenerative disease (6), traumatic brain injury (TBI) (7), various and mental health disorders (8-9). This reduction of NAA has been indirectly linked to the overall energetic status of the brain, which is also reduced during early stage neurodegenerative disease progression (178). NAA will also increase as energetic status and neuronal integrity improve, such as during periods of recovery from traumatic brain injury (184). This thesis work was undertaken in an effort to understand how and why NAA is reduced during early neurodegenerative disease progression, and to determine if this reduction can be linked to the overall energetic integrity of the brain. We hypothesize that the characteristic reduction of whole brain NAA in the early stages of neurodegenerative disease is an active response to the

simultaneous reduction of energetic integrity. We tested this hypothesis by analyzing the transcriptional regulation of the gene encoding for the NAA synthetic enzyme N-acetyl-transferase-8-like (*Nat8L*), during key periods of neurodegenerative disease in the 5xFAD model of Alzheimer's disease (AD).

NAA was discovered in 1956 through the analysis of metabolic components of protein free extracts from the cat brain (1). The extracts contained an N-substituted acetylated form of aspartate, which was eventually named N-acetyl-n-aspartic acid (NAA). NAA is found within neurons of the mammalian Central Nervous System (CNS) (6). It is synthesized from Acetyl Coenzyme A (AcCoA) and aspartate via Nat8L (Figure 1.1) either within the mitochondria (11) or the endoplasmic reticulum (12).

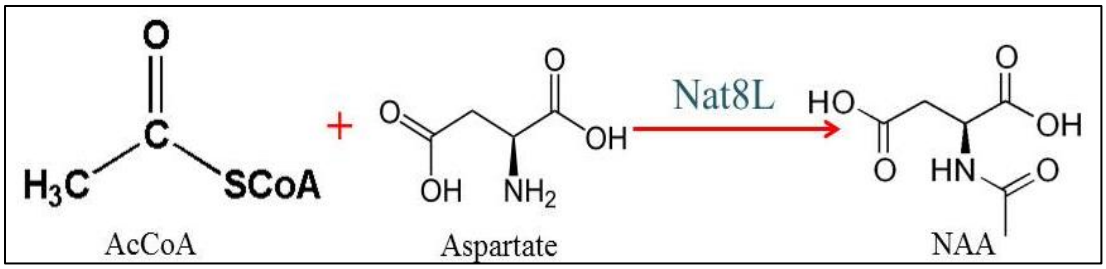

Figure 1.1 NAA Synthesis. AcCoA and aspartate react to form NAA via the enzyme Nat8L.

In order for NAA to be synthesized, AcCoA must be diverted from the neuronal Tricarboxylic acid (TCA) cycle while aspartate is converted from glutamate and malate (185), most likely diverted from the Malate Aspartate Shuttle (MAS). These diversions ultimately lead to a significant reduction in NADH available for oxidative phosphorylation. After synthesis, NAA is shuttled down neuronal axons and exported into oligodendrocytes through the sodium-dependent dicarboxylate

transporter (NaDC3) (14). Once within oligodendrocytes, NAA is catabolized by ASPA, in order to generate acetate and aspartate (15; Figure 1.2).

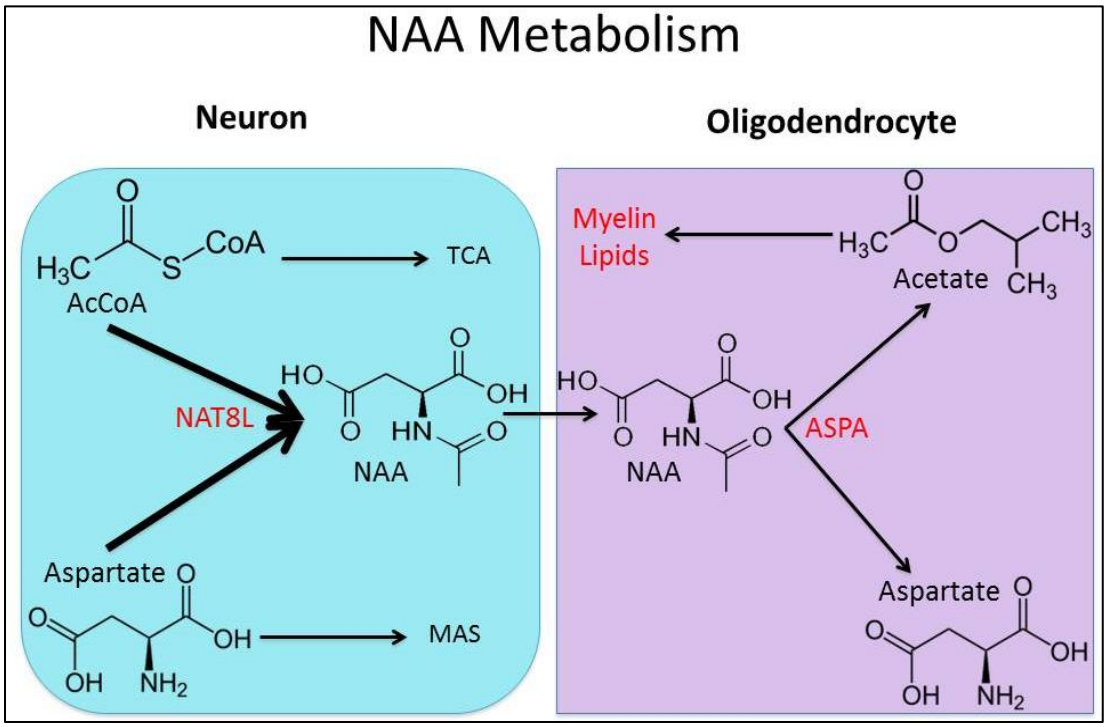

Figure 1.2 NAA Metabolism. NAA is synthesized within neurons when acetate and aspartate are diverted from the TCA cycle and MAS, respectively, and react in the presence of Nat8L. NAA is then shuttled into a neighboring oligodendrocyte where it is catabolized by ASPA back into acetate and aspartate. Acetate is then used to produce myelin lipids for the myelin sheath during early development.

The resulting acetate formed from NAA catabolism is used to synthesize various lipids. During early development, acetate will be converted into acetyl-CoA and malonyl-CoA and become incorporated into the myelin sheath (3; Figure 1.3), whereas post myelination acetate is incorporated into other lipids for the CNS (16-17)

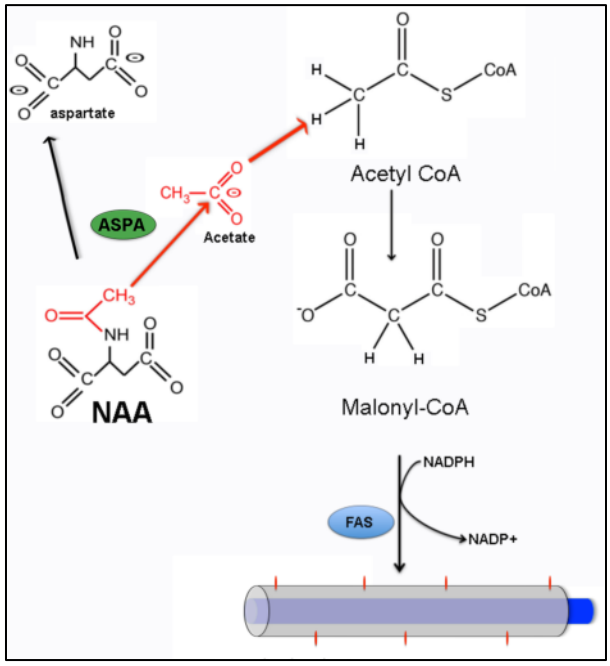

Figure 1.3 NAA Catabolized Acetate is Incorporated into Fatty Acids. NAA is catabolized by ASPA into aspartate and acetate. Acetate is used by oligodendrocytes to produce fatty acid precursors, such as malonyl Co-A, which will generate fatty acids and be incorporated into the myelin sheath during early development, or synaptic membranes during adulthood.

Through bioinformatics mining, it was revealed that only two N-acetyl transferases (NAT's; 18-20) were primarily expressed in the mammalian brain, *Nat8l*, and *Nat14*. These genes were isolated and cloned into expression cassettes and transfected into HEK293 cells in the presence of acetate and aspartate, the precursors to NAA. The only cells which were able to successfully synthesize NAA were those expressing *Nat8L*; therefore *Nat8L* was identified as the gene responsible for encoding the NAA synthetic enzyme. The identification of this gene also led to the determination that the disorder hypoacetylaspartia is directly caused by a mutation in the gene encoding *Nat8L* (21-25). Hypoacetylaspartia is the only known disorder

characterized by the complete lack of NAA. There is currently only one patient who has been identified to have had this disorder, but unfortunately it was a young child who has since passed. However, the identification of this disorder has revealed that NAA must have another role in the mammalian brain other than myelination. This is because, in spite of not being able to make any NAA, this patient somehow maintained a moderately normal level of myelination. Despite this, the patient still suffered from mental retardation, microcephaly, and seizures, eventually leading to his early death. This case study indicates not only that there are other means of myelination besides NAA metabolism but that the role of NAA in the adult brain is much more complicated than simply supplying oligodendrocytes with precursors for myelin fatty acids.

In order to synthesize NAA, AcCoA and aspartate must be diverted from the TCA cycle and the MAS, respectively. AcCoA is used to initiate the TCA cycle and produce NADH and $FADH_2$ for the electron transport chain (ETC) and oxidative phosphorylation. Therefore, when NAA is produced, AcCoA is diverted from the TCA cycle, eventually leading to a net loss of 11 ATP's (26). Aspartate is found within neuronal mitochondria as the source of aspartate for the MAS, a shuttle system which is responsible for supplying the ETC cycle with additional NADH (27). Therefore, when aspartate is diverted from the MAS, there will be significantly less NADH available for the ETC. Cumulatively, this causes a significant loss of neuronal ATP (Figure 1.4) that must be compensated for in order to maintain the brain's energetic homeostasis (28-29).

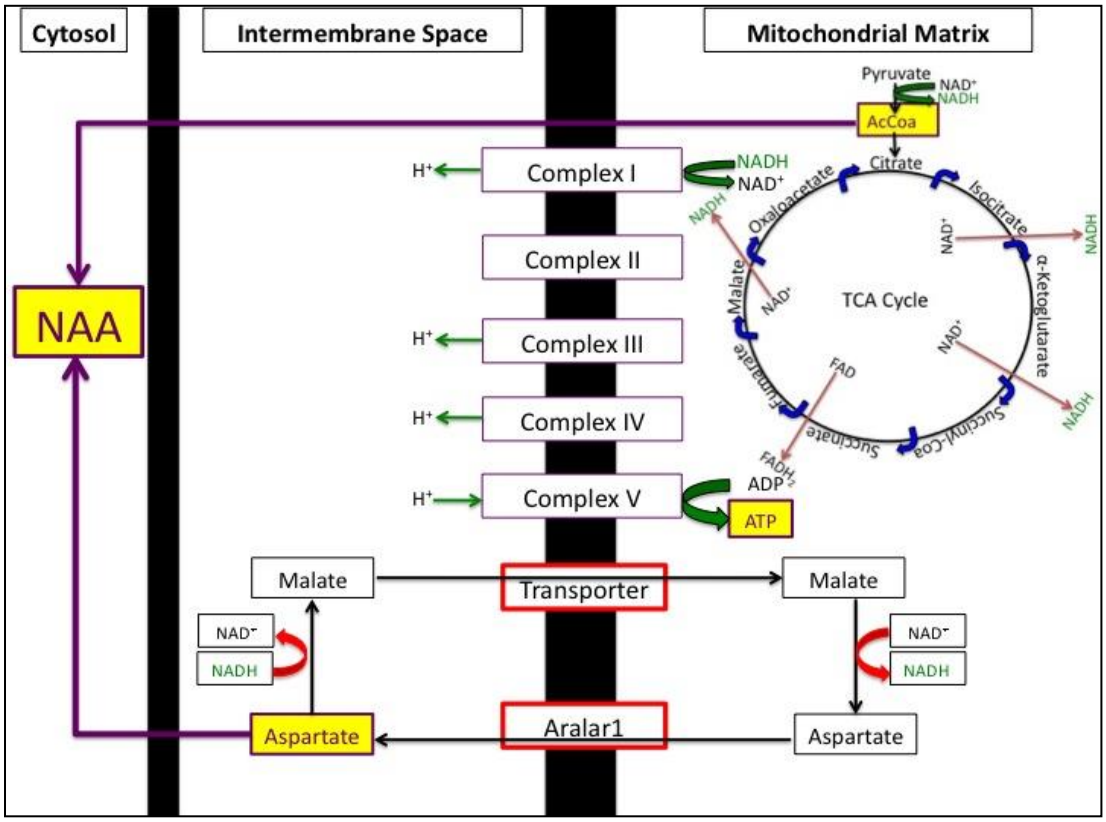

Figure 1.4 The Synthesis of NAA is an Energetically Unfavorable Process. The malate-aspartate shuttle uses malate and aspartate transporters to provide reducing power in the form of NADH for the mitochondrial matrix in times of energetic stress. The electron transport chain will then use the NADH to produce ATP via ATP Synthase. However, NAA synthesis diverts AcCoA and aspartate from these ATP producing mechanisms, leading to a direct loss of ATP.

The synthesis of NAA is indirectly linked to the function of various mitochondrial components. For example, in 1996 Bates et al published a manuscript describing the direct correlation between NAA production and ETC activity (132). Intact rat brain mitochondria exposed to various inhibitors of ETC complexes; complex I (NADH ubiquinone oxidoreductase), complex III (ubiquinone oxidase c

oxidoreductase), complex IV (cytochrome c oxidase), and complex V (ATP synthase), produced reduced levels of both ATP and NAA when exposed to sucrose containing respiration medium (figure 1.5). Therefore, it was concluded that the mitochondria's capability for oxidative phosphorylation has a direct effect on the neuron's ability to synthesize NAA, however the exact mechanism remains unknown (132). The results of this study were confirmed through numerous publications detailing the direct correlation between ETC complex activity and NAA production through the use of various ETC complex inhibitors (30-33). However, although these studies only highlighted the direct correlation between NAA synthesis and oxidative phosphorylation, they failed to identify a mechanism that could account for this relationship.

Glucose is the brain's main source of energy and is critical to maintain brain function. Therefore, any dysregulation of normal glucose metabolism could significantly alter the brains ability to perform normally (186). ETC activity and glucose availability both directly impact the bioavailability of NAA and energetic substrate. Therefore, since NAA and ETC activity were directly related to one another it was hypothesized that NAA synthesis and glucose utilization mechanisms would also be correlated to one another. Glucose utilization is significantly decreased in older mammals compared with younger controls (58). Therefore, it was hypothesized that older rats would not only present with decreased glucose utilization but may also show reduced levels of whole brain NAA. Metabolic flux analysis in older rats showed reduced bioavailability of glutamate and glutamine, indicating limited ability to generate ATP. The data also revealed a significant reduction of NAA levels, suggesting

that NAA mirrors changes in the brains ability to generate ATP (figure 1.5; 34). To further support this notion, clinical studies of patients with varying degrees of neurodegenerative disease present with reduced levels NAA simultaneously with decreases in glucose utilization as shown through positron emission tomography (PET) (35). Therefore age and neurodegenerative diseases both present with reduced glucose metabolism and NAA, suggesting substrate bioavailability is a limiting factor for the synthesis of NAA synthesis in both contexts.

The MAS is responsible for increasing the pool of reducing equivalents available for oxidative phosphorylation. It appears, on the basis of published data, to also be rate limiting for NAA synthesis due to the direct competition of mitochondrial aspartate. One of the main components of the MAS is the exchange of intra-mitochondrial aspartate for extra-mitochondrial glutamate through the inter-membrane transport protein aralar; encoded by *aralar1* (Figure 1.6). *Aralar1* knockout mice have essentially non-functional MAS's due the inability of aspartate to leave the mitochondrial matrix. Therefore, mitochondrial aspartate levels became significantly reduced and in turn are unavailable to synthesize NAA (figure 1.5; 36-38). Therefore Aralar1-knockout mice have significantly reduced levels of whole brain NAA, once again suggesting substrate competition between NAA synthesis and oxidative phosphorylation.

These studies revealed a mechanism in which the ability of the cell to produce NAA is directly affected by the cells overall mitochondrial integrity (Figure 1.5). However, none of these studies were able to analyze if reduced mitochondrial integrity had any direct effect on the regulation of NAA synthesis. Our previous data revealed

that ASPA was transcriptionally regulated during normal wild-type development (39). Therefore we became interested in determining if *Nat8L* is also transcriptionally regulated, and if so, if there is a difference in the regulation during wild-type development and disease progression.

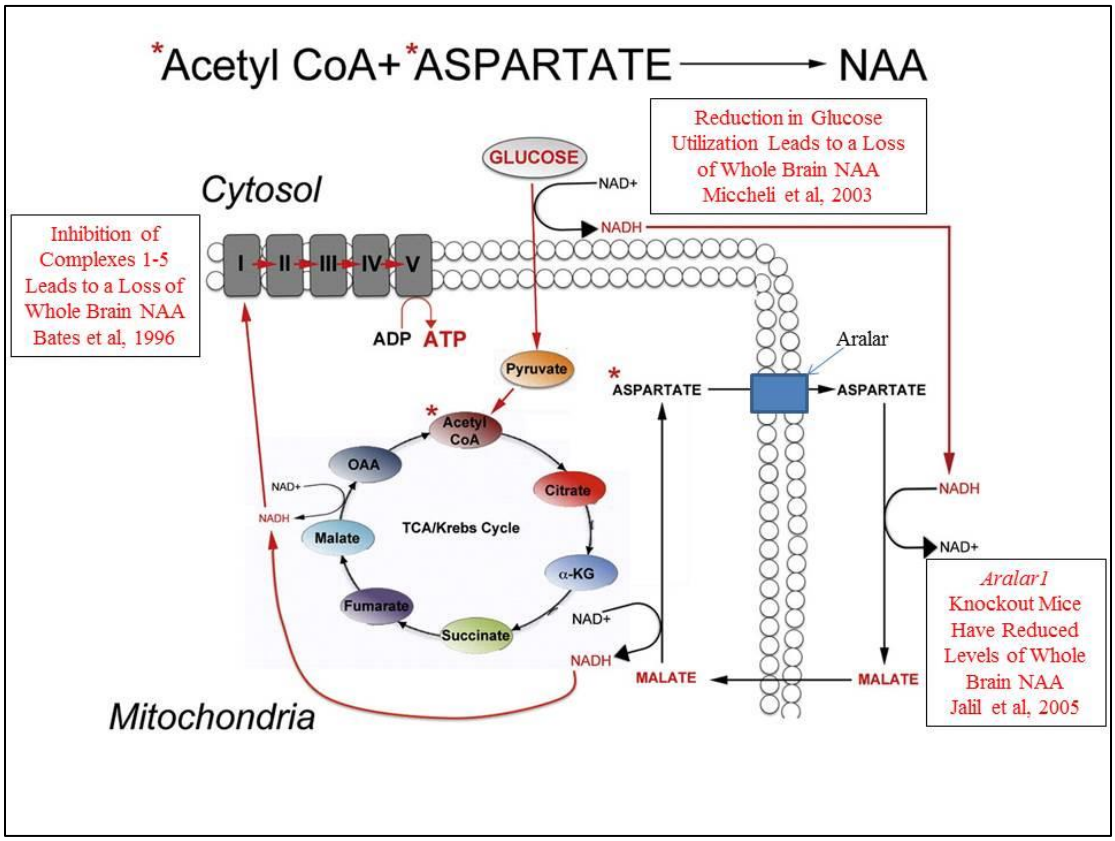

Figure 1.5 NAA Synthesis is Directly Correlated with Mitochondrial Oxidative Integrity. The production of NAA has been experimentally shown to be reduced during periods of reduced mitochondrial integrity. Levels of whole brain NAA are significantly reduced in mitochondria which have been exposed to inhibitors of complexes I to V of the ETC, during periods of reduced glucose utilization, and when the MAS is inhibited in *Aralar1* knockout mice.

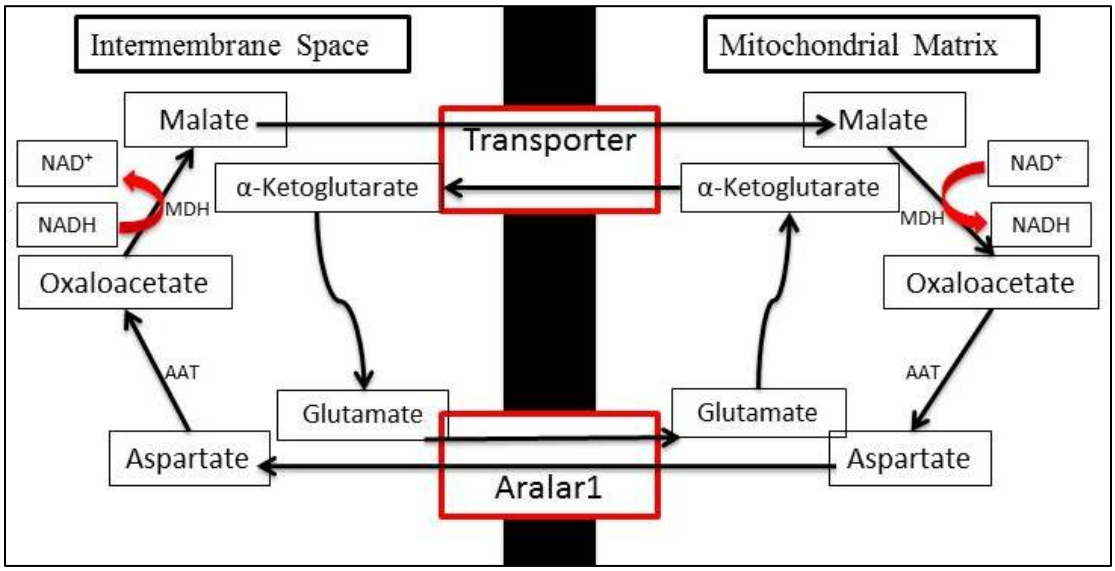

Figure 1.6 The MAS. The MAS is essential for the production of glycolytic NADH for oxidative phosphorylation. Intra-mitochondrial aspartate is converted to malate in a 2-step system which requires the oxidation of NADH. Malate is transported into the mitochondrial matrix in exchange for α-KG. Once within the matrix, malate is converted back to aspartate through a 2-step system which requires the reduction of NAD^+. Aspartate is transported back into the intermembrane space through the transporter aralar (encoded by *Aralar1*) in exchange for glutamate. Aspartate is then converted once again into malate to continue the shuttle.

A unifying feature of numerous neurodegenerative diseases and disorders is that reductions in whole brain NAA and oxidative integrity precede neurodegenerative pathology. For example, NAA is used as a marker of cognitive decline in Alzheimer's disease patients (41). The onset of reduced NAA coincides with the beginning stages of Mild Cognitive Impairment (MCI), a precursor to Alzheimer's. This stage in AD progression also presents with diminished glucose energy metabolism and overall mitochondrial dysfunction (41). A similar pattern has

been demonstrated in various transgenic models of AD (43-45). These findings have led to the hypothesis that Amyloid Beta 42 (Aβ42) attacks neuronal mitochondria and causes severe mitochondrial dysfunction, resulting in reduced levels of NAA and ATP (46-48). This pattern of a disease specific event leading to reduced mitochondrial integrity and whole brain NAA is repeated throughout the neurodegenerative spectrum. For example, Huntington's disease mice expressing the mutant *Htt* gene present with significantly reduced levels of NAA which coincide with symptomatic onset and profound metabolic dysfunction. This is because mutant HTT is a gain of function mutation which is hypothesized to cause reduced Ca^{2+}buffering capacity, loss of membrane potential and decreased expression of oxidative phosphorylation enzymes. Similarly, clinically NAA is significantly reduced during the early stages of Huntington's disease, occurring simultaneously with reduced oxidative capacity (49-52). NAA is also reduced during periods of global ischemia; or reduced oxygen availability to the brain. The reduced amount of available oxygen eventually leads to reduced mitochondrial integrity and neuronal cell death (53). Another example of a disease in which there is significant oxidative stress and reduced levels of NAA is Parkinson's disease; a debilitating disorder caused by mutations in numerous genes specific to mitochondrial function. Some of these genes include *pink1* which leads to reduced complex I activity (54), and *parkin*; a Ubiquitin Protein Ligase which assists in mitochondrial degradation (55). These mutations in mitochondrial function are hypothesized to be the reason for both oxidative stress and reduced levels of whole brain NAA during PD progression. The

list of neurodegenerative disorders which present with reduced oxidative integrity and reduced whole brain levels of NAA is endless (Table 1).

There is a wide variety of mitochondrial disorders which present with reduced levels of NAA and various CNS defects, such as strokes, seizures, or psychiatric abnormalities. Some of these disorders include mitochondrial encephalomyopathy, lactacidosis, stroke-like episodes syndrome, myoclonic epilepsy and ragged red fibers syndrome, and mitochondrial neuro-gastrointestinal encephalomyopathy syndrome (56-57). This connection between mitochondrial disorders, reduced NAA, and reduced CNS function is due to the large energetic investment made by synaptic mitochondria in order to maintain neuronal synaptic communication (58-59). Therefore, these disorders not only cause significant synaptic mitochondrial dysfunction but as a result, also present with reduced levels of NAA. These studies provide more evidence that abnormalities in levels of NAA are highly dependent on the overall neuronal mitochondrial integrity.

Numerous experiments have demonstrated that NAA and ATP are intimately linked to one another's production and are both affected by neurodegenerative disease progression. However, it remains unknown how *Nat8L* is regulated during these periods of reduced levels of NAA and if there is a link with reduced oxidative integrity. Therefore, this thesis work was undertaken to understand if *Nat8L* is actively regulated during periods of reduced levels of NAA and if it is affected by the energetic status of the brain during 5XFAD progression.

Disease	Energetic Stress	Low [NAA] Compared with Normal Biological Levels
Parkinson's	Przedborski, S. (2005). Pathogenesis of nigral cell death in Parkinson's disease. Parkinsonism & related disorders, 11, S3-S7.	Chahine, L. M., & Stern, M. B. (2011). Diagnostic markers for Parkinson's disease. Current opinion in neurology, 24(4), 309-317.
PTSD	Sapolsky, R. M. (2000). The possibility of neurotoxicity in the hippocampus in major depression: a primer on neuron death. Biological psychiatry, 48(8), 755-765.	Schuff, N., Meyerhoff, D., Mueller, S., Chao, L., Sacrey, D., Laxer, K., & Weiner, M. (2006). N-acetylaspartate as a marker of neuronal injury in neurodegenerative disease. *N-Acetylaspartate*, 241-262.
AIDS' Dementia Complex	Brooke, S. M., Howard, S. A., & Sapolsky, R. M. (1998). Energy dependency of glucocorticoid exacerbation of gp120 neurotoxicity. *Journal of neurochemistry*, *71*(3), 1187-1193.	Meyerhoff, D. J., MacKay, S., Bachman, L., Poole, N., Dillon, W. P., Weiner, M. W., & Fein, G. (1993). Reduced brain N-acetylaspartate suggests neuronal loss in cognitively impaired human immunodeficiency virus-seropositive individuals In vivo 1H magnetic resonance spectroscopic imaging. *Neurology*, *43*(3 Part 1), 509-509.
Traumatic Brain Injury	Signoretti, S., Marmarou, A., Tavazzi, B., Lazzarino, G., Beaumont, A., & Vagnozzi, R. (2001). N-Acetylaspartate reduction as a measure of injury severity and mitochondrial dysfunction following diffuse traumatic brain injury. *Journal of neurotrauma*, *18*(10), 977-991.	Shannon, R. J., van der Heide, S., Carter, E. L., Jalloh, I., Menon, D. K., Hutchinson, P. J., & Carpenter, K. L. (2016). Extracellular N-acetylaspartate in human traumatic brain injury. *Journal of neurotrauma*, *33*(4), 319-329.
ALS	Panov, A., Steuerwald, N., Vavilin, V., Dambinova, S., & Bonkovsky, H. L. (2012). Role of neuronal mitochondrial metabolic phenotype in pathogenesis of ALS. In *Amyotrophic Lateral Sclerosis*. InTech.	Rooney, W. D., Miller, R. G., Gelinas, D., Schuff, N., Maudsley, A. A., & Weiner, M. W. (1998). Decreased N-acetylaspartate in motor cortex and corticospinal tract in ALS. *Neurology*, *50*(6), 1800-1805.
Epilepsy	Yang, H., Wu, J., Guo, R., Peng, Y., Zheng, W., Liu, D., & Song, Z. (2013). Glycolysis in energy metabolism during seizures. *Neural regeneration research*, *8*(14), 1316.	Gadian, D. G. (1995). N-acetylaspartate and epilepsy. *Magnetic resonance imaging*, *13*(8), 1193-1195.
Alzheimer's Disease	De La Torre, J. C. (2008). Pathophysiology of neuronal energy crisis in Alzheimer's disease. Neuro-degenerative diseases, 5(3-4), 126.	Adalsteinsson, E., Sullivan, E. V., Kleinhans, N., Spielman, D. M., & Pfefferbaum, A. (2000). Longitudinal decline of the neuronal marker N-acetyl aspartate in Alzheimer's disease. *The Lancet*, *355*(9216), 1696-1697.

Table 1: Brain Disorders which present with reduced oxidative integrity and low levels of whole brain NAA

The Synthesis of NAA is Energetically Taxing on the Cell

Specific Aim One

Specific aim one was to determine the direct energetic cost of NAA synthesis on a non-diseased cell. Current literature suggests a direct link between compromised mitochondrial function and reduced NAA synthesis. However, prior to this thesis work, it was unknown how NAA synthesis affected the energetic status of the cell. Therefore, by promoting extracellular NAA synthesis in HEK293 cells in energetically stressed and non-stressed cells, we hoped to identify if/how energetic integrity actively regulates NAA metabolism in either context. We hypothesized that the overexpression of *Nat8L* in HEK293 cells would be energetically unfavorable to the cell and eventually lead to reduced levels of ATP. We also hypothesized that, during periods of energetic crisis, the cell would not be able to maintain concomitant NAA and ATP production due to the direct competition for AcCoA and aspartate, leading to much greater loss of ATP.

Introduction

Previous literature has demonstrated a direct link between compromised mitochondrial function; such as inhibited ETC activity, reduced glucose utilization, or abolished MAS activity, and reduced levels of NAA (Figure 1.5). However, since the gene responsible for the expression of the NAA synthetic enzyme was only recently identified and cloned, the effect *Nat8L* expression may have on ATP production has yet to be investigated. Therefore, in specific aim one, we were interested in providing experimental evidence for this effect. We hypothesized that since NAA and ATP

production require the same intermediates, that overexpressing *Nat8L* would ultimately decrease the cell's ability to produce ATP.

Materials and Methods

Experimental Protocol

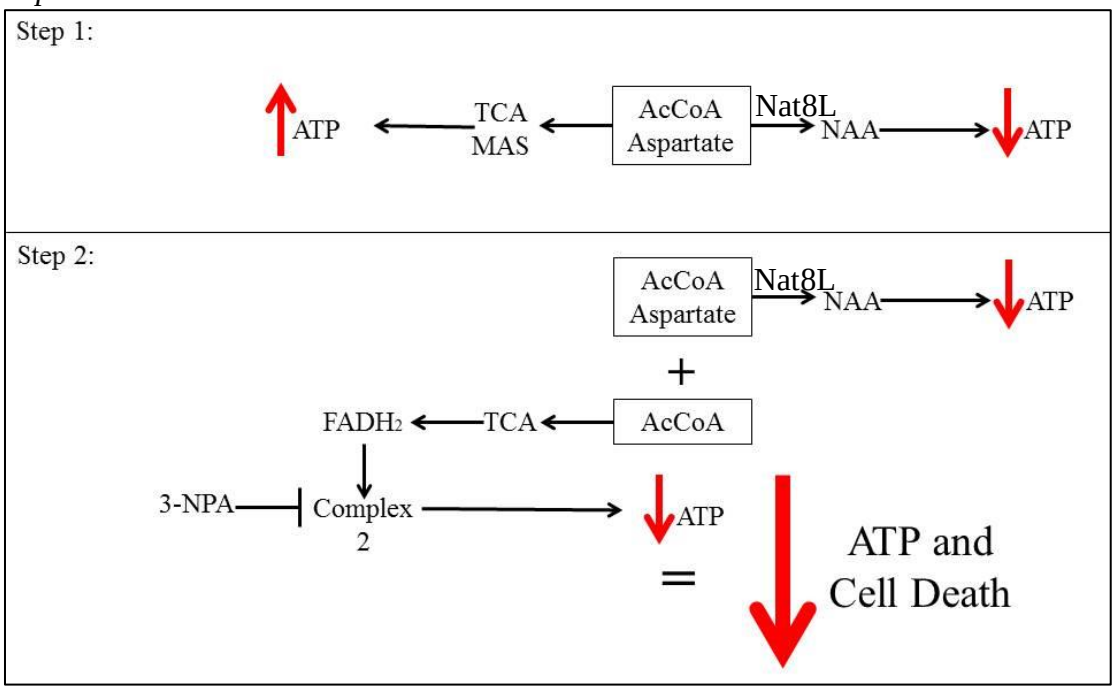

Figure 1.7 Experimental Protocol to Prove NAA Synthesis as an Energetic Stress on the Cell and is Therefore Incompatible with Reduced ETC Activity. Step 1 of this experiment will involve measuring the amount of ATP and NAA that is produced in HEK293 cells expressing exogenous *Nat8L*. The second step of this experiment will involve analyzing the effect that NAA synthesis has on levels of ATP in cells incubated with an inhibitor of complex II of the ETC (3-NPA). We hypothesize that expressing *Nat8L* in this system will result in a significant loss of ATP, and therefore will be energetically incompatible with reduced ETC activity and lead to a further reduction of ATP.

Transfections

Human embryonic kidney cells 293 (HEK293 cells) were plated at 50% confluence and incubated in 10% Fetal Bovine Serum (FBS) in Dulbecco's Modified Eagle Medium (DMEM) for approximately 24 hours. HEK293 cells were chosen due to their extensive use in a wide variety of research topics (187), their complete lack of NAA synthesis, as well as being the cell line in which *Nat8L* was originally transfected in to confirm Nat8L as the NAA synthetic enzyme. Once 80% confluent, the media was changed to 5% FBS Iscove's Modified Dulbecco's Medium (IMDM) and incubated for 2 hours. After incubation, a 1:1 mixture of 2X Hepes buffered saline (HeBS) buffer: transfection reaction (10ug gene of interest DNA (*Nat8L* or *GFP*), water, and 0.25 M $CaCl_2$) was added drop wise to each well. Media was replaced with 10% FBS in DMEM 24 hours later the cells were collected, counted, and used for HPLC sample preparation.

GW1CMV-Perceval (Addgene, Cambridge, MA) was isolated and sub cloned into pAM/CBA-pL to produce a lab stock of pAM/CBA-pL-Perceval using restriction sites Xbal and EcoR1. The Perceval plasmid was then isolated using a plasmid DNA maxiprep kit and stored at -80˚C for future transfections. Transfections began by seeding $1x10^3$ cells/cm^2 in each well of a 24 well plate in 10% FBS media. The next day co-transfections of Perceval with *Nat8L* or empty control plasmid were performed using Lipofectamine (Thermo-Fisher Scientific, Waltham Ma) reagent according to manufacturer's protocol. Briefly, Lipofectamine Reagent was diluted in Opti-MEM Medium and mixed in a 3:1 ratio with diluted DNA (per µg). The mixture was then incubated at RT for 15 minutes before being directly added to the

cells with a final concentration of 500 ng/DNA/well. The following morning, the media was replaced with 10% FBS in DMEM. The cells were counted via trypan blue 24 hours later prior to Perceval analysis.

Cells that were to be incubated in 3-NPA were plated into a 24-well plate at a density of 100,000 cells/cm^2 one day prior to transfection. On day two, 18 wells were transfected with *Nat8L* or *GFP* using Lipofectamine Reagent while the remaining six went through media replacement. The next day 500 uM 3-NPA was added to each well and allowed to incubate for a total of 16 hours. The cells were then collected, counted, and used for HPLC sample preparation.

HPLC of Transfected Cells

HPLC samples were isolated from each individual well by scraping all cells from the bottom of each well using a rubber policeman. The cells were pelleted by centrifugation 10 minutes at 10,000×g at 4°C prior to media aspiration. 100 ul of ice-cold precipitation solution 9 [3:1 acetonitrile: KH2PO4 (pH 7.4)] was added to the pellet before suspension through low-level sonication. The suspensions were centrifuged for 10 minutes at 10,000×g at 4°C. The supernatant was retained, and the remaining pellet was sonicated with an additional 100 µl of precipitation solution before centrifugation for 10 minutes at 10,000×g at 4°C. The two supernatants were combined and extracted twice with 2× volume of HPLC-grade chloroform. The samples were run on a Thermo scientific Surveyor-Plus HPLC system equipped with UV detection and a Hypersil BDS-C18 column (5 µm particle size; 25× 4.9 mm). An ion-paired reverse phase detection methodology was used to analyze samples using buffers and sequence as described previously (60). NAA, ATP, AcCoA, and MalCoA

were quantified in a single run using standard curves generated by purified HPLC-grade standards and the quantity was expressed as quantity/wet weight of tissue.

Perceval Analysis

10 wells of a 24 well plate were used for Perceval analysis. Of the 10 wells, five contained HEK293 cells co-transfected with Perceval-HR and *GFP* while the other five wells contained HEK293 cells co-transfected with Perceval-HR and *Nat8L*. Each well was placed under a fluorescent microscope and viewed under UV lighting in order to see Perceval-HR fluorescence. Once Perceval expression was visualized, five images were taken of each well using IP lab digital imaging software (Scanalytics Inc., Rockville, MD). Each image was sectioned into 4 equal parts and Perceval fluorescence was measured via mean densitometry readings with a minimum reading set to 500 (black) and a maximum reading set to 5000 (white) to establish background lighting. These readings were all determined using IP lab. The mean densitometry readings from all five wells of each experimental group (five images per well with four ROI per image) were averaged to determine the mean Perceval-HR florescence (and therefore expression).

Results

The Effect of Nat8L Expression on NAA and ATP: AMP in HEK293 Cells

The synthesis of NAA has been shown to be negatively affected by mitochondrial dysfunction (Figure 1.5). Considering that the synthesis of NAA requires the diversion of two prominent energetic substrates, AcCoA, and aspartate, we hypothesized that the overexpression of *Nat8L* in HEK293 cells, and therefore the exacerbated synthesis of NAA, would be energetically taxing on the cell. In order to test this hypothesis, *Nat8L* or *GFP* were expressed in HEK293 cells using Lipofectamine reagent. Once transfected, HPLC analysis of AMP, ATP, and NAA was performed on the cells in order to identify if high levels of NAA synthesis had a direct effect on energetic integrity. Cells overexpressing *Nat8L* showed significantly higher levels of NAA compared with GFP transfected controls (Figure 1.8A, $p<0.001$), indicating that the transfection protocol was generated NAA producing HEK293 cells. The cells overexpressing *Nat8L* also showed a significant reduction in ATP: AMP compared with GFP transfected controls (Figure 1.8 B, $p<0.001$), indicating significant energetic loss in *Nat8L* transfected cells. These data confirmed our hypothesis that NAA synthesis alone was indeed a direct energetic stress on the cell.

In order to confirm our observation that the overexpression of *Nat8L* led to a direct loss of ATP, HEK293 cells were co-transfected with *Nat8L* and *Perceval-HR*. *Perceval-HR* is an optimized form of Perceval, a construct which senses live cell alterations in ATP: ADP and in response directly increases cell fluorescence at 500 nm. The construct contains a Glnk (Ammonia transport signaling protein from

Methanococcus jannaschi) and cpmVenus region (circularly permuted monomeric GFP inserted into the T-Loop of GlnK) (188). This construct will competitively bind both ATP and ADP; however, the fluorescent output at 500nm will only increase when ATP is bound. Therefore, if the cell is under energetic stress and is producing significantly less ATP, ADP will increase and bind to Perceval-HR. If Perceval-HR is bound to ADP, then there will be no resulting fluorescent output when read at 500 nm (fluoresces as green).

When *Perceval-HR* and *Nat8L* were cotransfected into HEK293 cells, there was significantly less fluorescence in the *Nat8L* expressing cells compared with a control empty expression cassette (Figure 1.8 C&D, N=5 wells/treatment group) These results were obtained through the quantification of cellular fluorescence via the analysis of histograms displaying the count of fluorescent pixels at 500 nm. These results confirm our previous data that the overexpression of *Nat8L*, and the subsequent synthesis of NAA, leads to a direct energetic stress within the cell.

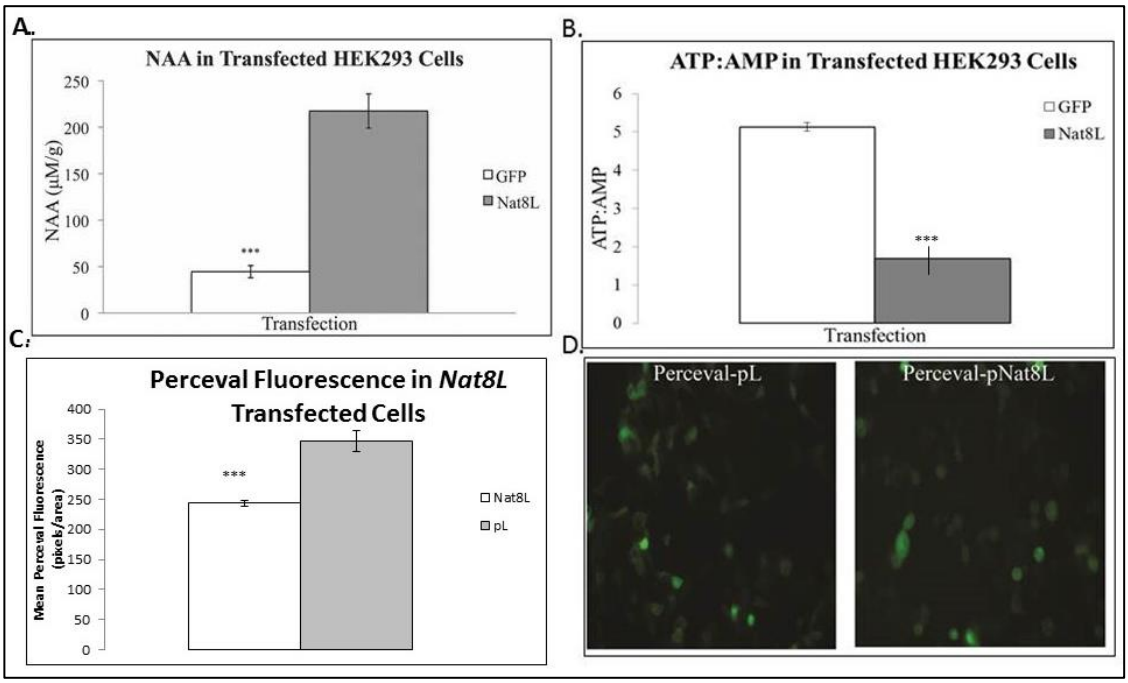

Figure 1.8 The Synthesis of NAA is Energetically Taxing on the Cell. HPLC analysis of NAA, ATP, and AMP was performed on *Nat8L* and *GFP* transfected cells. Once quantified the data revealed a significantly higher amount of NAA (A) in the *Nat8L* transfected cells compared with *GFP* controls. The analysis also revealed a significant reduction in ATP: AMP (B) in cells transfected with *Nat8L* compared with controls. These results were confirmed through the cotransfection of Perceval-HR with an empty expression cassette or one expressing *Nat8L*. The cells expressing *Nat8L* had significantly less Perceval fluorescence (C&D) compared with controls. (***≤0.001<**≤0.01<*≤0.05)

The Cell is Unable to Sustain NAA Synthesis and Oxidative Phosphorylation During Mitochondrial Dysfunction

As previously described, a common element of early stage neurodegenerative disease is significant mitochondrial dysfunction and oxidative stress occurring prior to neuronal loss or phenotypic changes in behavior or cognition. Another shared common element throughout this diverse pathological spectrum is the reduction of whole brain NAA, which occurs simultaneously with, and appears to be coordinated with oxidative stress.

As we have shown, the synthesis of NAA is energetically taxing on the cell. We hypothesize that this energetic deficit is due to the fact that NAA synthesis requires the oxidative intermediates AcCoA and aspartate. Therefore, if NAA synthesis were to occur simultaneously with oxidative phosphorylation the pool of available energetic substrate would significantly reduce. In order to test this hypothesis that concomitant NAA and ATP synthesis during periods of reduced ETC function is energetically detrimental to the cell, we expressed *Nat8L* in 3-NPA treated cells. 3-NPA treatment will eventually lead to the inhibition of both complex II and the MAS due to its inhibitory effect of succinate dehydrogenase. Succinate dehydrogenase is the main component of complex II, therefore, since complex II is the only component of the ETC which is directly linked TCA cycle, the inhibition by 3-NPA drastically reduces the cells capacity for oxidative phosphorylation. 3-NPA also inhibits the MAS because succinate dehydrogenase is required by the TCA cycle to produce fumarate from succinate, which in turn will reduce malate and oxaloacetate, both of which are required for the MAS. Therefore, 3-NPA also

inhibits the TCA cycle and the MAS, leading to an ablation of NADH availability. The inhibitory effect of 3-NPA was confirmed by HPLC analysis which revealed that 3-NPA treated cells had significantly less ATP than untreated controls (Figure 1.9). After this confirmation, we were interested in how *Nat8L* expression affected the ATP concentration in 3-NPA treated cells. HPLC analysis revealed that the cells transfected with *Nat8L* and treated with 3-NPA produced significantly less ATP compared with GFP transfected controls (Figure 1.8). Interestingly, these cells also seemed to die relatively quickly compared with any other group as shown via cell viability assay (data not shown). These data indicated that expressing *Nat8L* while in an energetically stressed environment was extremely unfavorable, to the point of possibly leading to cell death. When a cell senses a loss of ATP levels, various pathways of cell death may be induced. If the cell loses approximately 15% of its total ATP levels, cell death will occur via necrosis. However, if the cell loses anywhere from 25-75% of its total ATP levels, cells initiate apoptosis as opposed to necrosis. Whichever means of cell death occurs in response to ATP reduction, the rate of cell death will be directly proportional to the severity of ATP loss (177). Therefore, it is reasonable to assume that cells treated with 3-NPA and expressing *Nat8L* died at a much faster rate than other groups (data not shown) due to the significant and rapid loss of ATP levels. Specifically, *Nat8l* transfected cells had about 2.8 times lower ATP:AMP than GFP transfected cells (N=6/group; P<.001)

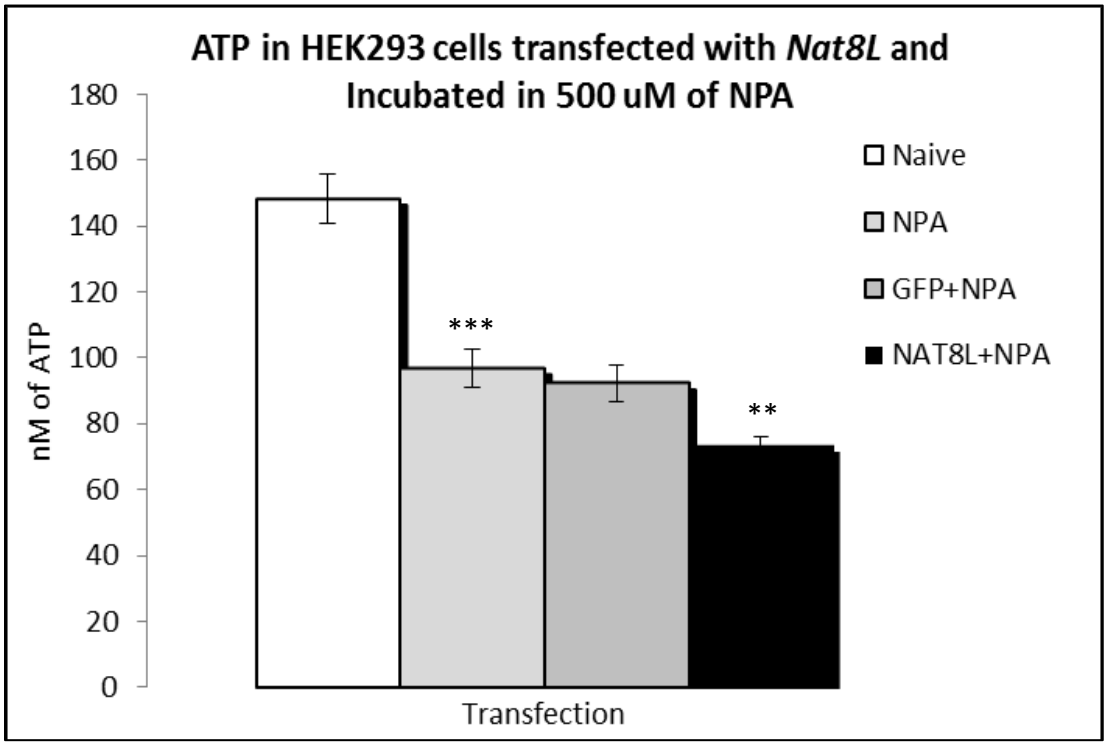

Figure 1.9 Cells Cannot Maintain Nat8L Expression During Disrupted Electron Transport Chain Activity. HEK293 cells were transfected with plasmids expressing *Nat8L*, *GFP*, and then treated with 500 µM of 3-NPA for 16 hours. The resulting cells were used for HPLC analysis and revealed a significant decrease in ATP in any cell given NPA, however cells given NPA and over expressing *Nat8L* had a much lower amount of ATP (N=6/group). (***≤0.001<**≤0.01<*≤0.05)

Conclusion

Our results revealed that the overexpression of *Nat8L* leads to a direct increase in levels of NAA (Figure 1.8A). We also demonstrated that the synthesis of NAA leads to a direct loss of ATP most likely due to the diversion of AcCoA and aspartate from the TCA cycle and the MAS (Figure 1.8 B-D). Lastly, we demonstrated that during periods of disrupted TCA cycle activity the synthesis of NAA is unfavorable for ATP production, and therefore has negative consequences to the cells (Figure 1.9). In fact, left unattended, cells overexpressing *Nat8L* while treated with 3-NPA eventually died, most likely due to severe energetic crisis. These results suggest that the synthesis of NAA is energetically costly to the cell and therefore incompatible with any existing energetic crisis. However, at this point, it remains unknown if the expression of *Nat8L* was altered during neurodegenerative disease progression.

Chapter Two

The Active Down-Regulation of NAA Synthesis Coincides with Reduced Energetic Integrity During Early Neurodegenerative Disease Progression

Specific Aim Two

Specific aim two sought to demonstrate that the reduction of NAA in a model of neurodegenerative disease is an active process. In order to accomplish this aim, the 5XFAD transgenic mouse model for Familial Alzheimer's Disease was analyzed for whole brain levels of NAA and ATP via HPLC, and expression of *Nat8L* via QRT-PCR and In Situ Hybridization (ISH), during periods of energetic crisis defined by various mitochondrial integrity assays. We hypothesized that NAA is reduced during the beginning stages of 5XFAD progression because of the down-regulation of *Nat8L*. We also predict that any revealed decrease in expression would occur in response to the reduced energetic integrity of the brain.

Introduction

A hallmark of neurodegenerative disease is the onset of reduced neuronal oxidative integrity prior to neuronal loss and disease specific symptoms (61-64). Depending on the specific disease type, oxidative integrity will coincide with a clinical reduction in whole brain levels of NAA, as determined via Proton Magnetic Resonance Spectroscopy (^{1}H-MRS). This is due to the intimate association of NAA synthesis with neuronal metabolic integrity. Because of this clinically proven link between NAA levels and energetic status, NAA is used to stage the progression of neuronal energetic stress throughout the neurodegenerative spectrum (65-69). One of the neurodegenerative diseases clinically characterized by the concomitant decrease

of whole brain NAA with reduced oxidative integrity is Alzheimer's disease (AD). AD can be described as the progressive degeneration of gray matter rich regions of the brain commonly associated with memory and cognition (70). The cause of most AD cases are unknown, however there is a small percentage of cases that have a heritable genetic component; the latter of which is known as Familial Alzheimer's disease (FAD). The genes causing FAD have been identified through the generation of multiple FAD mouse models which present with multiple FAD specific characteristics. In particular, we were interested in using one of these models, the 5XFAD model, to define if NAA was reduced and if the expression of *Nat8L* was involved in or correlated with any abnormalities in NAA level or mitochondrial integrity.

FAD is associated with the accumulation of the short peptide Amyloid-Beta 42 (Aβ42) within the cell body of neurons; this, in turn, leads to perturbations in energetic metabolism, disrupted synaptic processes, and eventually cell death (71). Recently, energy deficiency and mitochondrial dysfunction have been recognized as a prominent, early event in AD (72–82). One hypothesis for these AD pathologies is the accumulation of $A\beta_{42}$ interacting with intra-mitochondrial proteins and blocking mitochondrial import channels (83). The onset of energetic decline occurs simultaneously with reduced levels of whole brain NAA, as demonstrated through H-MRS. This relationship between AD pathology, oxidative integrity, and reduced levels of NAA has been shown through the analysis of human patients as well as various transgenic rodent models of AD as explained below.

During neurodegenerative disease progression NAA decreases at a similar rate to cognitive decline. This has been well-demonstrated through the direct correlation between whole brain levels of NAA and Alzheimer's patient's mini mental state exam (MMSE) scores (84; Figure 2.1), dementia rating scales (85), and auditory verbal learning test scores (86). Fluorodeoxyglucose Positron Emission Tomography (FDG PET) studies have also demonstrated that over 85% of AD patients have a reduced capacity for glucose utilization (87-89). The reduction of NAA directly correlates with glucose utilization and cognitive decline in a predictable manner. The correlation between glucose utilization, energetic integrity, and whole brain NAA levels has been experimentally demonstrated by revealing that NAA significantly reduced simultaneously with glutamate and glutamine in older rats which have a reduced ability to metabolize glucose (Figure 1.5; 34). This direct relationship between glucose, NAA, and energy is caused by the high reliance of brain specific ATP generation on glucose availability as well as the demonstrated connection between TCA cycle activity and NAA synthesis (Fig 1.8&1.9). Various transgenic mouse models for AD have also demonstrated the direct correlation between AD pathology, NAA reduction, and mitochondrial dysfunction in a similar timeline (90-95).

FAD is a rare genetic autosomal dominant disorder caused by mutations in the genes encoding *APP, PS1, PS2* (106). A mutation in either of these genes leads to an increase in $A\beta_{42}$ (107), a 42 amino acid peptide sequence which accumulates within neuronal cell bodies and can lead to AD pathology. The mechanism of $A\beta_{42}$ production is shown in figure 2.2; briefly, the membrane bound APP protein is

cleaved by a β and γ Secretase (contains PS1 and PS2) to produce $A\beta_{38-43}$. However, when there are mutations in the genes encoding APP, PS1, and/or PS2 the production mechanism leads to the favorable synthesis of $A\beta_{42}$ over other lengths of Aβ, eventually leading to the buildup of amyloid plaques and cell death.

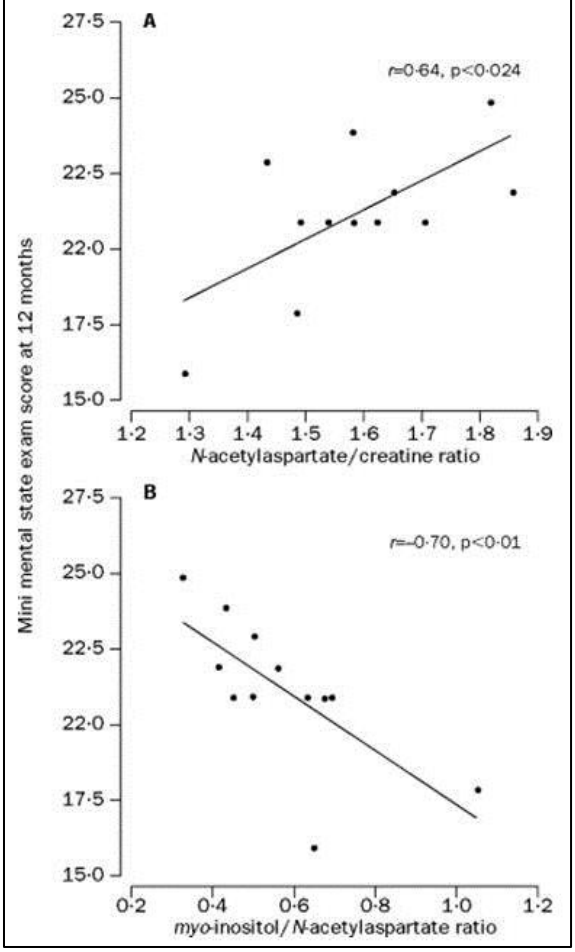

Figure 2.1. Whole Brain NAA Levels are Directly Correlated to MMS exam score in AD patients (84). 12 patients diagnosed with dementia of the Alzheimer type were given the MMS exam 1 year after diagnosis as well as an H-MRS through an axial slice to calculate NAA/creatine as well as myoinositol/NAA. Baseline *NAA* to creatine ratios were positively correlated with MMS exam scores at follow-up (Pearson's correlation coefficient r=0·64, p<0·024. Baseline *myo*inositol to *NAA* ratio was inversely correlated with the score at follow-up (*r*=−0·70, p<0·011; 84)

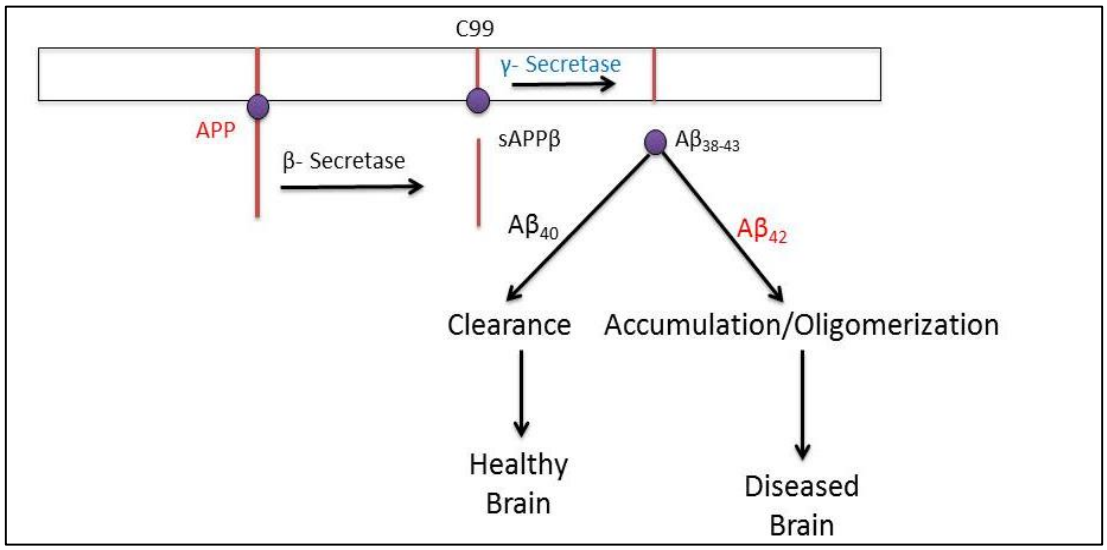

Figure 2.2 The Aβ42 model of FAD. APP is cleaved by β-secretase into a membrane bound C99 and a free sAPPβ region. C99 is then cleaved by gamma-Secretase, which contains both PS1 and PS2, into a peptide ranging from 38-43 amino acids in length. A peptide ranging from 38-41, or 43 amino acids will be cleared from the cell body. A 42 amino acid peptide will eventually accumulate and lead to amyloid plaques and disease.

The main difference between sporadic AD and FAD is that FAD not only has a specific genetic component but also develops much earlier in life. For example, specific *APP* mutations will lead to early onset AD from ages 43-65 (108), where mutations in *PS1* will induce AD progression as early as 28 years of age (109). For this reason, these mutations have been adapted into transgenic mouse models to be used to study AD progression and means of intervention. One of the most highly used models of AD is the Tg2576 transgenic mouse line. These mice overexpress a mutant form of Amyloid Precursor Protein (APP) which contains the Swedish mutation (KM670/671NL) (96). These mice develop relatively normally until 9-12 months of age when they begin to show signs of cognitive decline, $A\beta_{42}$ deposition,

and neuronal loss (96). They also show signs of oxidative damage and mitochondrial dysfunction by 5-8 months of age, leading to significant oxidative stress occurring prior to AD pathology (97-98). In order to develop a transgenic line that manifest cognitive abnormalities in proportion to amyloid load, transgenic models have been developed which express more than one mutant gene. The 3XTg model expresses 3 mutant genes; APP_{SWE}, $PS1_{M146V}$, and TAU_{P301L} leading to the accumulation of $A\beta_{42}$ and Tau (99). These mice develop AD pathology much more rapidly due to the additive nature of these mutations. Aβ accumulation begins around 4 months of age and is most apparent by 6 months; however, Tau immunoreactivity is not apparent until 12 months of age. These mice show minimal cognitive decline prior to Aβ formation, with most learning and memory deficits developing around 6 months of age (100-102). These mice also present with reduced glucose utilization and low levels of whole brain NAA around 6 months of age, coinciding with $A\beta_{42}$ accumulation (103-105). The transgenic model that was used in this thesis research are the 5XFAD transgenic mouse line (110). The 5XFAD mice are positive for five separate mutations within the genes encoding *APP* and *PS1*. The mutated APP contains three site-specific mutations, the Swedish (K670N/M671L), Florida (I716V), and London (V717I). The *PS1* gene also contains site-specific mutations, a M146L, and a L286V, which lead to an increase in $A\beta_{42}$ production.

Compared with wild-type or other transgenic mouse models of AD, 5XFAD mice present with FAD pathology at a much earlier age. As early as 1.5 months of age the 5XFAD mice begin to accumulate $A\beta_{42}$, as opposed to the Tg2576 line (Swedish mutation only) that does not begin to accumulate $A\beta_{42}$ until 9 months of

age. The 5XFAD mice also present with amyloid deposition and gliosis at 2 months of age rather than the 9-12 months it takes in the Tg2576 line. The 5XFAD mice are also positive for insoluble Aβ42 aggregates at 2 months of age, indicating the presence of amyloid deposits throughout the brain. The buildup of amyloid eventually leads to significant synaptic degeneration, neuronal loss, and spatial memory deficits occurring around 4-5 months of age (110). Therefore, the 5XFAD transgenic mouse line shows numerous pathologies present in human FAD patients in an accelerated timeline and is an excellent model for exacerbated amyloidosis. We were interested in when NAA reduction coincides with mitochondrial dysfunction in this model of AD. By doing so, we may be able to elucidate if *Nat8L* plays a role in this characteristic reduction of NAA and if there is any link between altered *Nat8L* expression and reduced oxidative integrity.

Materials and Methods

Animals

All mice in the 5XFAD colony were housed and maintained at the Rowan SOM animal facility with ad libitum access to food and water. The colony was established from founder mice purchased from the Mutant Mouse Regional Resource Center Network. The 5xFAD model has been described in detail elsewhere (110; https://www.mmrrc.org/catalog/sds.php?mmrrc_id=34840) All protocols performed were done so under an approved Rowan-SOM IACUC protocol, and adhered to national and institutional guidelines for animal care and use. For all analyses, mice were humanely euthanized with an intraperitoneal injection of sodium pentobarbital prior to tissue collection. Further detail on the 5XFAD model can be found elsewhere (110; https://www.mmrrc.org/catalog/sds.php?mmrrc_id=34840).

All mice began breeding around 2 months of age, once they had reached reproductive maturity. In order to produce wild-type and heterozygous 5XFAD offspring, a wild-type female (2 months- 1 year) was placed with one heterozygous 5XFAD male (2 months- 6 months) for 1 full gestation period of approximately 20 days. Once the female showed signs of pregnancy the male was removed and placed with another breeding female. Once the pups were born they were left with the dam until weaned (3 weeks of age).

All 5XFAD mice were genotyped between post-natal days three through five, prior to weaning. Pups were taken from their mothers and placed under cryoanesthesia. Once anesthetized, the pups were removed from anesthesia and placed on a sterile work area where one toe and the tip of their tail were removed

under sterile conditions. The remaining portions of the toe and tail were cauterized before the pup was placed back with the Dam. The removed portions of toe and tail were placed into a 1.5 ml micro centrifuge tube and used for DNA isolation using the Invitrogen Blood and Tissue DNA Isolation Kit (Qiagen 69506). Once isolated, the concentration of the resulting gDNA was determined by a Nanodrop (Thermo Scientific NanoDrop® ND-1000)

5XFAD mice were identified by the presence of an internal control gene as well as the mutated form of the *APP* in their genome. Since all five FAD mutations were contained on the same expression cassette, it was only necessary to identify the presence of one mutation in each mouse in order to identify it as 5XFAD. The gDNA was used to detect the presence of the APP transgene (5'-3'; F: AGGACTGACCACTCGACCAG,
R: CGGGGGGTCTAGTTCTGCAT) as well as the internal control (5'-3'; F: CTAGGCCACAGAATTGAAAGATCT,
R: GTAGGTGGAAATTCTAGCATCATCC) via PCR (Peltier Thermal Cycler-200). The gDNA and both primers were combined with a commercially available 2X Ranger mix (Bioline Bio-25051) containing Taq Polymerase to amplify the DNA. Once the PCR program was completed the amplified sample was resolved on a 2% agarose gel under low voltage for approximately 45 minutes. The internal control DNA band (324 base pairs), as well as the APP transgene band (377 base pairs), were detected under UV light (Figure 2.3). Wild-type pups were only positive for the internal control DNA while being positive for the internal control DNA as well as the APP transgene identified 5XFAD pups. It is impossible to distinguish between APP

heterozygotes and homozygotes. This is because the five mutations were introduced via pronuclear injections as a mixture (five different Thy1-driven cassettes), and the final strain was selected based on a combination of amyloid burden and memory deficit. Unfortunately, there was no reference for copy number of each of the five cassettes, making it impossible to generate an absolute copy number for the distinction of homo and heterozygotes. However, because the strain is inbred, the presence of the APP band is the only way of controlling for copy number and determining the expression of mutations (110)

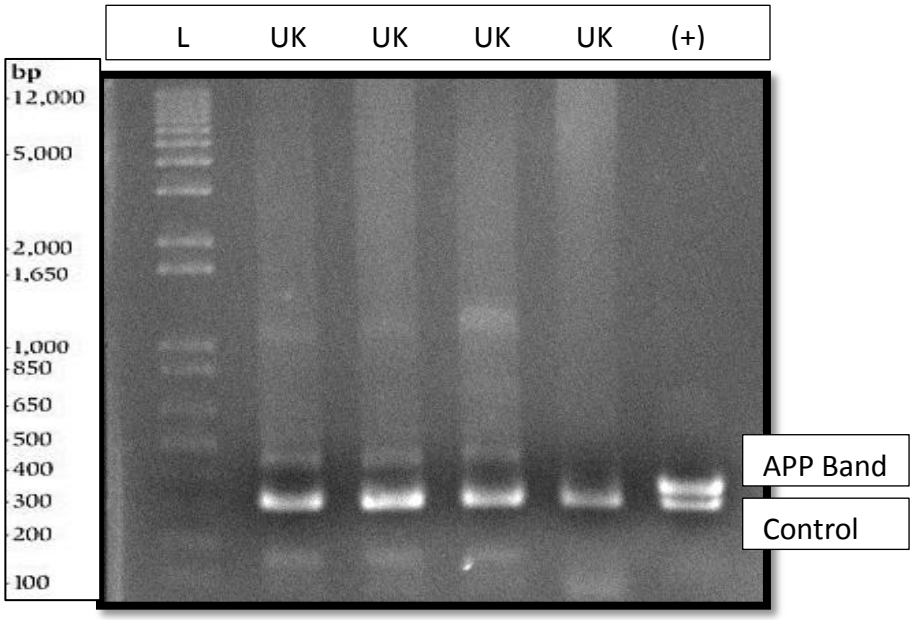

Figure 2.3 Representative Agarose Gel of 5XFAD Genotyping. 10 µl of gDNA PCR reaction was added to 2 µl of 6X loading dye and ran on a 2% agarose gel under low voltage for 45 minutes. A 1 Kb DNA Ladder was added to lane 1, followed by 4 lanes of PCR product from wild-type and 5XFAD animals, and lane 5 contained a 5XFAD positive control for the APP transgene. The bands were visualized under UV light.

HPLC

Tissue for HPLC analysis was collected from rapidly retrieved brains of deeply anesthetized 5XFAD mice. One hemisphere was homogenized with a dispersal element (Ultra Turrax, IKA Works Inc., Wilmington, NC), in 2× volume/weight of freshly prepared ice-cold precipitation solution (3:1 acetonitrile: KH_2PO_4 (pH 7.4). Homogenates were then centrifuged for 10 minutes at 10,000×g at 4°C. The supernatant was retained and the remaining pellet was sonicated with an additional 500 µl of precipitation solution before centrifugation for 10 minutes at 10,000×g at 4°C. The supernatants from the consecutive preparations were combined and were extracted twice with 2× volume of HPLC-grade chloroform. All samples were aliquoted and stored at -80°C until needed for HPLC analysis. The samples were analyzed on a Thermo Scientific Surveyor-Plus HPLC system equipped with UV detection and a Hypersil BDS-C18 column (5 µm particle size; 25× 4.9 mm). An ion-paired reverse phase detection methodology was used to analyze samples using buffers and sequence as described previously (51). NAA, ATP, and AMP were quantified in a single run using standard curves generated by purified HPLC-grade standards. Quantities of each metabolite were expressed as a molar concentration per wet weight of tissue.

Quantitative Real Time RT-PCR

Total RNA was prepared from one entire hemisphere of flash frozen mouse brain. Tissue was homogenized using Trizol reagent (Invitrogen Corp., Carlsbad, Ca) as per manufacturer's instructions (1 ml per 50-100 mg tissue). Purified RNA was treated with DNase to remove contaminating genomic DNA and cleaned using

RNeasy columns (Qiagen, Valencia, Ca). The concentration of all purified RNA was determined by spectrophotometry and the integrity of samples verified by denaturing agarose/formaldehyde gel electrophoresis. cDNA for QRT-PCR was generated from 1μg of purified RNA using a Superscript First Strand Synthesis Kit (Invitrogen, Carlsbad, CA). QRT-PCR was performed with SYBR-Green on an Applied Biosystems Step One Real Time PCR system (Applied Biosystems, Foster City, Ca). The primers for target transcripts were as follows: *Nat8L* (5′-3′; F: CTACCTGGAGTGCGCGCT, R: GGCGGCTTCATGTAGTACTGC), *NduSF2* (5′-3′; F: AGGTTGATGACGCCAAAGTGT, R: GACTCCATGGACGTCTTCATCTC), and *GAPDH* (5′-3′; F: AACTTTGGCATTGTGGAAGG, R: ACACATTGGGGGTAGGAACA). The Relative Standard curve method was used to analyze the expression of *Nat8L* and delta delta CT method was used for Ndusf2, both using GAPDH (Glyceraldehyde-3-phosphate dehydrogenase) expression as an internal control.

In Situ Hybridization

Total RNA from a 4-week old wild-type mouse brain was used to amplify an 830bp fragment of *Nat8L* to be used as a template for synthesis of a DIG-labeled RNA probe. This region was amplified by RT-PCR and sub cloned into a TOPO-TA sequencing plasmid. The *Nat8L* CDS was then sub cloned into the plasmid pSPT-19 for the synthesis of DIG-*Nat8L* using a commercially available kit, following the manufacturer's instructions (Roche Diagnostics, Indianapolis, IN). Prior to hybridization, coronal sections were sliced from 4-month-old RNase-free perfused 5XFAD and wild-type brains. The DIG-*Nat8L* probe was then hybridized to the

sections at a concentration of 30 ng/ml for 20 hours at 55°C. After hybridization, the sections were washed, blocked, and incubated for 2 hours with an anti-DIG-AP antibody (1:20,000; Roche Diagnostics, Indianapolis, IN). For co-labeling with NeuN, DIG-*Nat8L* labeled sections were then incubated overnight in NeuN (1:5000) as explained below prior to mounting and cover slipping.

Immunohistochemistry

All tissue samples for immunohistochemistry were prepared by the transcardial perfusion of deeply anesthetized animals with ice cold 0.9% saline followed by freshly prepared 4% buffered paraformaldehyde. Perfused brains were removed and post-fixed overnight in 4% paraformaldehyde, then cryopreserved in an ascending sucrose gradient. Cryopreserved brains were embedded in Tissue-Tek OCT compound (Sakura, Torrance, Ca), and flash frozen in an Isopentane/dry ice bath. Serial 45 um sections were collected from each brain (beginning approximately from Bregma 0.20 mm) and stored at -20°C in cryoprotectant until needed. Free-floating sections were incubated with primary antibodies overnight at room temperature (RT) in Immuno-buffer (1× PBS, 0.1% Triton X-100, and 1% normal goat serum; mouse A60 neuron-specific nuclear protein [NeuN] 1:500 [Millipore, Billerica, Ma]. After incubation in primary antibody, sections were incubated for 2 hours at RT in biotinylated secondary antibody (Sigma-Aldrich, St. Louis, Mo), followed by incubation at RT for 1 hour in extravadin peroxidase (Sigma-Aldrich, St. Louis, Mo). Positive cells were visualized using 3, 3′-diaminobenzidine (DAB; Sigma-Aldrich, St. Louis, Mo). Developed sections were mounted onto glass slides, dehydrated in an

ascending ethanol gradient, and then cleaned twice with xylene and coverslipped with DPX mountant (Sigma-Aldrich, St. Louis, Mo).

Unbiased Stereology

Estimates of NeuN-positive neurons were generated using the optical fractionator (k=4) and Stereologer software (Stereology Resource Center, Tampa, FL). Counts were performed on a single hemisphere of processed sections to generate estimates of NeuN for CA1 of the hippocampus and cortical layer V for 5xFAD and age matched control brains. All counts were performed at the 100× objective on an Olympus BX51 upright microscope equipped with an analog camera and motorized stage. Significance differences in N between experimental and control groups were determined by a 2-tailed student's T-test ($p \leq 0.05$).

Microarray Analysis of Mitochondrial Gene Expression

The expression of 84 nuclear-encoded transcripts for components of the mitochondrial electron transport chain (Complexes I-V) was analyzed using commercially available RT2 Profiler™ Mouse Mitochondrial Arrays (SA Biosciences/Qiagen, Frederick, MD). Total RNA was isolated from one hemisphere of flash frozen brains with Trizol reagent as described. Purified RNA (0.5 µg) from 4-month wild-type and 4-month 5X FAD brains was used to prepare cDNA using the RT2 First Strand Synthesis Kit, as per the manufacturer's instructions. The resulting cDNA was combined with RT2 Syber Green Master mix and added to the wells of a mouse mitochondrial energy metabolism RT2 Profiler PCR array. The prepared plate was run on an Eppendorf Mastercycler Ep Realplex 4S. The fold change of each target gene in 5X FAD samples relative to wild-type controls was determined using

the cycle threshold (CT) to fold change RT2 Profiler PCR Array Data Analysis Template V4.0. Significant differences in 5xFAD expression were determined using a threshold significance of $p<0.005$.

Mitochondria Isolation, Complex I Assay, and Malate Aspartate Shuttle Assay

Intact mitochondria were isolated from flash frozen brain tissue. Tissue was homogenized in 6 ml of homogenization buffer (320 mM Sucrose, 10 mM Tris-HCl [pH 7.4], 2 mM EDTA), and centrifuged for 10 minutes at 1000×g to pellet cell membranes and debris. The supernatant was removed and centrifuged for 20 minutes at 20,000×g to pellet mitochondria. The mitochondrial pellet was resuspended in 1ml of homogenization buffer without EDTA, and total protein concentration determined by BCA Protein Assay Kit (Thermo Fischer Scientific, Rockford, Il).

Malate aspartate shuttle (MAS) activity in intact mitochondria isolated from brains was assayed using previously published methodology (Jalil et al, 2006). Briefly, mitochondria (100 mg/sample) were placed in triplicate into a 96 well plate, and assay solution containing assay buffer (75 mM mannitol, 20 mM Tris-HCl, 0.5 mM EDTA, 100 mM KCL, 5 mM phosphate, 0.1% BSA) and reaction solution (66.6 mM NADH, 5 mM aspartate, 5 mM malate, 0.5 mM ADP, 16 mM CaCl2, and 5 mM glutamate) added. The reaction was started by the addition of 4U/ml aspartate aminotransferase and 6U/ml of malate dehydrogenase to each well. Shuttle activity was defined by the oxidation of NADH over 5 minutes as determined by the change in OD at 340 nm on an automated microplate reader (BioTek Instruments Inc. Winooski, VT).

Mitochondrial complex I activity was determined for the same intact mitochondrial samples using a commercially available immune-capture microplate format kit (Abcam, Cambridge, Ma). Briefly, mitochondrial proteins were generated by detergent extraction of intact samples followed by centrifugation. Lysed samples were then diluted to 250 ug/ml with supplied buffer, and 200 µl added in triplicate to the microplate supplied with the kit. Samples were incubated at room temperature for 3 hours, washed, and 200 ul of assay solution (1× Buffer, 1× NADH, and 1× dye) added. The absorbance of wells was read at 450 nm every minute for 30 minutes using a Microplate reader (BioTek, Winooski, VT). Complex I activity was expressed as the average change in absorbance/min/ug of total protein over 30 minutes.

Results

NAA is Significantly Reduced at 4 Months of Age in the 5XFAD Mouse

As the reduction of NAA has been clinically and experimentally shown to occur during the early stages of AD progression, we were first interested in identifying which period of time in 5XFAD pathology was defined by abnormally low levels of NAA. In order to accomplish this, we first had to uncover if/when NAA was reduced in the 5XFAD mouse model. Other models have demonstrated a significant reduction of NAA occurring prior to, or simultaneously with the onset of AD pathology (103-105). Therefore, we analyzed the months prior to and during the symptomatic onset of the 5XFAD mouse. As described in the literature, the 5XFAD mouse begins accumulating amyloid as early as 2 months of age; however neuronal loss and cognitive decline occur between 5-6 months of age (110). Therefore, we decided to analyze the level of whole brain NAA in 2- and 4-month 5XFAD brains via HPLC. Our analysis of these time points revealed a significant reduction of whole brain NAA occurring by 4 months of age (Figure 2.4). Therefore, we focused most of our future experiments around this time period, as we were mainly interested in uncovering the regulatory mechanism controlling this reduction.

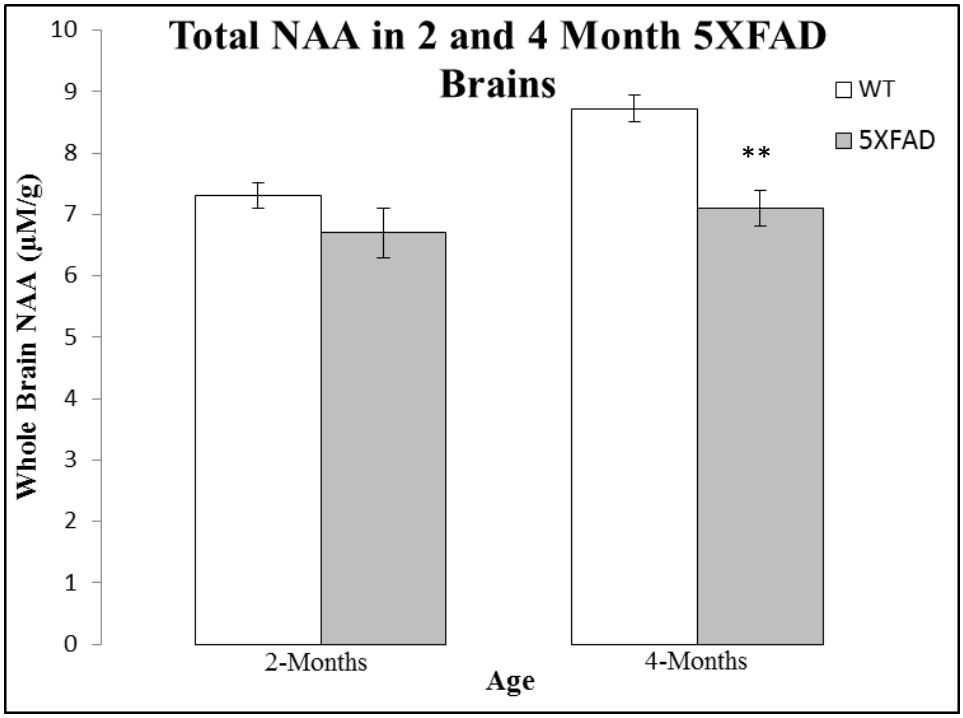

Figure 2.4 NAA is Significantly Reduced at 4 Months of Age in the 5XFAD Mouse. Whole brain homogenates analyzed by HPLC show a significant reduction in NAA from 2-4 months of age in 5xFAD brains (N=7 per age and genotype). (***≤0.001<**≤0.01<*≤0.05)

Nat8L is Down-Regulated at 4 months of Age in the 5XFAD Mouse

After confirming that NAA is reduced at 4 months of age in the 5XFAD brain it was important to determine if this reduction was due to an active response to energetic integrity. In order to determine if the reduction of NAA is due to altered transcriptional regulation of NAA synthesis, the expression of *Nat8L* was analyzed in the 5XFAD mouse brain via QRT-PCR. This analysis was performed on 2 and 4-month 5XFAD brains in order to determine if altered *Nat8L* expression could account for the observed reduction in NAA. The QRT-PCR results revealed a significant down -regulation of *Nat8L* at 4 months of age in the 5XFAD brains compared with wild-type controls (Figure 2.5A). This decrease in expression was confirmed

using an in house produced anti-*Nat8L* mRNA probe for in house ISH. This probe confirmed that Nat8L was down-regulated, and confirmed co-localization of *Nat8L* mRNA with neurons specifically (Figure 2.5B&C). *Nat8L* mRNA expression was determined through the side by side comparison of control and 5XFAD sections. Qualitatively, it was apparent that *Nat8L* mRNA was significantly reduced in 4-month 5XFAD brains compared with wild-type, particularly within CA1 of the hippocampus; a brain region of high interest in AD progression (Figure 2.5D). The hippocampus is followed during AD progression because it has a well cited history of having a strong role in memory formation and maintenance as well as being one of the first areas to suffer from significant neuronal loss, particularly within region CA1 (189). In order to confirm that the reduction in NAA was directly due to the down-regulation of *Nat8L* and not because of neuronal loss, we performed neuronal cell counts via unbiased stereology of NeuN (neuronal marker) positive nuclei within the cortex (191) (Figure 2.6A) and CA1 of the hippocampus (190) (Figure 2.6B) of wild-type and 5XFAD brains (110)). These counts confirmed that there was no neuronal loss at 4 months of age in the 5XFAD mouse brain compared with wild-type controls. Therefore, NAA was significantly reduced at 4 months of age in the 5XFAD mouse due to the down-regulation of the NAA synthetic enzyme, Nat8L.

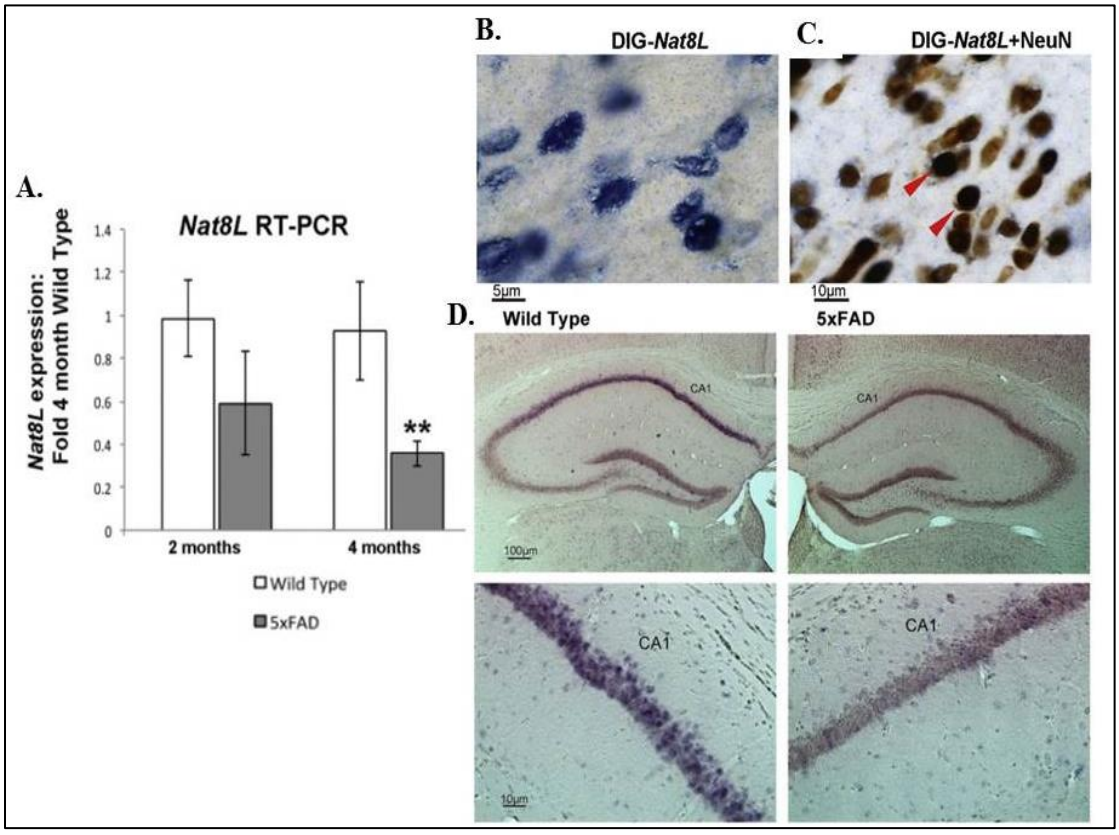

Figure 2.5 Nat8L is Down-regulated in the 4-Month 5XFAD Brain. (A) QRT-PCR of 1 hemisphere from 2 and 4-month wild-type and 5XFAD mouse brains revealed a significant down-regulation of *Nat8L* at 4 months of age in 4-month 5XFAD brains compared with wild-type controls (expression presented as fold- 4-month wild type, N=5/ group). (B-D) This reduction was confirmed through ISH via an in house made anti-*Nat8L* mRNA. The probe co-localized to (B) *Nat8L* within (C) neurons. (D) When hybridized to 4-month wild-type and 5XFAD brain sections, there was significantly less hybridization within 4-month 5XFAD brains compared with the wild-type controls, indicating a significant reduction of *Nat8L* expression. (***≤0.001<**≤0.01<*≤0.05)

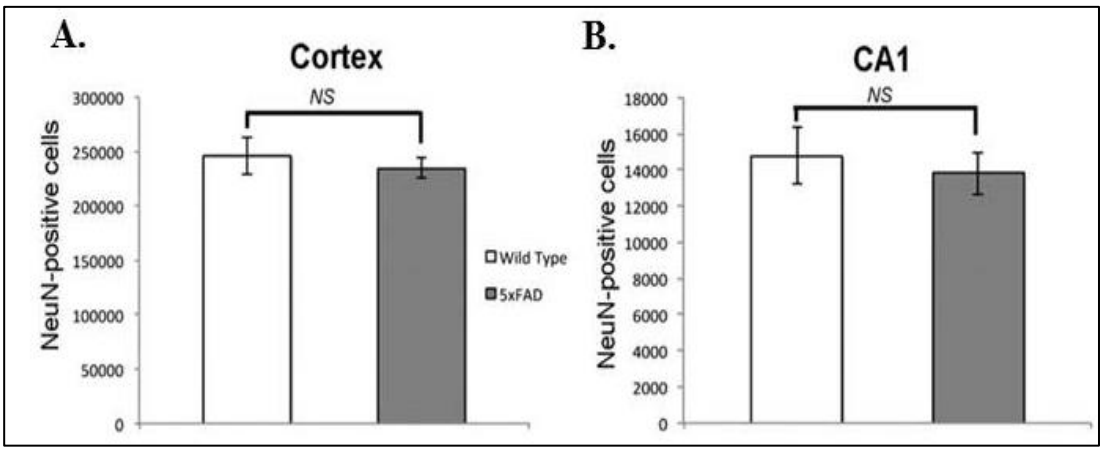

Figure 2.6 No Neuronal Loss in 4-Month 5XFAD Brains. Stereological estimates of NeuN-positive cells in (A) cortical layer V and (B) CA1 of the hippocampus indicate no significant difference in neuron content in 4-month 5XFAD brains relative to wild type (N=4/group).

ATP is Reduced at 2 and 4 Months of Age in the 5XFAD Mouse

A common hallmark of neurodegenerative disease is the onset of simultaneous loss of mitochondrial function (178) and whole brain levels of NAA (6) prior to symptomatic onset. We hypothesized that this simultaneous loss of mitochondrial function and NAA is not a coincidence, but due to the intimately linked synthetic pathways of both NAA and ATP. We predicted that *Nat8L* would be actively down-regulated during periods of energetic stress in order to minimize the negative impact NAA synthesis has on the pool of oxidative substrates. Therefore, we decided to investigate the time period of 5XFAD development which presents with reduced levels of NAA (4 months) in order to identify if mitochondrial dysfunction coincided with reduced *Nat8L* expression. To determine if/when energetic crisis began in the

5XFAD model, HPLC of 2 and 4-month 5XFAD and wild-type brains was performed to reveal any differences in ATP production. The results showed that ATP was significantly reduced and AMP was significantly increased at 2 and 4 months of age in the 5XFAD mouse compared with controls (Figure 2.7) prior to the down-regulation of *Nat8L* and the loss of whole brain NAA.

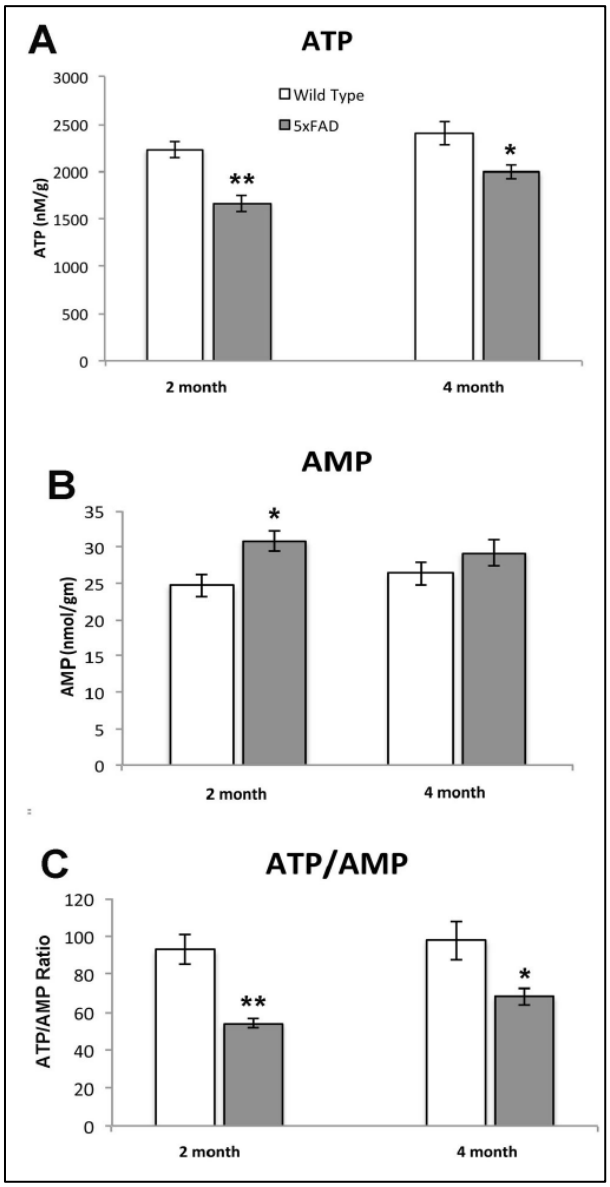

Figure 2.7 ATP: AMP is decreased in 2 and 4-month 5XFAD brains. HPLC analysis of ATP (A) and AMP (B) reveal significant decreases and significant increases, respectively at 2 and 4-months in 5xFAD brains, resulting in a reduction in the ATP/AMP ratio (C). Levels of ATP and AMP expressed as nmol/wet weight of tissue (N=7). (***≤0.001<**≤0.01<*≤0.05)

Mitochondrial Dysfunction as a Possible Transcriptional Regulator of NAA Synthesis

In order to properly assess the level of mitochondrial dysfunction in the 5XFAD brain, 2- and 4-month 5XFAD and wild-type brains were analyzed for various aspects of mitochondrial function. We were first interested in identifying if there were any differences in ETC gene expression between wild-type and 5XFAD brains. The results of this analysis would identify if the progression of 5XFAD had any effect on the transcriptional regulation of genes utilized for oxidative phosphorylation. Since ATP and NAA production are so intimately associated, any significant differences in expression may reveal an upstream mechanism involved in the transcriptional regulation of ATP and/or NAA. In order to undertake this analysis, we performed a microarray on 84 nuclear encoded ETC genes in 2- and 4-month 5XFAD brains and compared them to wild-type controls. Despite earlier data reporting a significant loss of ATP at 2 months (Fig 2.7A), we did not see any significant down-regulation of ETC related genes until 4 months of age. In depth analysis of the resulting delta Ct values revealed that the top 13 most down-regulated genes (Figure 2.8A) were representative of complexes I, III, IV and V. In order to confirm this overall reduction in gene expression of components of the ETC, we performed in house independent validation of the most significantly down-regulated gene, *Ndufs2* (Figure 2.8B). Our results confirmed our microarray data that this gene, and most likely the other ETC genes, were down-regulated at 4 months of age in the 5XFAD brain compared with wild-type, not at 2 months.

A. Table 1: Signficantly Down Regulated Nuclear Encoded ETC Genes in 4 Month 5XFAD Brains Compared with Age Matched WT Controls

Gene	Complex	Fold WT
Ndufs2	I	-1.71
Uqcrh	III	-1.71
Bcs11	III	-1.67
ATP5g3	V	-1.59
Cox5a	IV	-1.59
Ndufb3	I	-1.51
ATP5h	V	-1.46
Ndufa2	I	-1.44
Cox8c	IV	-1.44
Ndufs7	I	-1.41
Uqcrfs1	III	-1.41
ATP5j2	V	-1.39
Ndufb6	I	-1.37

B.

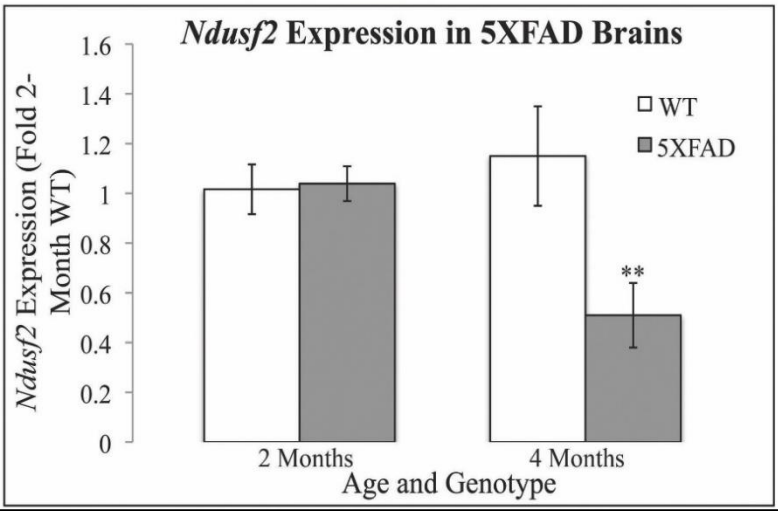

Figure 2.8 Nuclear Encoded ETC genes are Significantly Down –regulated at 4 Months of Age in the 5XFAD Brain. (A) Table 1: The 13 most significantly down-regulated nuclear encoded ETC genes in 4-month 5XFAD brains as identified via microarray. The threshold significance for the above-mentioned genes was $p \leq 0.005$. (B) QRT-PCR confirmation of the most significantly down-regulated Complex one gene, *Ndusf2*, from the 4-month array data (Fold- 2-month wild type values, N=5). (***$\leq$0.001<**$\leq$0.01<*$\leq$0.05)

Considering the microarray revealed that the most down-regulated nuclear encoded ETC gene was a component of complex I of the ETC, we were interested in determining if this down-regulation led to a reduction in complex one activity. If this correlation was proven correct, then we could assume that complexes III, IV, and V activities would also be reduced; and therefore the entire ETC would be compromised during this time period. In order to evaluate complex one activity, intact mitochondria were isolated from 2- and 4-month wild-type and 5XFAD brains and used in a commercially available complex one activity assay. The results of the assay revealed a significant reduction in complex I activity in 4-month 5xFAD mitochondria compared with wild-type controls (Figure 2.9). The data also revealed that once again, there was no difference between the activity of 2-month wild-type and 5XFAD brains. From these data, we concluded that overall mitochondrial dysfunction occurs at 4 months of age in the 5XFAD mouse brain. This dysfunction occurred simultaneously with reduced *Nat8L* expression and NAA synthesis. However, a significant reduction in ATP: AMP occurs at 2 months of age in the 5XFAD brain, prior to reduced NAA. Therefore, we hypothesize that NAA is actively reduced in response to this reduction in ATP: AMP. However, it is also possible that ATP: AMP and NAA are being actively reduced by a different, yet common active mechanism related to cellular energetic integrity. At this time the data was not comprehensive enough to discern between these two possible mechanisms, and was only sufficient to identify the timeline of correlated events.

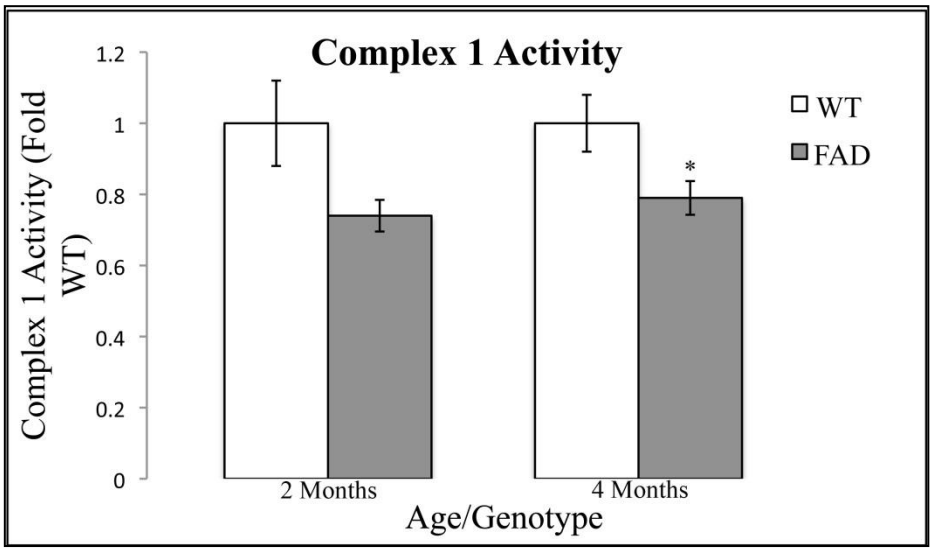

Figure 2.9 Complex I Activity is Significantly Reduced at 4 Months of Age in the 5XFAD Mouse Brain. Reduced *Ndusf2* expression correlates with a significant decrease in 4-month 5xFAD mitochondrial Complex one activity. Activity defined as the mean change in OD@450 nm over 30 minutes. Values presented as fold-wild type activity, N=5). (***≤0.001<**≤0.01<*≤0.05)

NAA Reduction is Not due to Insufficient Aspartate Availability as Shown Through Increased MAS Activity in 4-Month 5XFAD Mouse

The synthesis of NAA has been demonstrated to be dependent on the activity of the MAS (13). This is because NAA synthesis and the MAS both rely on the intra-mitochondrial pool of aspartate to maintain their activity. To determine the contribution of MAS activity to NAA synthesis during 5XFAD progression, intact mitochondria were isolated from 4-month wild-type and 5XFAD brains and used for a MAS activity assay. The resulting data revealed a significant up-regulation of MAS activity in 4-month 5XFAD brains compared with wild-type controls (Figure 2.10).

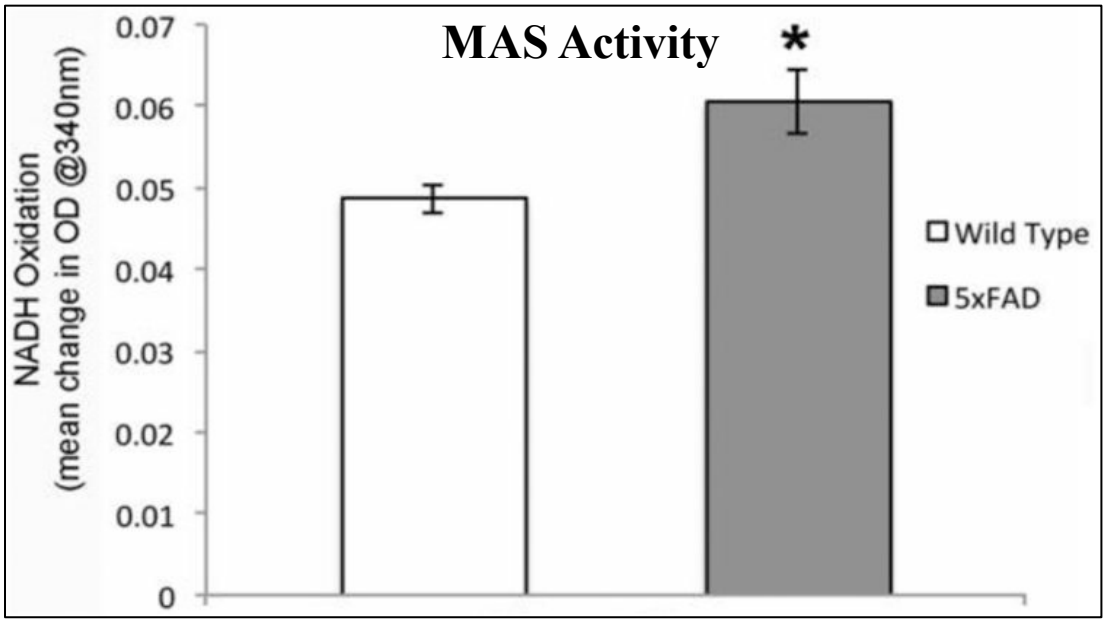

Figure 2.10 Increased MAS activity in 4-month 5xFAD brains relative to wild type controls. NADH oxidation, determined by the mean change in OD @ 340 nm over 5 minutes for 4-month 5xFAD and wild type mitochondrial preparations. Data expressed as mean change in OD +/- SEM, n=5. (***≤0.001<**≤0.01<*≤0.05)

Therefore, it is highly unlikely that reduced NAA levels in the 5XFAD mouse are caused by decreased availability of rate-limiting aspartate. However, since the MAS is responsible for sending reducing equivalents to the ETC, the significant increase in MAS activity in 4-month 5XFAD brains could indicate the beginning of an energetic stress response mechanism. This mechanism could also be responsible for the active down-regulation of NAA synthesis in order to save mitochondrial aspartate for increased MAS activity.

Conclusions

The main conclusion from this chapter is that NAA is reduced due to the active down-regulation of *Nat8L*. This reduction in whole brain levels of NAA and the expression of *Nat8L* occur after the reduction in whole brain levels of ATP: AMP, but simultaneously with significant mitochondrial dysfunction and increased MAS activity. Therefore, we hypothesize that *Nat8L* expression is either actively regulated by reduced levels of ATP: AMP or directly down-regulated by an upstream energetic stress response cascade which serves to reduce mechanisms which reduce the pool of oxidative intermediates while simultaneously increasing ATP generation.

To identify if NAA synthesis and/or metabolism was transcriptionally regulated in response to neuronal insult, the brains of TBI mouse models were analyzed for NAA levels, ATP levels, and transcriptional regulation of *ASPA* and *Nat8L*. The results of this study revealed a significant up-regulation of *ASPA* which occurred prior to a decrease in NAA, *Nat8L*, and mitochondrial function (40). Therefore, it is possible that ASPA is a primary responder to reduced levels of ATP and not *Nat8L*. ASPA may also be an upstream regulator of *Nat8L* expression in the 5XFAD model, in models of TBI, and/or other models of neurodegenerative disease/disorder. If this hypothesis were to be proven correct, it would be direct evidence of oligodendrocytes and neurons participating in the mutual regulation of their transcriptomes and both contributing to one regulatory mechanism.

Chapter Three

The Possible Role of ASPA in Nat8L Regulation

Specific Aim Three

The first goal of specific aim three was to determine if *ASPA*, similar to *Nat8L*, showed any difference in expression between wild-type and 5XFAD mice during previously defined periods of energetic crisis and reduced levels of whole brain NAA. We hypothesized that *ASPA* would be up-regulated at 4 months of age in the 5XFAD mouse, occurring simultaneously with reduced levels of whole brain NAA and mitochondrial dysfunction. The second goal of specific aim three was to determine if in vivo *ASPA* expression had any direct effect on the expression of *Nat8L*. This aim was carried out by analyzing the expression of *Nat8L* within the brains of wild-type and *ASPA* null mice. Specifically, the expression of *Nat8L* was analyzed during 1-8-weeks of age, as this time period is defined by the normal induction of both *ASPA* and *Nat8L* expression. We hypothesized that the expression of *Nat8L* would be down-regulated in response to the ablation of *ASPA* expression, possibly indicating *ASPA* as a regulatory signal for *Nat8L* expression.

Introduction

The reduction of NAA is considered a hallmark of most neurodegenerative diseases, however, it is also a prominent marker in other brain-specific disorders or injuries. In 2015 DiPetro et al (111) published a paper revealing the direct relationship between Traumatic Brain Injury (TBI) severity and whole brain levels of NAA in rats. During periods of injury (both moderate and severe), the rat brains also

presented with significantly reduced expression levels of *Nat8L*, increased expression levels of *ASPA*, and reduced levels of ATP.

TBI is an umbrella term for any direct insult to the brain due to trauma. This can vary from a simple concussion (mild TBI) to an accident leading to complete paralysis (severe TBI) (112). A key means of grading a TBI is the reduction of whole brain NAA and the amount of time it remains at a low level. This is because, similarly to neurodegenerative disorders, NAA is used as a marker of overall neuronal mitochondrial integrity during TBI progression (116-118). However, unlike neurodegenerative disorders, patients suffering from mild TBIs can, and usually do, recover. In order to track the progression of TBI recovery, clinicians continue to monitor whole brain levels of NAA until they return to normal levels (5-10 mM in adult humans; 113-115).

Rat models of TBI have been extremely useful in distinguishing the thin line between mild and severe TBIs. These models have shown that rats subjected to mild TBI will present with decreased levels of whole brain NAA which recover after a few hours to basal levels (111). On the other hand, rats exposed to multiple mild TBI's or one severe TBI will present with reduced levels of NAA which do not recover over time. This pattern of NAA fluctuation seems to follow ATP levels, during recoverable and non-recoverable TBI's. The reduction of both NAA and ATP is hypothesized to be caused by injury-induced mitochondrial malfunction, and therefore will only increase once mitochondrial function returns to normal.

DiPietro's manuscript was the first of its kind to highlight that reduced levels of NAA during TBI occur simultaneously with the significant down-regulation of

Nat8L, the up-regulation of *ASPA*, and the reduction of ATP (111). This timeline of events seemed quite similar to what we had demonstrated as occurring during the progression of FAD in 5XFAD mice. However, despite revealing that *Nat8L* expression is significantly down-regulated simultaneously with reduced levels of NAA and energetic crisis, we still need to determine if FAD progression affects the expression of *ASPA*. Therefore, the results of this study prompted our investigation into the regulation of *ASPA* during 5XFAD progression.

The Nur7 transgenic mouse line was named after a specific nonsense point mutation within the gene encoding the ASPA protein which seemed to cause neurological damage (120). This mutation generated an early stop codon that led to the translation of a truncated, non-functional form of ASPA (120). Because these mice express limited *ASPA* RNA and have no functional ASPA protein, they are unable to break down NAA, and consequently have significantly higher amounts of NAA in their cerebral cortex, brainstem, cerebellum, and spinal cord compared with wild-type controls (120). They also present with significant hypo-myelination throughout the CNS and begin showing signs of physical disability by three weeks of age, a period normally defined by myelination and ASPA expression (120). Due to these characteristics, Nur7 mice are a widely accepted model of the human pediatric leukodystrophy called Canavan's Disease; the only disorder characterized by high levels of NAA and non-functional ASPA (193).

Unlike *Nat8L*, the *ASPA* gene and its function in NAA metabolism were identified decades ago (194). However, until recently, it was unknown how the activity of ASPA was regulated during wild-type development. ASPA expression has

been shown to be up-regulated between the first and third weeks of postnatal rodent development (123). This increase was hypothesized to be transcriptionally controlled, occurring simultaneously with myelination (123-124). A subsequent study analyzed the expression of *ASPA* during wild-type rat development and revealed a significant 5-fold increase in *ASPA* expression occurring between postnatal days 7-14 (125) (Figure 3.1A). These results were confirmed via Immunohistochemistry (IHC) of ASPA-positive oligodendrocytes within white matter tracts of 1, 2, 4 and 8-week old rat brains followed by unbiased stereology. The results revealed a 12-fold increase in ASPA positive cells (Figure 3.1B) in 2-week wild-type brains compared with 1-week brains, despite there being no significant difference in oligodendrocyte number (Figure 3.1C). These results indicated that the increase in *ASPA* was due to the transcriptional up-regulation of *ASPA* mRNA, and not an increase in oligodendrocyte number (125).

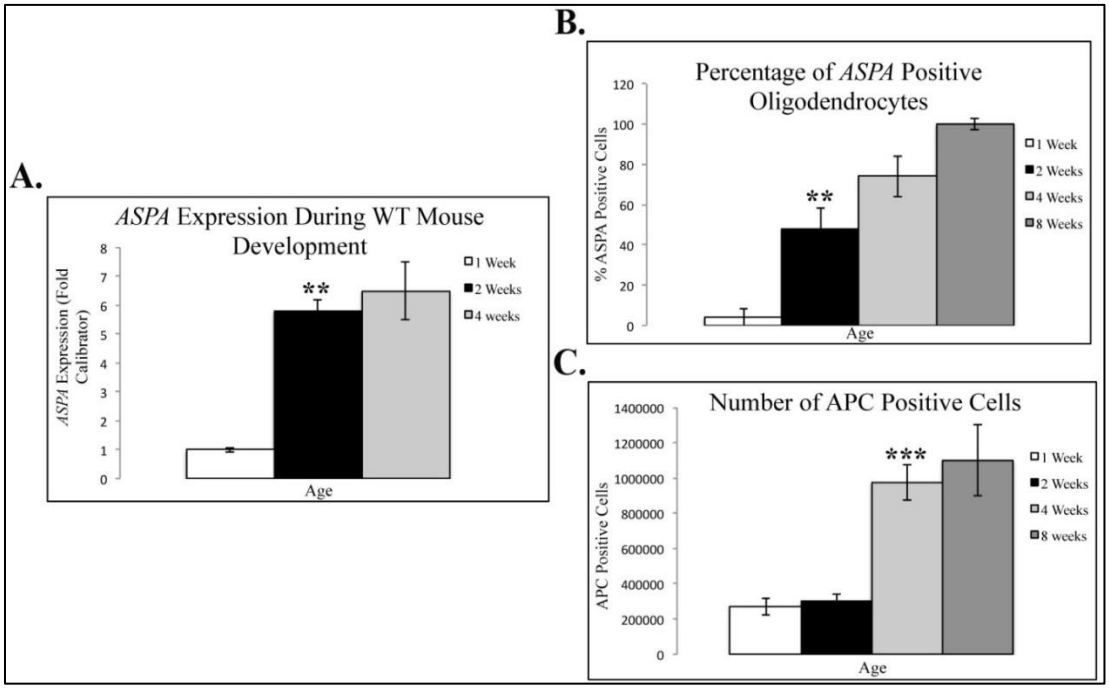

Figure 3.1 ASPA and APC Expression during Postnatal Mouse Development. (A) The expression is shown at 1, 2, and 4-weeks of age expressed as a fold difference relative to 1-week (N = 3/age). (B) ASPA-positive oligodendrocytes in wild-type brain at ages 1, 2, 4, and 8-weeks of age (N=3/age) for the white matter tracts of the external capsule. (C) Total count of APC positive cells within the white matter tracts of the external capsule in wild-type brains ages 1, 2, 4, and 8-weeks (N=3/age). ***≤0.001<**≤0.01<*≤0.05 (125)

Materials and Methods

Animals

All mice used in this study were housed and maintained at the RowanSOM vivarium under approved Institutional Animal Care and Use Committee (IACUC) guidelines and protocols. All mice were given food and water ad libitum. All mice used in this aim had a C57BL/6J background with either a wild-type or Nur7 genotype. The *nur7* genotype has been described previously (120; Traka *et al*, 2008) and the colony was established from founder mice purchased from the Mutant Mouse Regional Resource Center Network (https://www.mmrrc.org).

All mice began breeding around 2 months of age, once they had reached reproductive maturity. To breed the Nur7 mouse line one heterozygous Nur7 female was placed with one heterozygous Nur7 male for 1 gestational period. Once the female was noticeably pregnant, the male was removed and placed with a different heterozygous Nur7 female. Heterozygotes are used for breeding to ensure sufficient impregnation as well as the production of healthy offspring. Homozygous Nur7 mutant mice suffer from disrupted myelin synthesis weeks before they are sexually mature; therefore they are incapable of adequately conceiving and caring for their young. Once the pups were born they were genotyped at day 2 and left with the dam until weaned. Wild-type and heterozygous Nur7 mice were left with the Dam for 3 weeks before being placed in their own cages, while the homozygous Nur7 mutants must be left with the mother for an extra week to increase chance of survival.

The Jackson Nur7 mouse line can be identified as wild-type, heterozygous for the Nur7 mutation, or homozygous for the Nur7 mutation. In order to correctly

identify the genotype of each pup the genomic DNA had to go through 2 rounds of PCR in order to determine the normalized copy number of the Nur7 SNP. Briefly, after the gDNA was preliminarily quantified using a NanoDrop Spectrophotometer, it was diluted to a concentration of 4 ng/μl in DNase-free water. It then went through Quantitative Real-Time -PCR (QRT-PCR) using an Applied Biosystems Step One Real Time PCR system (Applied Biosystems, Foster City, Ca) to amplify the housekeeping gene GAPDH. This was done using a 2X TaqMan Universal PCR Master Mix (Applied Biosystems 4324018) and a 20X TaqMan Gene Expression Assay Master Mix Solution containing primers and a 6FAM/MGB probe (Applied Biosystems 4352932E) specific for mouse GAPDH. Once completed, the QRT-PCR results were used to determine a more accurate concentration of the gDNA using a GAPDH expression standard curve.

Equal amounts of gDNA were added to a master mix containing 2X TaqMan Universal PCR Master Mix containing primers and a 6FAM and 1Vic, 40X commercially available custom SNP Genotyping Assay Solution (Thermo Fischer), and DNase-free water. The custom SNP genotyping assay was designed in house in order to identify the copy number of the Nur7 single nucleotide mutation. The PCR was performed using an Applied Biosystems Step One Real Time PCR system and following completion, each gDNA sample was analyzed for the absence/presence of either dye using a dot plot. Wild-type mice have two copies of the aspa ^{wt} allele which is visualized by 1Vic, represented by the blue dots. Homozygous mutant mice have 2 copies of the aspa^{nur7} allele which are visualized by 6Fam; represented by the red

dots. Heterozygotes contain 1 wild-type allele and one nur7 allele, so the DNA is visualized by both dyes, represented by the green dots (Figure 3.2).

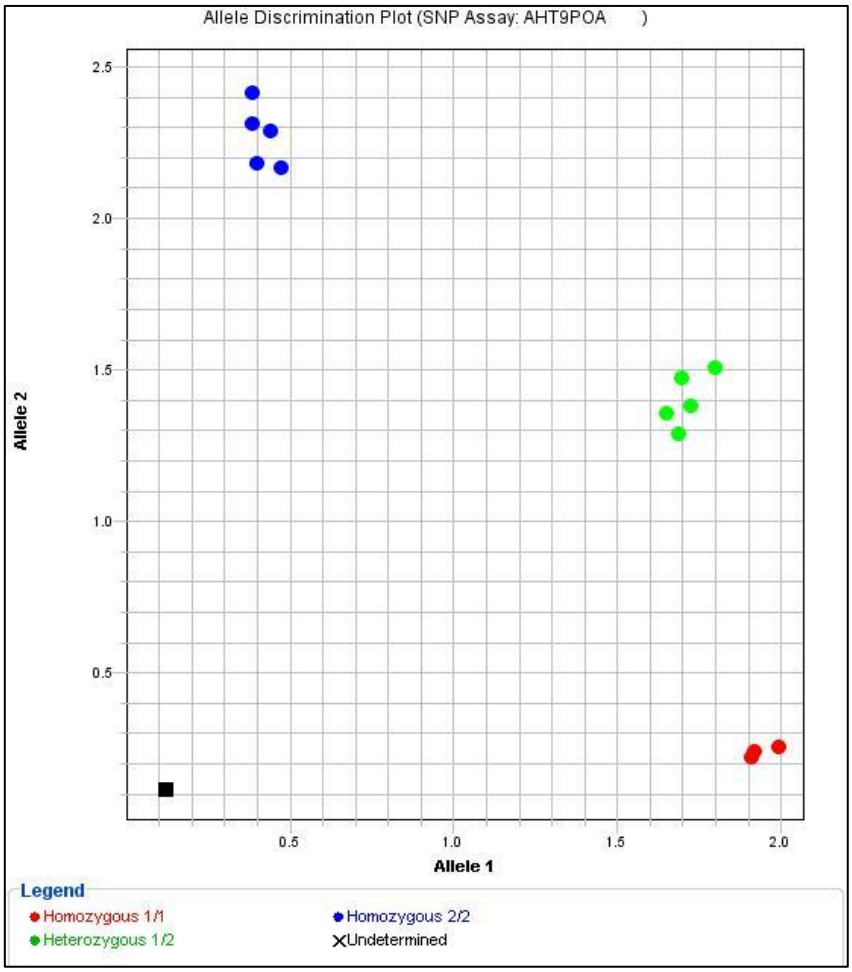

Figure 3.2. Representative Allelic Discrimination Plot of Nur7 Genotyping. Homozygous wild-type mice have two copies of the aspa ^{wt} allele which is visualized by 1Vic, represented by the blue dots. Homozygous mutant mice have two copies of the aspa^{nur7} allele which are visualized by 6Fam; represented by the red dots. Heterozygotes contain one wild-type allele and one nur7 allele, so the DNA is visualized by both dyes, represented by the green dots

QRT-PCR

Total RNA was prepared from one entire hemisphere of flash frozen mouse brain. Tissue was homogenized using Trizol reagent (Invitrogen Corp., Carlsbad, Ca) as per manufacturer's instructions (1 ml per 50-100 mg tissue). Purified RNA was treated with DNase to remove contaminating genomic DNA and cleaned using RNeasy columns (Qiagen, Valencia, Ca). The concentration of all purified RNA was determined by spectrophotometry and the integrity of samples verified by denaturing agarose/formaldehyde gel electrophoresis. cDNA for QRT-PCR was generated from 1 μg of purified RNA using a Superscript First Strand Synthesis Kit (Invitrogen, Carlsbad, CA). QRT-PCR was performed with SYBR-Green on an Applied Biosystems Step One Real Time PCR system (Applied Biosystems, Foster City, Ca). The primers for target transcripts were as follows: *Nat8L* (5′-3′; F: CTACCTGGAGTGCGCGCT, R: GGCGGCTTCATGTAGTACTGC), ASPA (5'-3'; F: TGAGCATCCTTCACTCAAATATGC,
R: GGCTGAGGACCAACTTCTATACCA) and GAPDH (5′-3′; F: AACTTTGGCATTGTGGAAGG, R: ACACATTGGGGGTAGGAACA). The Relative Standard curve method was used to analyze the expression of *Nat8L* and delta delta CT method was used for ASPA, both using GAPDH (Glyceraldehyde-3-phosphate dehydrogenase) as an internal control.

Immunohistochemistry

All tissue samples for immunohistochemistry were prepared by the transcardial perfusion of deeply anesthetized animals with ice cold 0.9% saline followed by freshly prepared 4% buffered paraformaldehyde. Perfused brains were

removed and post-fixed overnight in 4% paraformaldehyde, then cryoprotected in an ascending sucrose gradient. Cryoprotected brains were embedded in Tissue-Tek OCT compound (Sakura, Torrance, Ca), and flash frozen in an Isopentane/dry ice bath. Serial 45 um sections were collected from each brain (beginning approximately from Bregma 0.20 mm) and stored at -20°C in cryoprotectant until needed. Free-floating sections were incubated with primary antibodies overnight at room temperature (RT) in Immuno buffer (1× PBS, 0.1% Triton X-100, 1% normal goat serum, and primary antibody). Primary antibody for mouse A60 neuron-specific nuclear protein [NeuN] 1:500 [Millipore, Billerica, Ma] and ASPA (1:250) was generated by immunizing rabbits with a recombinant human ASPA peptide (77), generously provided by Dr. R.E. Viola at the University of Toledo, OH. After incubation in primary antibody, sections were incubated for 2 hours at RT in biotinylated secondary antibody (Sigma-Aldrich, St. Louis, Mo), followed by incubation at RT for 1 hour in extravadin peroxidase (Sigma-Aldrich, St. Louis, Mo). Positive cells were visualized using 3, 3′-diaminobenzidine (DAB). Developed sections were mounted onto glass slides, dehydrated in an ascending ethanol gradient, and then cleaned twice with xylene and cover slipped with DPX mountant (Sigma-Aldrich, St. Louis, Mo).

Stereology

Estimates of NeuN-positive neurons were generated using the optical fractionator (k=4) and Stereologer software (Stereology Resource Center, Tampa, FL). Counts were performed on a single hemisphere of processed sections to generate estimates of NeuN for cortical layer V of 2-week old wild-type and Nur7. All counts were performed with a 100× objective on an Olympus BX51 upright microscope

equipped with an analog camera and motorized stage. Significance differences in *N* between experimental and control groups were determined by a 2-tailed students T-test ($p \leq 0.05$).

In Situ Hybridization

45 µM free floating coronal brain sections were washed with 5X SSC (750 mM NaCl and 75 mM sodium citrate), PBS, PBST, 0.1M TEA, and 0.25M Acid Anhydride. They were pre-hybridized in hybridization solution (DIG wash and block buffer set, Roche) while the probe was being denatured. The probe was hybridized to the tissue sections with 30 ng/ml of *Nat8L* probe for 20 hours at 55˚C. After the hybridization, the sections were washed thoroughly and blocked with 1X DIG wash buffer (Roche Diagnostics). The sections were incubated for 2 hours with the anti-DIG-AP antibody provided in the DIG Nuclear Detection kit at a dilution of 1:20,000. They were then developed using the detection reagents from the DIG nuclear detection Kit (Roche) according to the provided protocol. The processed sections were mounted onto glass slides and cover slipped with DPX mountant.

Results

ASPA is Up-regulated During 5XFAD Progression

Following the recent publication of a paper describing the up-regulation of ASPA prior to reduction in levels of NAA in a model of TBI (111), we became interested in the possible involvement of ASPA in the regulation of *Nat8L* expression. In order to determine if *ASPA* was transcriptionally regulated during the progression of FAD, we analyzed the expression of *ASPA* in 2 and 4-month wild-type and 5XFAD brains via QRT-PCR. The resulting data revealed a significant increase in *ASPA* expression occurring at 2 months of age in 5XFAD brains compared with wild-type controls. However, *ASPA* expression seemed to be unaffected by 5XFAD pathology at 4 months of age (Figure 3.3A). In order to confirm this up-regulation of *ASPA*, 2-month 5XFAD brains were sectioned and used for IHC to detect ASPA protein. The IHC showed a visually qualitative increase in ASPA protein in 2-month 5XFAD brains compared with wild-type controls, confirming the quantitative QRT-PCR data. These increases occurred within white matter-rich regions of the internal capsule (Figure 3.3B & C), subcortical white matter tracts of the external capsule overlying the hippocampus (Figure 3.3D & E), and white matter of the fornix of the hippocampus (Figure 3.3 F & G). These data showed that *ASPA* is up-regulated simultaneously with reduced ATP levels but prior to the down-regulation of *Nat8L* and mitochondrial dysfunction. Therefore, *ASPA* may be an upstream responder to the onset of energetic stress which affects the expression of *Nat8L*, implicating oligodendrocytes in the regulation of *Nat8L*.

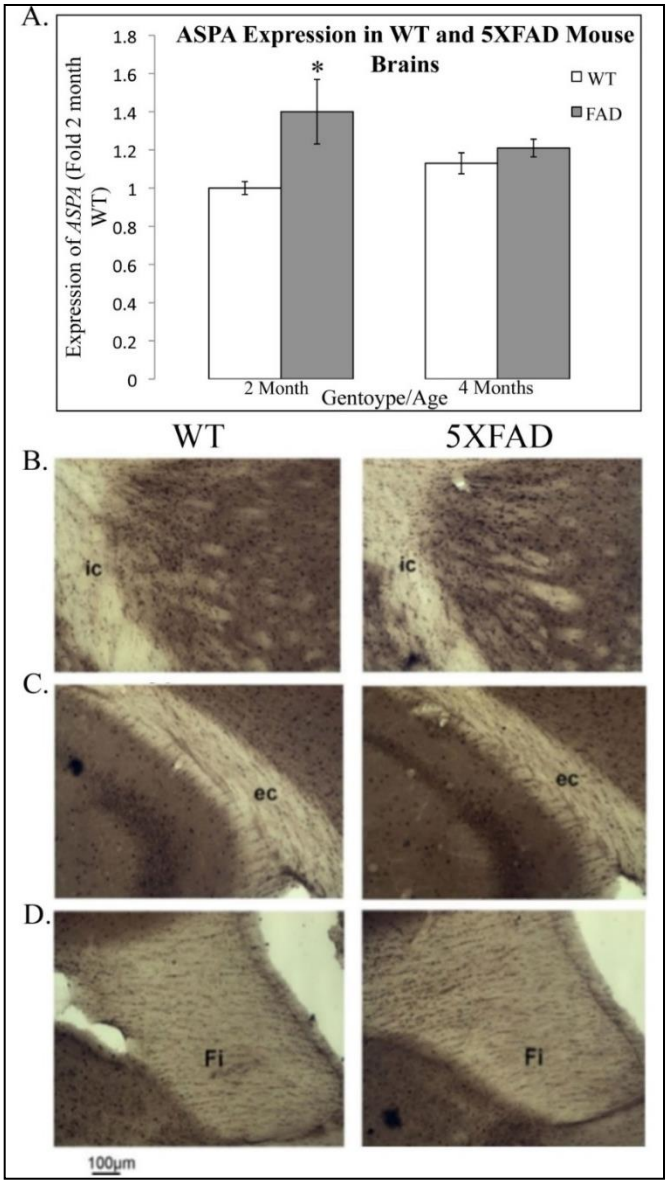

Figure 3.3 ASPA is Up-Regulated at 2 Months of Age in the 5XFAD Mouse Brain. (A) ASPA is up-regulated at 2 months of age in the 5XFAD mouse brain compared with wild-type as assessed by QRT-PCR. There was no observed difference in ASPA expression between 4-month wild-type and 5XFAD brains. *ASPA* expression presented as fold- wild-type 2-month levels for each group, n=5. Immunohistochemical confirmation of increased ASPA expression in 2-month 5xFAD brains within white matter tracts of the internal capsule (ic) **(B-C),** the external capsule (EC) **(D-E**) and the white matter of the fimbria (Fi) of the fornix (**F-G**). ***≤0.001<**≤0.01<*≤0.05

Nat8L is Abnormally Regulated During ASPA Null/Nur7 Mouse Development

In order to determine if the expression of *ASPA* has a regulatory effect on *Nat8L*, we examined *Nat8L* expression in *ASPA* null mice during the first 4-weeks of development. The first four weeks were chosen in light of previous data which showed that ASPA is up-regulated between 1-2-weeks of age in the developing mouse (195). ASPA expression was also shown to remain high throughout the first 4-weeks of development (123); the time point in which developmental myelination will be mostly completed (196). *Nat8L* expression was analyzed at 1, 2, and 4-weeks of age in the wild-type and Nur7 mouse by QRT-PCR (Figure 3.4 A). *Nat8l* is significantly increased at 1-week of age in the Nur7 mouse compared with wild-type controls, but this increase became more significant (lower p value) at 2-weeks of age, indicating that is it highly likely that the true increase in expression occurs closer to 2-weeks of age. This increase in expression was confirmed by In Situ Hybridization (ISH) for *Nat8L* in 2-week Nur7 and wild-type brains. The ISH images revealed a visually prominent increase in *Nat8L* mRNA in 2-week Nur7 brains compared with wild-type controls. This increase was most prominent within the thalamus and interneurons of the hippocampus (Figure 3.4 B-I). In order to confirm that the up-regulation of *Nat8L* was not due to an increased number of neurons, 2-week Nur7 brains and wild-type brains were stained with the neuronal nuclei marker, NeuN. The sections were then subjected to unbiased stereology counts of NeuN positive nuclei within the thalamus and the hippocampus. The results of these counts revealed no significant differences in neuronal content of Nur7 brains relative to wild-type

controls (data not shown). Therefore, the up-regulation of *Nat8L* in Nur7 mice is not due to an increase in neuronal number, but to an actual increase in *Nat8L* expression.

The data presented here revealed that ASPA function may play a direct role in the expression of *Nat8L* during mouse development. This deduction is due to the significant difference in *Nat8L* expression which occurs either in the presence or absence of a functional ASPA protein. As we have shown, during normal mouse development when ASPA is fully functional, *Nat8L* expression starts to increase between 2 and 4-weeks of age (Figure 3.4). However, without the presence of a functional ASPA protein, as shown in the ASPA Null/Nur7 mouse model, *Nat8L* becomes significantly up-regulated as early as 1-week of age (figure 3.4). These results indicate that without ASPA, *Nat8L* is uncontrollably up-regulated, either due to the lack of an inhibitory signal or the early introduction of an excitatory signal. To further support this hypothesis, as we have previously stated, ASPA expression begins prior to *Nat8L* expression during wild-type mouse development, indicating that ASPA expression is regulated upstream of *Nat8L*. Therefore, we hypothesize that ASPA activity plays a direct role on the timely expression of Nat8L during wild-type mouse development.

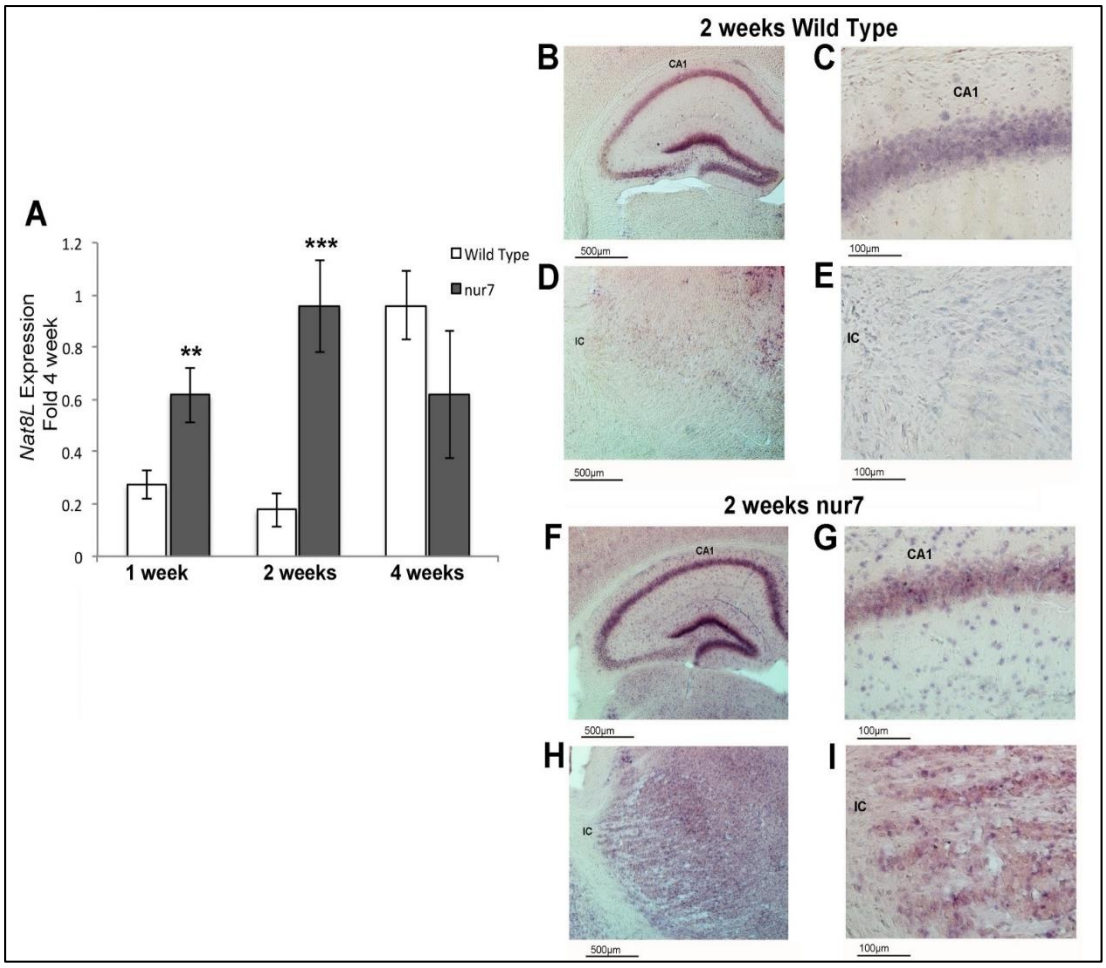

Figure 3.4. Nat8L is Up-Regulated at 2-weeks in the Nur7 Mouse Brain. Nat8L is prematurely up-regulated at 2-weeks of age in the ASPA null/Nur7 mouse as shown through QRT-PCR (A, N=5). This up-regulation was confirmed via ISH with clear increase of expression within the interneurons of the hippocampus **(**7B-C & F-G) and the thalamus (7D-E & H-I). IC: Internal Capsule, CA1: Region CA1 of the hippocampus.

Conclusion

The main conclusion from this chapter is that NAA may be reduced during the development of FAD pathology in 5XFAD mice due to down-regulation of *Nat8L* and up-regulation of *ASPA*. ASPA is up-regulated 2 months prior to the reduction of NAA, *Nat8L* expression, or reduced oxidative integrity. Therefore, we tested to see if *ASPA* had any effect on the expression of *Nat8L* through an analysis of *Nat8L* expression in *ASPA* null/Nur7 Mice. The results revealed that *Nat8L* is significantly and prematurely up-regulated in the absence of *ASPA*. Our analysis of *ASPA* and *Nat8L* expression in 5XFAD and Nur7 mice indicate that ASPA could be a negative regulator of *Nat8L*.

Discussion

Substrate Availability as a Possible Means of Regulation for NAA Metabolism

The synthesis of NAA is dependent on the mitochondria's ability to fully metabolize glucose into ATP (28, 34, & 36-38). This is because the brain relies on glucose as its oxidative substrate; (127) therefore any disruption of mitochondrial integrity could potentially lead to a significant loss of brain function (128). Because of this sensitivity to energetic status, the CNS has developed acute responses to combat mitochondrial dysfunction through the minimization of energetically taxing pathways (129-130). It is our hypothesis, that the active down-regulation of NAA synthesis during early stage neurodegenerative disease is one of these neuroprotective pathways (Figure 4.1)

Prior to this thesis work, it was proven that any disruption of mitochondrial function, including reduced ETC activity (131-132), reduced glucose utilization (133), or inhibited MAS activity (134-135), led to a significant reduction of detectable NAA. The tight coupling of oxidative phosphorylation with NAA synthesis is most likely due to direct competition for the energetic substrates AcCoA and aspartate (132). This hypothesis is supported by our in vitro data revealing that exacerbated NAA synthesis results in reduced bioavailability of energetic currency (ATP). Therefore, it is reasonable to hypothesize that increasing NAA synthesis reduces the pool of available AcCoA and aspartate required for TCA driven oxidative phosphorylation (Figure 1.8). The mathematical reasoning behind this is that there are approximately $4.22X\ 10^{23}$ molecules of NAA in the adult brain which are only turned over once every 70 hours (197). For every molecule of NAA that is

synthesized, one AcCoA and one aspartate molecule are diverted from their respective ATP-generating mechanisms. The loss of one AcCoA results in the loss of one round of the TCA cycle, or three NADHs and one $FADH_2$, which is equivalent to 10 ATP molecules. The loss of one aspartate molecule results in a loss of one NADH molecule from the MAS, with a net loss of three ATP molecules. Therefore, every molecule of synthesized NAA leads to a direct loss of 13 ATP molecules. This means that every 70 hours the brain uses 8×10^{21} molecules of ATP just to produce NAA. To put this in some perspective, the brain requires 1.64×10^5 ATP to release one synaptic vesicle (182). This means that the brain could release 4.9×10^{16} synaptic vesicles for the cost of producing one round of NAA. Taken together, these numbers indicate that these two substrates are extremely important to NAA synthesis and oxidative phosphorylation, and also that NAA synthesis is an extremely expensive process, in terms of energy cost, within the brain. For these reasons, we hypothesize that NAA synthesis must be actively reduced during periods of energetic stress (such as neurodegenerative disease progression) in order to save these valuable substrates for ATP production and subsequent necessary brain function.

The balance of NAA synthesis and oxidative phosphorylation is highly dependent on substrate availability of numerous cellular pathways. For example, the availability of intra-mitochondrial aspartate is rate limiting not only for NAA synthesis but also for the continuous activity of the MAS (136). During periods of reduced oxidative phosphorylation, glycolytic NADH will be used to convert pyruvate into lactate rather than be used in the ETC for oxidative phosphorylation (137). As we have shown (Figure 2.7) 5XFAD mice, as well as multiple other

neurodegenerative disease models (Table 1), show mitochondrial dysfunction. Therefore, any disruption of NADH delivery to ETC will cause a drastic reduction in the diseased mitochondria's ability to generate ATP. This reduction of NADH can only be compensated for by increasing the activity of the MAS. The MAS functions by bringing NADH into the mitochondrial matrix through the oxidation of malate to oxaloacetate (138). NAA synthesis directly competes with the MAS for the limited pool of intra-mitochondrial aspartate (136-137& 139). Therefore, we hypothesize that NAA synthesis is actively down-regulated in 5XFAD mice to ensure that the MAS has a sufficient pool of available aspartate to continue supplying the ETC with NADH (Figure 1.4).

AcCoA is produced within neuronal mitochondria through the pyruvate dehydrogenase complex. AcCoA is used to initiate the TCA cycle, however, neurons are unable to produce de novo oxaloacetate because they do not contain pyruvate carboxylase (140). Therefore, the neurons ability to metabolize glucose is completely dependent on the TCA cycle and the MAS. Thus, when NAA synthesis diverts neuronal AcCoA and aspartate from these ATP producing processes it is damaging to the overall energetic integrity of the cell.

Determining the Time Period Defined by Altered NAA Metabolism in 5XFAD mice

Our primary goal for undertaking this thesis work was to understand why NAA is significantly reduced during the early stages of numerous neurodegenerative diseases, including AD, PD, MS, and HD (141-144). In particular, we were interested in revealing a time period in which NAA was reduced during FAD

progression, and if this reduction coincided with any pronounced change in oxidative metabolism.

The onset of severe mitochondrial dysfunction and oxidative stress has been clinically and experimentally proven to play a significant role in the onset of various neurodegenerative diseases, particularly AD (145-147). Since we were able to reveal that NAA synthesis was a significant energetic stress in vitro (Figures 1.8 & 1.9), we were interested in determining if NAA was reduced during AD progression and if so, if there was a direct link with overall oxidative integrity. Our hypothesis was that NAA was reduced during early stage AD in response to reduced mitochondrial integrity in order to save key energetic substrate for oxidative phosphorylation. This hypothesis was based on our findings that the cell is unable to maintain NAA synthesis and ATP production during periods of compromised ETC activity (figure 1.9) as well as the characteristic metabolic decline present during AD progression.

First, we showed that NAA is reduced (Figure 2.3) at 4-months of age in 5XFAD mice, prior to the onset of severe FAD pathology. As demonstrated by Oakley et al (110), 5XFAD mice present with multiple types of FAD pathology. This includes, but is not limited to, cerebral $A\beta_{42}$ deposition around 2 months of age with a steady increase up to 9 months of age (the latest age examined), significant synaptic degeneration beginning around 4 months of age, neuronal loss by 6 months of age (figure 2.5), and spatial memory deficits by 4-5 months.

After identifying that NAA was reduced at 4 months of age in 5XFAD mice, we were then able to reveal that the reduction was caused by the down-regulation of

Nat8L and occurred simultaneously with reduced mitochondrial function; as shown through ATP analysis (Figure 2.6), ETC gene microarrays (2.7), and complex I assays (Figure 2.8). We also demonstrated that the reduction of *Nat8L* expression occurred simultaneously with increased MAS activity (Figure 2.9), indicating that NAA was not reduced due to limited aspartate availability, but because of an active response to reduced oxidative integrity. These experiments indicate that our hypothesis is most likely correct, in that NAA is reduced during 5XFAD progression due to the active down-regulation of *Nat8L* in response to mitochondrial dysfunction. We also hypothesize that this mechanism is a possible novel neuroprotective mechanism against any neuronal energetic deficit, such as during TBI and neurodegeneration.

AMPK as a Possible Means of Regulation for Nat8L

Although we did not directly investigate possible regulatory mechanisms of NAA metabolism other than ASPA functionality, our hypothesis is that *Nat8L* is actively down-regulated in response to the onset of energetic stress. Therefore, we believe that *Nat8L* could be regulated by a cellular energy signaling cascade. The key energy sensing regulatory protein in the eukaryotic cell is AMP-activated protein kinase (AMPK) (148). AMPK is highly distributed in regions of the body which consume the most energy; therefore it is not surprising that it is highly expressed in the brain (149-150). AMPK is expressed in all cell types of the CNS, however, most of this expression is within Purkinje neurons of the cerebellum and hippocampal pyramidal neurons; cell types which have been well established as having high metabolic rates and increased levels of glucose utilization (151). AMPK is able to modulate gene expression of downstream targets, eventually leading to the activation

of various catabolic processes such as glycolysis, lipolysis, fatty acid oxidation, and autophagy (152). AMPK can also inhibit synthetic processes such as gluconeogenesis, lipogenesis, and steroid synthesis (153-155). AMPK is activated by the upstream calcium sensing kinase CamKKβ and AMP binding (156-157). Therefore, any mechanism which leads to the increase of intracellular calcium, and/or the increase of cellular AMP, will lead to the activation of AMPK and its downstream targets (158). Calcium is a prominent secondary messenger in the brain that can alter neuronal gene expression, energy production, membrane excitability, and synaptic transmission based on its intracellular concentration. Significant increases in intracellular calcium have been shown to negatively affect the pathology of numerous neurodegenerative diseases including Parkinson's (159), Huntington's (160), and Alzheimer's (161). This relationship is directly demonstrated through the up or down regulation of AMPK occurring simultaneously with energy metabolism defects during the progression of neurodegenerative diseases including Alzheimer's, Parkinson's, and Huntington's (181). Specifically, AMPK activity is significantly increased in the brains of patients affected by various neurodegenerative diseases, however, the specific role AMPK plays in each of these disorders individually has yet to be established (181). Since we predict that the down-regulation of NAA during FAD progression in 5XFAD mice (Figure 2.5) is a neuronal protective mechanism against energetic stress (Figure 2.7, 2.8, & 2.9) and AMPK is an energetic response element whose expression is responsive to energetic status, we hypothesize that AMPK may be responsible for regulating *Nat8L* and/or *ASPA* during FAD progression.

An example of a neuronal gene which is down-regulated by AMPK is Insulin Receptor Substrate 2 (IRS2); a gene that plays an important role in the nonpathogenic metabolic homeostasis of hypothalamic neurons (162). IRS2 is responsible for nutrient intake in response to reduced levels of available energetic substrate within the hypothalamic–pituitary–adrenal axis (HPA) (162). The expression of IRS2 is activated by the transcriptional activator CREB-regulated transcription co-activator 2 (CrTC2). Within hypothalamic neurons, CrTC2 becomes inhibited when it is phosphorylated by AMPK during periods of limited energetic resources (163). From this example, we believe that *Nat8L* is regulated in a similar manner, and could become down-regulated by downstream targets of AMPK phosphorylation in response to reduced mitochondrial integrity.

The Regulation of Nat8L through Neuronal miRNA's

One possible means of down-regulating the expression of *Nat8L* is by silencing *Nat8L* transcription through microRNA's (miRNA's). A recent publication has revealed that the expression of *Nat8L* in non-neuronal cells can be regulated by miRNA4488 (164). A miRNA ChIP assay was performed to determine which miRNA's were affected by the overexpression of transforming growth factor β2 (TGFβ2 -OT1) in human vascular endothelial cells. The assay revealed three distinct miRNA targets regulated by the expression of TGFβ2 -OT1; miRNA4488, miRNA 3960, and miRNA 4459. These targets were then used in bio-informative prediction software to determine their possible binding targets. The analysis of that data revealed that miRNA4488 could to bind to the 3'UTR of the gene encoding *Nat8L*, acting to inhibit its expression. To determine if miRNA4488 could inhibit *Nat8L* expression, a

miRNA4488 mimic and an inhibitor were transfected into human vascular endothelial cells and used for QRT-PCR of the *Nat8L* transcript. The results revealed that miRNA4488 was indeed able to inhibit the expression of *Nat8L* (164). The repression of miRNA4488 was also found to occur through the binding of miRNA4488 to a competing endogenous RNA TGFβ2 -OT1. This protein is able to sequester numerous miRNA's through a competitive binding site and increase the expression of various miRNA targets, such as *Nat8L*. Interestingly, TGFβ2 is down-regulated in response to amyloid deposition as well as during the progression of Alzheimer's disease pathology in transgenic mouse models (165). Therefore, it is possible that the reduction of TGFβ2 during Alzheimer's disease could lead to an increase in miRNA4488, and subsequently inhibit the expression of *Nat8L*.

The Possible Down-Regulation of Nat8L through a Bi-Compartmental System

As we have demonstrated, the catabolic side of NAA metabolism is also transcriptionally regulated during early 5XFAD pathology. Specifically, ASPA is up-regulated at 2 months of age (Figure 3.3), occurring prior to any alteration in *Nat8L* expression, NAA concentration, or mitochondrial dysfunction, but simultaneous with the onset of energetic stress as shown through reduced levels of whole brain ATP: AMP (Figure 2.6). The possibility of *Nat8L* down-regulation through neuron-oligodendrocyte cross talk is novel. However since ASPA seems to be a potential primary responder to early reductions in energetic status during 5XFAD progression, and Nat8L expression is significantly up-regulated in the absence of functional ASPA (Figure 3.4), it is possible that *Nat8L* is negatively regulated by ASPA through the communication between neurons and oligodendrocytes.

Considering NAA is synthesized within neurons and catabolized within oligodendrocytes, the regulation of *Nat8L* could come from within either cell type. However, the concept of oligodendrocyte to neuronal communication is relatively unstudied other than in the context of myelination. However, recent research has highlighted a possible means of oligo-neuronal communication through the release of signaling molecules contained within oligodendrocytic exosomes. In these studies, primary oligodendrocytes were co-cultured with primary cortical neurons within a Boyden chamber, allowing both cell types constant access to one another's media. Upon glucose and oxygen deprivation, primary neurons exposed to oligodendrocytic exosomes had significantly higher activation of pro-survival signaling pathways (MEK/ERK and PI3K/AKT) compared with neurons not exposed to oligodendrocytic exosomes (166-167). These signaling pathways have numerous downstream targets which have direct effects on neuronal survival (166-167). In order to determine if the regulation of any neuronal genes were affected in response to oligodendrocytic exosomes, the author's cultured primary neurons and oligodendrocytes within a boyden chamber and stimulated oligodendrytic exosomal release. After exosome exposure, mRNA was isolated from the primary neurons and used in a microarray to determine if gene expression was affected by exposure to the oligodendrytic exosomes. Compared to unexposed neurons, neurons exposed to exosomes presented with significantly down-regulated genes, including immediate early response 3 (Ier3), cortistastin, VGF nerve growth factor, and Brain Derived Neurotrophic Factor (BDNF); all are genes which affect neuronal plasticity, memory function, and neuro-protection (166-167). The study also revealed that oligodendrocytic exosomes

contained miRNA's (MiRNA-9 and 19a) which have the ability to inhibit the expression of the gene doublecortin (DCX); a microtubule stabilizing protein that is down-regulated during neuronal differentiation. This study was the first of its kind to demonstrate a direct transcriptional effect of neuronal genes from the internalization of oligodendrocytic exosomal content (166-167). Therefore, the down-regulation of *Nat8L* in 4-month 5XFAD brains could be in response from neuronal cues or controlled through exosomal communication with neighboring oligodendrocytes.

The Link Between NAA Metabolism and Histone Modification

A recently discovered means of gene regulation by ASPA activity, and therefore oligodendrocytes, is through the acetylation of histones. This hypothesis is based on recent data revealing an indirect correlation between ASPA expression and histone lysine acetylation in brown adipose tissue (168). This study investigated the effect of inhibiting NAA production through *Nat8L* knock down in immortalized brown adipose cells (iBacs), a cell type which has recently been shown to express similar amount of *Nat8L* AND *ASPA* compared with neurons and oligodendrocytes, respectively (198). The study revealed that when NAA production was blocked in iBacs, ASPA expression became significantly down-regulated and Histone3K became acetylated and unwound. To support the connection between NAA metabolism and histone acetylation, other studies have shown that the white matter of ASPA null mice also exhibited highly acetylated levels of H3K9 and H2B (168-169). Cumulatively, these studies indicate that ASPA is indeed an upstream regulator of histone acetylation.

Histone de/acetylation is a common means of transcriptional regulation for nuclear-encoded genes (170-171) Histone acetylation is regulated by two main classes of proteins; histone deacetylases (HDACs) and histone acetyltransferases (HATs) (170-172). HATs are lysine acetyltransferases which acetylate lysine residues on histones for the main purpose of un-winding chromatin and allowing transcriptional enzymes access to a gene. On the other hand, HDACs are lysine acetyltransferases which remove acetate from histones in order to condense chromatin and block transcription (173). The acetylation of histones depends on the availability of AcCoA; the sole donor for histone and protein acetylation through lysine acetyltransferases and primary substrate of NAA synthesis (174). The indirect association of ASPA expression and histone acetylation, therefore, indicates ASPA as a possible regulator of histone controlled gene expression. Currently, it remains unknown if *Nat8L* expression is regulated by histone acetylation, however, this finding opens the door to the possibility of ASPA expression directly regulating gene expression, and maybe even *Nat8L*.

Histone acetylation is not the only demonstrated epigenetic modification regulated by NAA metabolism. A recent publication has demonstrated that oligodendrocytes from *Nat8L* knockout mice had a significant increase in histone H3 methylation in H3K4me3, H3K9me2, and H3K9me3 when treated with NAA. These histones have been shown to regulate cellular energetics, growth, and oligodendrocyte differentiation (176). This finding suggests that one role of NAA in the adult brain may be to regulate various histone modifications in both neurons and oligodendrocytes, perchance in response to overall mitochondrial integrity. There is

also a possibility, that since histone acetylation is responsive to ASPA expression within fat cells, this may also be true in the brain. As we have shown, ASPA becomes up-regulated at two months of age in the brains of 5XFAD mice (figure 3.3), this up-regulation may lead to the modification of various histones within oligodendrocytes. Since histone modification is a key means of gene regulation, the resulting modification of histones in response to *ASPA* could have a regulatory effect on neuronal *Nat8L* expression through cell to cell communication.

Future Experiments

There are endless means of possible regulation in response to energetic crisis, especially to down-regulate an energetically taxing reaction. However, the bi-compartmental metabolism of NAA only makes deciphering this mechanism much more difficult. Therefore, any future experiments based on this research would focus on our finding that *Nat8L* is actively down-regulated during periods of reduced mitochondrial function prior to disease pathology. First, it would be important to show an identical sequence of metabolic and transcriptional events in other brain specific diseases/disorders which present with reduced levels of NAA besides 5XFAD and TBI. The hypothesized sequence of events would be a reduction in ATP: ADP, an increase in *ASPA* expression, mitochondrial dysfunction, the down-regulation of *Nat8L*, a reduction of whole brain NAA, and the onset of disease/disorder specific pathology. The disorders of most interest would be ones characterized by significant energetic stress, reduced levels of NAA, and at least one well-studied mouse model. Examples of these disorders include Parkinson's disease, Huntington's disease, epilepsy, and amyotrophic laterals sclerosis (ALS).

A key hypothesis of this thesis is that NAA synthesis is reduced during the progression of FAD in order to save AcCoA and aspartate for oxidative phosphorylation. Therefore, in order to determine if this hypothesis is true, it is important to define whether or not substrate deprivation is a key factor in the transcriptional regulation of *Nat8L*. This analysis would begin by analyzing the effect of increased levels of AcCoA on the transcriptional regulation of *Nat8L* and *ASPA*. AcCoA is the NAA synthetic substrate which contributes the most to the energetic deficit caused by NAA synthesis (10 ATP/13 ATP), therefore we hypothesize that if any substrate were to have a regulatory effect on the regulation of NAA metabolism it would be AcCoA. One way to do this would be to increase the production of AcCoA in mice using the drug Dichloroacetate (DCA). DCA is known to increase the activity of the pyruvate dehydrogenase complex, and therefore would increase the amount of available AcCoA (183). The treated mice would be given DCA intraperitoneally, injected daily over a course of three days, before being sacrificed. The brain tissue would be flash-frozen and subsequently used to analyze NAA levels, *Nat8L* and *ASPA* expression, as well as used for a control assay to confirm an increase in AcCoA levels. This assay can be purchased commercially, such as the PicoProbe Acetyl CoA colorimetric Assay Kit. By performing this analysis, we would be able to determine if AcCoA availability has a direct effect on the regulation of *Nat8L* and/or *ASPA*, or if it is simply a substrate of NAA synthesis.

In order to determine if ASPA negatively regulates *Nat8L*, we are currently working on overexpressing ASPA in oligodendrocytes of Nur7 and 5XFAD mice using an oligodendrocyte specific adeno-associated viral vector (AAV). Specifically,

we plan to overexpress ASPA into developing wild-type and Nur7 mice to see if reconstituting ASPA has any effect on the expression of *Nat8L*. We hypothesize that since *Nat8L* is significantly up-regulated in ASPA null/Nur7 mice and because *ASPA* is up-regulated 2 months before *Nat8L* is down-regulated in 5XFAD mice, reconstituting ASPA expression into its native cell type might return *Nat8l* expression to a control level. We are also interested in overexpressing ASPA directly into the brains of 5XFAD mice and measuring the resulting expression of *Nat8L* and the energetic status of the brain at 2 and 4 months of age. Since ASPA catabolism is an energy yielding reaction (199), we hypothesize that the overexpression of ASPA in 5XFAD brains would lead to a significant increase in whole brain levels of ATP due to the down regulation of *Nat8L* and the reduction of NAA synthesis. This is because, as we have shown in a non-neuronal cell type, increased expression of *Nat8L* and NAA synthesis leads to a direct loss of ATP with (figure 1.9) or without energetic crisis (figure 1.8). Therefore, if the exacerbated expression of *ASPA* did down-regulate *Nat8L*, the energetic substrates AcCoA and aspartate would be diverted from NAA synthesis and could be used to generate more ATP.

Another future experiment would be to analyze if AMPK is activated by amyloidosis, and if so, does it lead to the down-regulation of *Nat8L*. An important preliminary experiment would be to determine the activity of AMPK in hippocampal slices when treated with soluble amyloid. Amyloid deposition has been shown to lead to a direct induction of oxidative stress (200) and therefore, should increase the activity of AMPK. AMPK activity could be measured by many different means, such as an ELISA activity assay, western blot, or by the phosphorylation of downstream

targets such as AcCoA carboxylase or HDAC4 *(201)*. If it was confirmed that AMPK activity was increased in response to amyloidosis, we could then alter activity of AMPK during periods of oxidative stress and analyze the expression of *Nat8L* and *ASPA*. In order to accomplish this, we would first need to identify a time period in which AMPK activity was increased in 5XFAD development, which also corresponded to abnormal expression of *Nat8L* or *ASPA*. Then, we could selectively inhibit AMPK activity through pharmacological intervention with compound C ((6-[4-(2-Piperidin-1-Cyl-ethoxy)-phenyl)]-3-pyridin-4-yl-pyrrazolo[1,5-a]-pyrimidine) (177) and measure the expression of Nat8L and ASPA via QRT-PCR. If the results showed that either *Nat8L* or *ASPA* expression, and the concentration of whole brain NAA, were changed in response to the inhibition of AMPK, then we could prove that AMPK was indeed an upstream regulator of NAA metabolism during neurodegenerative disease progression.

Conclusion

The data from this thesis work supports the hypothesis that NAA levels in the brain are reduced during the early stages of neurodegenerative disease through the active down-regulation of *Nat8L* and the up-regulation of *ASPA*. Our data also suggest that ASPA is a primary responder to reductions in whole brain ATP: AMP while *Nat8L* expression is not reduced until significant mitochondrial dysfunction during the progression of 5XFAD. Recent literature has revealed that this metabolic pattern of events is identical to what occurs in TBI progression. Therefore, we hypothesize that *Nat8L* will be down-regulated and *ASPA* will be up-regulated during any brain specific disease or injury which presents with reduced mitochondrial

integrity. Despite not revealing a specific signaling pathway responsible for the transcriptional regulation of *Nat8L* and *ASPA*, we hypothesize that NAA synthesis is reduced in direct response to the energetic crisis caused by these various brain specific diseases due to the direct competition of NAA synthesis and ATP synthesis for the substrates AcCoA and aspartate. Therefore, we predict that *Nat8L* and *ASPA* are regulated within their own cell types or through neuron-oligodendrocyte communication by either the metabolism of AcCoA or an energy sensing signaling molecule such as AMPK.

References

1. Tallan HH (1957) Studies on the distribution of N-Acetyl-L-aspartic acid in the brain. J Biol Chem 224:41–45

2. TkacI, Rao R, Georgieff ML, Gruetter R (2003) Developmental and regional changes in the neurochemical profile of the rat brain determined by in vivo 1H NMR spectroscopy. Magn Reson Med 50:24-32

3. Chakraborty G, Mekala P, Yahya D, Wu G, Ledeen RW (2001) Intraneuronal N-acetylaspartate supplies acetyl groups for myelin lipid synthesis: evidence for myelin-associated aspartoacylase. J Neurochem 78:736–745

4. D'Adamo AF, Gidez LI, Yatsu FM (1968) Acetyl transport mechanisms. Involvement of N-acetyl aspartic acid inde novo fatty acid biosynthesis in the developing rat brain. Exp Brain Res 5:267–273.

5. William E. Wu,[a] Achim Gass,[c] Lidia Glodzik,[b] James S. Babb,[a] Jochen Hirsch,[c] Marc Sollberger,[c,d] Lutz Achtnichts,[c]Michael Amann,[c] Andreas U. Monsch,[c] and Oded Gonen[a,*] (2012) Whole brain N-acetylaspartate concentration is conserved throughout normal aging. Neuro Biol of Aging 33(10): 2440-2447

6. Moffett J, Ross B, Arun P, Madhavarao C, and Namboodiri A (2007). N-Acetylaspartate in the CNS: from neurodiagnostics to neurobiology Progress in Neurobiology 81:89–131

8. Kirtaş D, Karadağ R, Balci Şengül M, Kiroğlu Y (2016). 1H-magnetic resonance spectroscopy in first episode and chronic schizophrenia patients. Turk J Med Sci. Apr 19;46(3):862-71. doi: 10.3906/sag-1502-9.

7. Tavazzi B, et al (2007). Temporal window of metabolic brain vulnerability to concussions: oxidative and nitrosative stresses—part II. Neurosurgery. 61:390–5.

9. Rigotti DJ, Inglese M, Gonen O (2007). Whole-brain N-acetylaspartate as a surrogate marker of neuronal damage in diffuse neurologic disorders. AJNR Am J Neuroradiol. 28:1843–9.

10. Vagnozzi R, Signoretti S, Tavazzi B, Cimatti M, Amorini AM, Donzelli S, Delfini R, Lazzarino G (2005). Hypothesis of the postconcussive vulnerable brain: experimental evidence of its metabolic occurrence Neurosurgery 57:164–171.

11. Ariyannur P. S., Moffett J. R., Madhavarao C. N., Arun P., Vishnu N., Jacobowitz D., et al. (2010). Nuclear-cytoplasmic localization of acetyl coenzyme A synthetase-1 in the rat brain. *J. Comp. Neurol.*

12. Rajinder Kaul, Guang Ping Gao, Kuppareddi Balamurugan & Reuben Matalon (1993) Cloning of the human aspartoacylase cDNA and a common missense mutation in Canavan disease. Nature Genetics 5, 118 – 123

13. Jalil MA, Begum L, Contreras L, Pardo B, Iijima M, Li MX, Ramos M, Marmol P, Horiuchi M, Shimotsu K, Nakagawa S, Okubo A, Sameshima M, Isashiki Y, Del Arco A, Kobayashi K, Satrústegui J, Saheki T (2005). Reduced N-acetylaspartate levels in mice lacking aralar, a brain- and muscle-type mitochondrial aspartate-glutamate carrier. J Biol Chem. 280:31333–31339.

14. George, R. L., Huang, W., Naggar, H. A., Smith, S. B., & Ganapathy, V. (2004). Transport of N-acetylaspartate via murine sodium/dicarboxylate cotransporter NaDC3 and expression of this transporter and aspartoacylase II in ocular tissues in mouse. Biochimica et Biophysica Acta (BBA)-Molecular Basis of Disease, 1690(1), 63-69.

15. Tahay G., Wiame E., Tyteca D., Courtoy P. J., Van S. E. (2012). Determinants of the enzymatic activity and the subcellular localization of aspartate N-acetyltransferase.*Biochem. J.*

16. Mehta V., Namboodiri M. A. (1995). N-acetylaspartate as an acetyl source in the nervous system. *Brain Res. Mol. Brain Res.*

17. Ariyannur P. S., Moffett J. R., Manickam P., Pattabiraman N., Arun P., Nitta A., et al. (2010). Methamphetamine-induced neuronal protein NAT8L is the NAA biosynthetic enzyme: implications for specialized acetyl coenzyme A metabolism in the CNS. *Brain Res.* 1335 1–13

18. Goldstein, F. B. (1959). Biosynthesis of N-acetyl-L-aspartic acid. Biochim. Biophys. Acta 33, 583–584. doi: 10.1016/0006-3002(59)90161-1

19. Goldstein, F. B. (1969). The enzymatic synthesis of N-acetyl-L-aspartic acid by subcellular preparations of rat brain. J. Biol. Chem. 244, 4257–4260.

20. Knizley, H. Jr. (1967). The enzymatic synthesis of N-acetyl-L-aspartic acid by a water-insoluble preparation of a cat brain acetone powder. J. Biol. Chem. 242, 4619–4622.

21. Martin E., Capone A., Schneider J., Hennig J., Thiel T. (2001) Absence of N-acetylaspartate in the human brain: impact on neurospectroscopy? Ann. Neurol. 49:518–21.

22. Boltshauser E., Schmitt B., Wevers R. A., Engelke U., Burlina A. B., Burlina A. P. (2004) Follow-up of a child with hypoacetylaspartia. Neuropediatrics 35:255–258.CrossRefPubMedGoogle Scholar

23. Burlina A. P., Schmitt B., Engelke U., Wevers R. A., Burlina A. B., Boltshauser E. (2006) Hypoacetylaspartia: clinical and biochemical follow-up of a patient.

24. Wiame, E., Tyteca, D., Pierrot, N., Collard, F., Amyere, M., Noel, G., et al. (2010). Molecular identification of aspartate N-acetyltransferase and its mutation in hypoacetylaspartia. Biochem. J. 425, 127–136

25. Martin E., Capone A., Schneider J., Hennig J., Thiel T. (2001) Absence of N-acetylaspartate in the human brain: impact on neurospectroscopy? Ann. Neurol. 49:518–21.

26. Lehninger, A. L., Nelson, D. L., & Cox, M. M. (2000). Lehninger principles of biochemistry. New York: Worth Publishers.

27. Gellerich, F. N., Gizatullina, Z., Gainutdinov, T., Muth, K., Seppet, E., Orynbayeva, Z., et al. (2013). The control of brain mitochondrial energization by cytosolic calcium: the mitochondrial gas pedal. IUBMB Life, 65(3), 180-190.

28. Zilberter, Y. (2012). Understanding how the brain ensures its energy supply. Frontiers in neuroenergetics, 4.

29. Shetty, P. K., Galeffi, F., & Turner, D. A. (2012). Cellular links between neuronal activity and energy homeostasis. The link between brain energy homeostasis and neuronal activity, 82.

30. Heales, S. J., Davies, S. E., Bates, T. E., & Clark, J. B. (1995). Depletion of brain glutathione is accompanied by impaired mitochondrial function and decreased N-acetyl aspartate concentration. Neurochem Res, 20(1), 31-38.

31. Demougeot, C., Garnier, P., Mossiat, C., Bertrand, N., Giroud, M., Beley, A., et al. (2001). N-Acetylaspartate, a marker of both cellular dysfunction and neuronal loss: its relevance to studies of acute brain injury. J Neurochem, 77(2), 408-415.

31. Andreassen, O. A., Dedeoglu, A., Ferrante, R. J., Jenkins, B. G., Ferrante, K. L., Thomas, M., et al. (2001). Creatine increase survival and delays motor symptoms in a transgenic animal model of Huntington's disease. Neurobiol Dis, 8(3), 479-491.

33. Miccheli, A., Puccetti, C., Capuani, G., Di Cocco, M. E., Giardino, L., Calzà, L., et al. (2003). [1-13C]Glucose entry in neuronal and astrocytic intermediary

metabolism of aged rats. A study of the effects of nicergoline treatment by 13C NMR spectroscopy. Brain Res, 966(1), 116-125.

34. Miccheli, A., Puccetti, C., Capuani, G., Di Cocco, M. E., Giardino, L., Calzà, L., et al. (2003). [1-13C]Glucose entry in neuronal and astrocytic intermediary metabolism of aged rats. A study of the effects of nicergoline treatment by 13C NMR spectroscopy. Brain Res, 966(1), 116-125.

35. Shokouhi S, Claassen D, Riddle W (2014). Imaging Brain Metabolism and Pathology in Alzheimer's Disease with Positron Emission Tomography. J Alzheimers Dis Parkinsonism. Apr;4(2). pii: 143.

36. Jalil MA, Begum L, Contreras L, Pardo B, Iijima M, Li MX, Ramos M, Marmol P, Horiuchi M, Shimotsu K, Nakagawa S, Okubo A, Sameshima M, Isashiki Y, Del Arco A, Kobayashi K, Satrústegui J, Saheki T (2005). Reduced N-acetylaspartate levels in mice lacking aralar, a brain- and muscle-type mitochondrial aspartate-glutamate carrier. J Biol Chem. 280:31333–31339.

37. Satrústegui, J., Contreras, L., Ramos, M., Marmol, P., del Arco, A., Saheki, T., et al. (2007). Role of aralar, the mitochondrial transporter of aspartate-glutamate, in brain N-acetylaspartate formation and Ca(2+) signaling in neuronal mitochondria. J Neurosci Res, 85(15), 3359-3366.

38. Wibom, R., Lasorsa, F. M., Töhönen, V., Barbaro, M., Sterky, F. H., Kucinski, T., et al. (2009). AGC1 deficiency associated with global cerebral hypomyelination. N Engl J Med, 361(5), 489-495.

39. Francis J, Strande L, Pu A, and Leone P (2011) Endogenous Aspartoacylase Expression is Responsive to Glutmatergic Activity in vitro and in vivo. Glia 59: 1435-1446

40. Di Pietro V, Amorini AM, Tavazzi B, Vagnozzi R, Logan A, Lazzarino G, Signoretti S, Lazzarino G, Belli A (2014). The molecular mechanisms affecting N-acetylaspartate homeostasis following experimental graded traumatic brain injury. Mol Med. 20:147–157.

41. Falini, A., Bozzali, M., Magnani, G., Pero, G., Gambini, A., Benedetti, B., ... & Filippi, M. (2005). A whole brain MR spectroscopy study from patients with Alzheimer's disease and mild cognitive impairment. Neuroimage, 26(4), 1159-1163.

42. Lee, S. H., Kim, K. R., Ryu, S. Y., Son, S., Hong, H. S., Mook-Jung, I., ... & Ho, W. K. (2012). Impaired short-term plasticity in mossy fiber synapses caused by

mitochondrial dysfunction of dentate granule cells is the earliest synaptic deficit in a mouse model of Alzheimer's disease. Journal of Neuroscience, 32(17), 5953-5963.

43. Braak H, Braak E (1991). Neuropathological stageing of Alzheimer-related changes. Acta Neuropathol. 82:239–259.

44. Price JL, Ko AI, Wade MJ, Tsou SK, McKeel DW, Morris JC (2001). Neuron number in the entorhinal cortex and CA1 in preclinical Alzheimer disease. Arch Neurol. 58:1395–1402.

45. Selkoe DJ (1997). Alzheimer's disease: genotypes, phenotypes, and treatments. Science. 275:630–631.

46. M. Catani, A. Cherubini, R. Howard (2001). 1H MR spectroscopy differentiates mild cognitive impairment from normal brain aging. NeuroReport, 12 pp. 2315–2317

47. S. Chantal, M. Labelle, R.W. Bouchard, et al (2002). Correlation of regional proton magnetic resonance spectroscopic metabolic changes with cognitive deficits in mild Alzheimer disease. Arch. Neurol., 59 pp. 955–962

48. K. Kantarci, G. Reynolds, R.C. Petersen, et al (2003). Proton MR spectroscopy in mild cognitive impairment and Alzheimer disease: comparison of 1.5 and 5 T. AJNR Am. J. Neuroradiol., 24 pp. 843–849

49. The Huntington's Disease Collaborative Research Group (1993). A novel gene containing a trinucleotide repeat that is expanded and unstable on Huntington's disease chromosomes. Cell. Mar 26;72(6):971-83.

50 Damiano M1, Galvan L, Déglon N, Brouillet E (2009). Mitochondria in Huntington's disease. Biochim Biophys Acta. 2010 Jan;1802(1):52-61. doi: 10.1016/j.bbadis.2009.07.012. Epub

51. Padowski, J. M., Weaver, K. E., Richards, T. L., Laurino, M. Y., Samii, A., Aylward, E. H., & Conley, K. E. (2014). Neurochemical correlates of caudate atrophy in Huntington's disease. Movement Disorders, 29(3), 327-335.

52. Negi, R. S., Manchanda, K. L., & Sanga, S. (2014). Imaging of Huntington's disease. Medical Journal, Armed Forces India, 70(4), 386.

53. Demougeot C, Marie C, Giroud M, Beley A (2004). N-acetylaspartate: a literature review of animal research on brain ischaemia. . J Neurochem. Aug;90(4):776-83.

54. H. Chen, D.C. Chan (2009). Mitochondrial dynamics – fusion, fission, movement, and mitophagy – in neurodegenerative diseases. Hum Mol Genet, 18, pp. 169–176

55. J Brooks,1 J Ding,1 J Simon-Sanchez,1 C Paisan-Ruiz,2 A B Singleton,1 and S W Scholz (2009). Parkin and PINK1 mutations in early-onset Parkinson's disease: comprehensive screening in publicly available cases and control. J Med Genet. Jun; 46(6): 375–381.

56. Finsterer, J. (2006). Central nervous system manifestations of mitochondrial disorders. Acta neurologica Scandinavica, 114(4), 217-238.

57. Haas, R. H., & Zolkipli, Z. (2014, July). Mitochondrial disorders affecting the nervous system. In Seminars in neurology (Vol. 34, No. 03, pp. 321-340). Thieme Medical Publishers.

58. Sanford L. Palay (1956). Synapses in the Central Nervous System. J Biophys Biochem Cytol. Jul 25; 2(4): 193–202.

59. DiMauro S1, Schon EA (2008). Mitochondrial disorders in the nervous system. Annu Rev Neurosci. 31:91-123.

60. 1. Simons M and Nave K (2015) Oligodendrocytes: Myelination and Axonal Support. Cold Spring Harb Perspect Bio

61. Butterfield D.A., Bader Lange M.L., Sultana R (2010). Involvements of the lipid peroxidation product, HNE, in the pathogenesis and progression of Alzheimer's disease. Biochim. Biophys. Acta. 1801:924–929. doi: 10.1016/j.bbalip.2010.02.005. [PMC free article] [PubMed] [Cross Ref]

62. Ruiperez V., Darios F., Davletov B (2010). Alpha-synuclein, lipids and Parkinson's disease. Prog. Lipid Res. 49:420–428. doi: 10.1016/j.plipres.2010.05.004. [PubMed] [Cross Ref]

63. Lee J., Kosaras B., del Signore S.J., Cormier K., McKe A., Ratan R.R., Kowall N.W., Ryu H (2011). Modulation of lipid peroxidation and mitochondrial function improves neuropathology in Huntington's disease mice. Acta Neuropathol. 121:487–498.

64. Shichiri M., Yoshida Y., Ishida N., Hagihara Y., Iwahashi H., Tamai H., Niki E (2011). Alpha-tocopgerol suppresses lipid peroxidation and behavioral and cognitive impairments in the Ts65Dn mouse model of Down syndrome. Free Radic. Biol. Med.50:1801–1811.

65. Jessen F, Block W, Traber F, et al (2000). Proton MR spectroscopy detects a relative decrease of N-acetylaspartate in the medial temporal lobe of patients with AD. Neurology. 55(5):684–688.

66. Chen SQ, Cai Q, Shen YY, et al (2012). Age-related changes in brain metabolites and cognitive function in APP/PS1 transgenic mice. Behav Brain Res. 235(1):1–6.

67. Kirtaş D, Karadağ R, Balci Şengül M, Kiroğlu Y (2016). 1H-magnetic resonance spectroscopy in first episode and chronic schizophrenia patients. Turk J Med Sci. Apr 19;46(3):862-71. doi: 10.3906/sag-1502-9.

68. Tavazzi B, et al (2007). Temporal window of metabolic brain vulnerability to concussions: oxidative and nitrosative stresses—part II. Neurosurgery. 61:390–5.

69. Rigotti DJ, Inglese M, Gonen O (2007). Whole-brain N-acetylaspartate as a surrogate marker of neuronal damage in diffuse neurologic disorders. AJNR Am J Neuroradiol. 28:1843–9.

70. Seab JP, Jagust WJ, Wong ST, Roos MS, Reed BR, Budinger TF (1988). Quantitative NMR measurements of hippocampal atrophy in Alzheimer's disease Magn Reson Med 8(2):200-8.

71. Kapogiannis D and Mattson M (2011). Perturbed energy metabolism and neuronal circuit dysfunction in cognitive impairment Lancet Neurol 10(2): 187-198

72. 1. Kukull WA, Higdon R, Bowen JD, et al (2002). Dementia and Alzheimer disease incidence: a prospective cohort study. Arch Neurol. 59:1737–1746.

73. Braak H, Braak E (1991). Neuropathological stageing of Alzheimer-related changes. Acta Neuropathol. 82:239–259.

74. Delacourte A, David JP, Sergeant N, et al (1991). The biochemical pathway of neurofibrillary degeneration in aging and Alzheimer’s disease. Neurology. 52:1158–1165.

75. Price JL, Ko AI, Wade MJ, Tsou SK, McKeel DW, Morris JC (2001). Neuron number in the entorhinal cortex and CA1 in preclinical Alzheimer disease. Arch Neurol. 58:1395–1402.

76. Haass C, Selkoe DJ (2007). Soluble protein oligomers in neurodegeneration: lessons from the Alzheimer’s amyloid beta-peptide. Nat Rev Mol Cell Biol. 8:101–112.

77. Pratico D, Uryu K, Leight S, Trojanoswki JQ, Lee VM (2001). Increased lipid peroxidation precedes amyloid plaque formation in an animal model of Alzheimer amyloidosis. J Neurosci. 21:4183–4187.

78. Tanzi RE, Bertram L (2001). New frontiers in Alzheimer's disease genetics. Neuron. 32:181–184.

79. Selkoe DJ (2002). Alzheimer's disease is a synaptic failure. Science. 298:789–791.

80. Selkoe DJ (1997). Alzheimer's disease: genotypes, phenotypes, and treatments. Science. 275:630–631.

81. Blennow K, Hampel H, Weiner M, Zetterberg H (2010). Cerebrospinal fluid and plasma biomarkers in Alzheimer disease. Nat Rev Neurol.6:131–144.

82. Swerdlow RH, Burns JM, Khan SM (2010). The Alzheimer's disease mitochondrial cascade hypothesis. J Alzheimers Dis. 20(Suppl 2):S265–279.

83. Swerdlow RH (2012). Mitochondria and cell bioenergetics: increasingly recognized components and a possible etiologic cause of Alzheimer's disease. Antioxid Redox Signal. 16:1434–1455

84. Doraiswamya P, Charlesa H, K Ranga, and Krishnana R (1998). Prediction of cognitive decline in early Alzheimer's disease The Lancet 352(9141) 1678

85. Guo, F., Bannerman, P., Mills Ko, E., Miers, L., Xu, J., Burns, T., et al. (2015). Ablating N-acetylaspartate prevents leukodystrophy in a Canavan disease model. Ann Neurol, 77(5), 884-888.

86. Kantarci K, Smith G, Ivnik R, Petersen R, Boeve B, Knopman D, Tangalos E, and C Jack (2002). 1H Magnetic Resonance Spectroscopy, Cognitive Function, and Apolipoprotein E Genotype in Normal Aging, Mild Cognitive Impairment and Alzheimer's Disease J. Int Neuropsychol Soc 8(7): 934–942

87. Chugani HT, Phelps ME, Mazziotta JC (1987). Positron emission tomography study of human brain functional development. Ann Neurol. 22:487–497.

88. Mosconi L (2005). Brain glucose metabolism in the early and specific diagnosis of Alzheimer's disease. FDG-PET studies in MCI and AD. Eur J Nucl Med Mol Imaging. 32:486–510.

89. Silverman DH, Small GW, Chang CY, et al (2001). Positron emission tomography in evaluation of dementia: regional brain metabolism and long-term outcome. JAMA. 286:2120–2127.

90. Eckert A, et al (2008). Soluble beta-amyloid leads to mitochondrial defects in amyloid precursor protein and tau transgenic mice. Neurodegener Dis. 5:157–159. [PubMed]

91. Yao J, et al (2009). Mitochondrial bioenergetic deficit precedes Alzheimer's pathology in female mouse model of Alzheimer's disease. Proc Natl Acad Sci USA. 106:14670–14675.

92. Caspersen C, et al (2005). Mitochondrial Abeta: A potential focal point for neuronal metabolic dysfunction in Alzheimer's disease. FASEB J.19:2040–2041. [PubMed]

93. Takuma K, et al (2005). ABAD enhances Abeta-induced cell stress via mitochondrial dysfunction. FASEB J. 19:597–598. [PubMed]

94. Shukkur EA, et al (2006). Mitochondrial dysfunction and tau hyperphosphorylation in Ts1Cje, a mouse model for Down syndrome. Hum Mol Genet.15:2752–2762.

95. Manczak M, et al (2006). Mitochondria are a direct site of A beta accumulation in Alzheimer's disease neurons: Implications for free radical generation and oxidative damage in disease progression. Hum Mol Genet.15:1437–1449

96. Hsiao K, Chapman P, Nilsen S, Eckman C, Harigaya Y, Younkin S, Yang F, Cole G (1996). Correlative memory deficits, Abeta elevation, and amyloid plaques in transgenic mice. Science. Oct 4;274(5284):99-102.

97. Irizarry MC, McNamara M, Fedorchak K, Hsiao K, Hyman BT (1997). APPSw transgenic mice develop age-related A beta deposits and neuropil abnormalities, but no neuronal loss in CA1. J Neuropathol Exp Neurol. 56(9):965-73.

98. Varghese, M., Zhao, W., Wang, J., Cheng, A., Qian, X., Chaudhry, A.& Pasinetti, G. M. (2011). Mitochondrial bioenergetics is defective in presymptomatic Tg2576 AD mice. Translational neuroscience, 2(1), 1-5.

99. S. Oddo, A. Caccamo, J.D. Shepherd, M.P. Murphy, T.E. Golde, R. Kayed, R. Metherate, M.P. Mattson, Y. Akbari, F.M. LaFerla (2003). Triple-transgenic model of Alzheimer's disease with plaques and tangles: intracellular Abeta and synaptic dysfunction. Neuron, 39, pp. 409–421

100. S. Oddo, A. Caccamo, M. Kitazawa, B.P. Tseng, F.M. LaFerla (2003). Amyloid deposition precedes tangle formation in a triple transgenic model of Alzheimer's disease. Neurobiol. Aging, 24, pp. 1063–1070

101. L. Gimenez-Llort, G. Blazquez, T. Canete, B. Johansson, S. Oddo, A. Tobena, F.M. Laferla, A. Fernandez-Teruel (2007). Modeling behavioral and neuronal symptoms of Alzheimer's disease in mice: a role for intraneuronal amyloid. Neurosci. Biobehav. Rev., 31, pp. 125–147

102. L.M. Billings, S. Oddo, K.N. Green, J.L. McGaugh, F.M. LaFerla (2005). Intraneuronal Abeta causes the onset of early Alzheimer's disease-related cognitive deficits in transgenic mice. Neuron, 45, pp. 675–688

103. Sancheti, H., Kanamori, K., Patil, I., Díaz Brinton, R., Ross, B. D., & Cadenas, E. (2014). Reversal of metabolic deficits by lipoic acid in a triple transgenic mouse model of Alzheimer's disease: a 13C NMR study. Journal of Cerebral Blood Flow & Metabolism, 34(2), 288-296.

104. Sancheti, H., Akopian, G., Yin, F., Brinton, R. D., Walsh, J. P., & Cadenas, E. (2013). Age-dependent modulation of synaptic plasticity and insulin mimetic effect of lipoic acid on a mouse model of Alzheimer’s disease. PLoS One, 8(7), e69830.

105. Sancheti, H., Patil, I., Kanamori, K., Brinton, R. D., Zhang, W., Lin, A. L., & Cadenas, E. (2014). Hypermetabolic state in the 7-month-old triple transgenic mouse model of Alzheimer's disease and the effect of lipoic acid: a 13C-NMR study. Journal of Cerebral Blood Flow & Metabolism, 34(11), 1749-1760.

106. Hutton M, Perez-Tur J, Hardy J (1998). Genetics of Alzheimer's disease. Essays Biochem 33:117–131.

107. Iwatsubo T, Odak A, Suzuki N, et al. (1994). Visualization of A42(43) and A40 in senile plaques with end-specific A monoclonals: evidence that an initially deposited species is A42(43) Neuron 13: 45–53

108. Selkoe, D.J. (1996). Amyloid ß-protein and the genetics of Alzheimer’s disease. J. Biol. Chem. 271:18295–18298

109. Cruts, M, Backhovens, H, Wang, S, et al. (1995). Molecular genetics analysis of familial early onset Alzheimer’s disease linked to chromosome 14q24.3 Hum. Mol. Genet 12, 2363–2371

110. Oakley H, Cole SL, Logan S, Maus E, Shao P, Craft J, Guillozet-Bongaarts A, Ohno M, Disterhoft J, Van Eldik L, Berry R, Vassar R (2006). Intraneuronal beta-

amyloid aggregates, neurodegeneration, and neuron loss in transgenic mice with five familial Alzheimer's disease mutations: potential factors in amyloid plaque formation. J Neurosci.;26:10129–10140.

111. Di Pietro, V., Amorini, A. M., Tavazzi, B., Vagnozzi, R., Logan, A., Lazzarino, G., ... & Belli, A. (2014). The molecular mechanisms affecting N-acetylaspartate homeostasis following experimental graded traumatic brain injury. Molecular Medicine, 20(1), 147.

112.Vagnozzi R, et al (2007). Temporal window of metabolic brain vulnerability to concussions: mitochondrial-related impairment—part I. Neurosurgery.61:379–88.

113. Kamada K, Houkin K, Hida K, Iwasaki Y, Abe H (1995). Serial changes in metabolism and histology in the cold-injury trauma rat brain model-proton magnetic resonance imaging and spectroscopy study. Neurol Med Chir (Tokyo) 35:1–7.

114. Ricci R, et al (1997). Localised proton MR spectroscopy of brain metabolism changes in vegetative patients. Neuroradiology.39:313–9.

115. Tavazzi B, et al (2007). Temporal window of metabolic brain vulnerability to concussions: oxidative and nitrosative stresses—part II. Neurosurgery.61:390–5.

116. Signoretti S, et al (2004). The protective effect of cyclosporin A upon N-acetylaspartate and mitochondrial dysfunction following experimental diffuse traumatic brain injury. J Neurotrauma.21:1154–67.

117. Rubin Y, et al (1997). High-resolution 1H NMR spectroscopy following experimental brain trauma. J Neurotrauma.14:441–9.

118. Di Pietro V, et al (2013). Potentially neuroprotective gene modulation in an in vitro model of mild traumatic brain injury. Mol Cell Biochem.375:185–98.

119. Kile BT, Hentges KE, Clark AT, Nakamura H, Salinger AP, Liu B, Box N, Stockton DW, Johnson RL, Behringer RR, Bradley A, Justice MJ (2003). Functional genetic analysis of mouse chromosome 11. Nature. 425:81–86.

120.Traka M, Wollmann R, Cerda S, Dugas J, Barres B, and Popko B (2008) Nur7 is a nonsence mutation in the mouse aspartoacylase gene that cause spongy degeneration of the CNS. Neuro of Dis 28(45) 11537-11549.

121. 27. Kaul R, Gao GP, Balamurugan K, Matalon R, (1993) Cloning of the human aspartoacylase cDNA and a common missense mutation in Canavan Disease. Nat Genet 5: 118-123

122. Matalon R, Michaels K, Sebasta D, Deanching M, Gashkoff P, and Cassanova J (1988) Aspartoacylase Deficiency and N-acetylaspartic aciduria in patients with Canavan Disease. Am J. Med Genet 29: 463-471

123.Bhakoo K, Craig T, Styles P (2001) Developmental and regional distribution of aspartoacylase in rat brain tissue. J. Neurochem 79: 211-220

124. Kirmani B, Jacobowitz D, Namboodiri M (2003) Developmental increase of aspartoacylase in oligodendrocytes parallels CNS myelination. Brain Res Dev Brain Res 140 105-115

125. Francis J, Strande L, Pu A, and Leone P (2011) Endogenous Aspartoacylase Expression is Responsive to Glutmatergic Activity in vitro and in vivo. Glia 59: 1435-1446

126. Kirmani BF, Jacobowitz DM, Namboodiri MA (2004). Developmental increase of aspartoacylase in oligodendrocytes parallels CNS myelination. Brain Res Dev Brain Res.140:105–115.

127. Attwell D, Laughlin SB (2001). An energy budget for signaling in the grey matter of the brain. J Cereb Blood Flow Metab.21:1133–1145.

128. Magistretti PJ. Brain Eenergy Metabolism (2008). In: Squire, Berg, Bloom, du Lac, Ghosh, Spitzer, editors. Fundamental Neuroscience. San Diego: Academic Press. pp. 271–293.

129. Scheper, W., & Hoozemans, J. J. (2015). The unfolded protein response in neurodegenerative diseases: a neuropathological perspective. Acta neuropathologica, 130(3), 315-331.

130. Narciso, L., Parlanti, E., Racaniello, M., Simonelli, V., Cardinale, A., Merlo, D., & Dogliotti, E. (2016). The response to oxidative DNA damage in neurons: mechanisms and disease. Neural plasticity, 2016.

131. Koroshetz, W. J., & Bonventre, J. V. (1991). Heat shock protects cultured neurons from glutamate toxicity. Neuron, 7(6), 1043-1051.

132. Bates TE, Strangward M, Keelan J, Davey GP, Munro PM, Clark JB (1996). Inhibition of N-acetylaspartate production: implications for 1H MRS studies in vivo Neuroreport 7:1397–1400

133. Heales, S. J., Davies, S. E., Bates, T. E., & Clark, J. B. (1995). Depletion of brain glutathione is accompanied by impaired mitochondrial function and decreased N-acetyl aspartate concentration. Neurochem Res, 20(1), 31-38.

134. Miccheli, A., Puccetti, C., Capuani, G., Di Cocco, M. E., Giardino, L., Calzà, L., et al. (2003). [1-13C]Glucose entry in neuronal and astrocytic intermediary metabolism of aged rats. A study of the effects of nicergoline treatment by 13C NMR spectroscopy. Brain Res, 966(1), 116-125.

135. Ramos M, Pardo B, Llorente-Folch I, Saheki T, Del Arco A, Satrústegui J (2011). Deficiency of the mitochondrial transporter of aspartate/glutamate aralar/AGC1 causes hypomyelination and neuronal defects unrelated to myelin deficits in mouse brain. J Neurosci Res. ;89:

136. Rogatzki, M. J., Ferguson, B. S., Goodwin, M. L., & Gladden, L. B. (2015). Lactate is always the end product of glycolysis. Frontiers in Neuroscience, 9, 22.

137. Kane, D. A. (2014). Lactate oxidation at the mitochondria: a lactate-malate-aspartate shuttle at work. Frontiers in Neuroscience, 8, 366.

138. Jalil MA, Begum L, Contreras L, Pardo B, Iijima M, Li MX, Ramos M, Marmol P, Horiuchi M, Shimotsu K, Nakagawa S, Okubo A, Sameshima M, Isashiki Y, Del Arco A,
Kobayashi K, Satrústegui J, Saheki T (2005). Reduced N-acetylaspartate levels in mice lacking aralar, a brain- and muscle-type mitochondrial aspartate-glutamate carrier. J Biol Chem. 280:31333–31339.

140. Panov, A., Orynbayeva, Z., Vavilin, V., & Lyakhovich, V. (2014). Fatty Acids in Energy Metabolism of the Central Nervous System. BioMed Research International, 2014, 472459.

141. Ge Y, Gonen O, Inglese M, et al (2004). Neuronal cell injury precedes brain atrophy in multiple sclerosis. Neurology;62:624–27

142. Falini, A., Bozzali, M., Magnani, G., Pero, G., Gambini, A., Benedetti, B., ... & Filippi, M. (2005). A whole brain MR spectroscopy study from patients with Alzheimer's disease and mild cognitive impairment. Neuroimage, 26(4), 1159-1163.

143. H. Chen, D.C. Chan (2009). Mitochondrial dynamics – fusion, fission, movement, and mitophagy – in neurodegenerative diseases. Hum Mol Genet, 18, pp. 169–176

144. The Huntington's Disease Collaborative Research Group (1993). A novel gene containing a trinucleotide repeat that is expanded and unstable on Huntington's disease chromosomes. Cell. Mar 26;72(6):971-83.

145. Marcus, C., Mena, E., & Subramaniam, R. M. (2014). Brain PET in the diagnosis of Alzheimer’s disease. Clinical nuclear medicine, 39(10), e413.

146. Wang, X., Wang, W., Li, L., Perry, G., Lee, H. G., & Zhu, X. (2014). Oxidative stress and mitochondrial dysfunction in Alzheimer's disease. Biochimica et Biophysica Acta (BBA)-Molecular Basis of Disease, 1842(8), 1240-1247.

147. Morais VA1, De Strooper B (2010). Mitochondria dysfunction and neurodegenerative disorders: cause or consequence. J Alzheimers Dis. 20 Suppl 2:S255-63

148. Hardie, D. G. (2011). AMP-activated protein kinase—an energy sensor that regulates all aspects of cell function. Genes & development, 25(18), 1895-1908.

149. Gao G, Widmer J, Stapleton D, Teh T, Cox T, Kemp BE, Witters LA (1995). Catalytic subunits of the porcine and rat 5′-AMP-activated protein kinase are members of the SNF1 protein kinase family. Biochim Biophys Acta.1266:73–82.

150. Stapleton D, Mitchelhill KI, Gao G, Widmer J, Michell BJ, Teh T, House CM, Fernandez CS, Cox T, Witters LA, Kemp BE (1996). Mammalian AMP-activated protein kinase subfamily. J Biol Chem.

151. Pertsch M, Duncan GE, Stumpf WE, Pilgrim C (1998). A histochemical study of the regional distribution in the rat brain of enzymatic activity hydrolyzing glucose- and 2-deoxyglucose-6-phosphate. Histochemistry.

152. Kahn BB, Alquier T, Carling D, Hardie DG (2005). AMP-activated protein kinase: ancient energy gauge provides clues to modern understanding of metabolism. Cell Metab 1: 15–25

153. Leff T (2003). AMP-activated protein kinase regulates gene expression by direct phosphorylation of nuclear proteins. Biochem Soc Trans.

154. Hardie DG (2005). New roles for the LKB1→AMPK pathway. Curr Opin Cell Biol. 05;17:167–173

155. Lows KR (2005). Emerging role of AMP-activated protein kinase in coupling membrane transport to cellular metabolism. Curr Opin Nephrol Hypertens.

156. Anderson KA, Means RL, Huang QH, Kemp BE, Goldstein EG, Selbert MA, Edelman AM, Fremeau RT, Means AR (1998). Components of a calmodulin-dependent protein kinase cascade. Molecular cloning, functional characterization and cellular localization of Ca2+/calmodulin-dependent protein kinase kinase β J Biol Chem.

157. Stein SC, Woods A, Jones NA, Davison MD, Carling D (200). The regulation of AMP-activated protein kinase by phosphorylation. Biochem J.

158. Hardie DG (2004). The AMP-activated protein kinase pathway – new players upstream and downstream. J Cell Sci.

159. Chang C. S., Gertler T. S., Sumeier D. J. (2009). Calcium homeostasis, selective vulnerability and Parkinson's disease. Trends Neurosci. 32, 249–256

160. Lancelot E., Beal M. F. (1998). Glutamate toxicity in chronic neurodegenerative disease. Prog. Brain Res. 116, 331–347

161. Chohan M. O., Iqbal K. (2006). From tau to toxicity: emerging roles of NMDA receptor in Alzheimer's disease. J. Alzheimers Dis. 10, 81–87

162. Lerner, R. G., Depatie, C., Rutter, G. A., Screaton, R. A., & Balthasar, N. (2009). A role for the CREB co-activator CRTC2 in the hypothalamic mechanisms linking glucose sensing with gene regulation. EMBO reports, 10(10), 1175-1181.

163. Kubota N, Terauchi Y, Tobe K, Yano W, Suzuki R, Ueki K, Takamoto I, Satoh H, Maki T, Kubota T, Moroi M, Okada-Iwabu M, Ezaki O, Nagai R, Ueta Y, Kadowaki T, Noda T (2004).
J Clin Invest. Oct; 114(7):917-27.

164. Huang, S., Lu, W., Ge, D., Meng, N., Li, Y., Su, L., ... & Miao, J. (2015). A new microRNA signal pathway regulated by long noncoding RNA TGFB2-OT1 in autophagy and inflammation of vascular endothelial cells. Autophagy, 11(12), 2172-2183.

165. Schonrock, N., Ke, Y. D., Humphreys, D., Staufenbiel, M., Ittner, L. M., Preiss, T., & Götz, J. (2010). Neuronal microRNA deregulation in response to Alzheimer's disease amyloid-β. *PloS one*, *5*(6), e11070.

166. Fröhlich, D., Kuo, W. P., Frühbeis, C., Sun, J. J., Zehendner, C. M., Luhmann, H. J., ... & Krämer-Albers, E. M. (2014). Multifaceted effects of oligodendroglial exosomes on neurons: impact on neuronal firing rate, signal transduction and gene regulation. *Phil. Trans. R. Soc. B*, *369*(1652), 20130510.

167. Frühbeis C, et al. 2013. Neurotransmitter-triggered transfer of exosomes mediates oligodendrocyte-neuron communication. PLoS Biol. 11, e1001604

168. Prokesch, A., Pelzmann, H. J., Pessentheiner, A. R., Huber, K., Madreiter-Sokolowski, C. T., Drougard, A., ... & Graier, W. F. (2016). N-acetylaspartate catabolism determines cytosolic acetyl-CoA levels and histone acetylation in brown adipocytes. Scientific reports, 6.4

169. Kumar S., Biancotti J. C., Matalon R. & de V. J. Lack of aspartoacylase activity disrupts survival and differentiation of neural progenitors and oligodendrocytes in a mouse model of Canavan disease. J. Neurosci. Res. 87, 3415–3427

170. Frontini A. & Cinti S (2010). Distribution and development of brown adipocytes in the murine and human adipose organ. Cell Metab 11, 253–256

171. Kajimura S., Spiegelman B. M. & Seale P (2015). Brown and Beige Fat: Physiological Roles beyond Heat Generation. Cell Metab 22, 546–559

172. Cypess A. M. et al (2009). Identification and importance of brown adipose tissue in adult humans. N. Engl. J. Med. 360, 1509–1517.

173. Takahashi H., McCaffery J. M., Irizarry R. A., Boeke J. D. (2006). Nucleocytosolic acetyl-coenzyme a synthetase is required for histone acetylation and global transcription. Mol. Cell 23 207–217 10.1016

174. Prokesch, A., Pelzmann, H. J., Pessentheiner, A. R., Huber, K., Madreiter-Sokolowski, C. T., Drougard, A., ... & Graier, W. F. (2016). N-acetylaspartate catabolism determines cytosolic acetyl-CoA levels and histone acetylation in brown adipocytes. Scientific reports, 6.

175. Dash P. K., Orsi S. A., Moore A. N. (2009). HDAC inhibition combined with behavioral therapy enhances learning and memory following traumatic brain injury. Neuroscience 163 1–8 10.1016/j.neuroscience

176. Li J, Zeng Z, Viollet B, Ronnett GV, McCullough LD (2007). Neuroprotective effects of adenosine monophosphate-activated protein kinase inhibition and gene deletion in stroke. Stroke. 38:2992–2999.

177. Bajaj, S. K., Misra, R., Gupta, R., Chandra, R., & Malik, A. (2013). Megalencephalic leukoencephalopathy with sub cortical cysts: An inherited dysmyelinating disorder. Journal of pediatric neurosciences, 8(1), 77.

178. Beal M.F(1998). Mitochondria dysfunction in neurodegenerative diseases. Biochimica et Biophysica Acta (BBA)- Bioenergetics. 1366(1), 211-223.

179. Llorente-Folch, ect (2015). The regulation of neuronal mitochondrial metabolism by calcium. J. Physiol 593.16, 3447-3462.

180. Mattson MP (2007). Calcium and neurodegeneration. Aging Cell. 6(3): 337-350.

181. Domise M and Vingtdeux V (2016). “AMPK in neurodegenerative diseases”, AMP-activated protein kiase. Springer International Publishing. 153-177

182. Harris, J. J., Jolivet, R., & Attwell, D. (2012). Synaptic energy use and supply. Neuron, 75(5), 762-777.

183. Sun, Y., Li, T., Xie, C., Zhang, Y., Zhou, K., Wang, X., ... & Zhu, C. (2016). Dichloroacetate treatment improves mitochondrial metabolism and reduces brain injury in neonatal mice. Oncotarget, 7(22), 31708.

184. Vagnozzi, Roberto, et al. (2010) Assessment of metabolic brain damage and recovery following mild traumatic brain injury: a multicentre, proton magnetic resonance spectroscopic study in concussed patients. Brain 133.11

185. Patel, Tarun B., and John B. Clark. (1979) Synthesis of N-acetyl-L-aspartate by rat brain mitochondria and its involvement in mitochondrial/cytosolic carbon transport." Biochemical Journal 184.3 539-546.

186. Mergenthaler, P., Lindauer, U., Dienel, G. A., & Meisel, A. (2013). Sugar for the brain: the role of glucose in physiological and pathological brain function. Trends in neurosciences, 36(10), 587-597.

187. Thomas, P., & Smart, T. G. (2005). HEK293 cell line: a vehicle for the expression of recombinant proteins. Journal of pharmacological and toxicological methods, 51(3), 187-200.

188. Tantama, M., Martínez-François, J. R., Mongeon, R., & Yellen, G. (2013). Imaging energy status in live cells with a fluorescent biosensor of the intracellular ATP-to-ADP ratio. Nature communications, 4, 2550.

189. Padurariu, M., Ciobica, A., Mavroudis, I., Fotiou, D., & Baloyannis, S. (2012). Hippocampal neuronal loss in the CA1 and CA3 areas of Alzheimer's disease patients. Psychiatria Danubina, 24(2.), 152-158.

190. Bartsch, T., Döhring, J., Rohr, A., Jansen, O., & Deuschl, G. (2011). CA1 neurons in the human hippocampus are critical for autobiographical memory, mental time travel, and autonoetic consciousness. *Proceedings of the National Academy of Sciences*, *108*(42), 17562-17567.

191. Preston, A. R., & Eichenbaum, H. (2013). Interplay of hippocampus and prefrontal cortex in memory. Current Biology, 23(17), R764-R773.

192. Madhavarao, C. N., Moffett, J. R., Moore, R. A., Viola, R. E., Namboodiri, M. A., & Jacobowitz, D. M. (2004). Immunohistochemical localization of aspartoacylase in the rat central nervous system. Journal of Comparative Neurology, 472(3), 318-329.

193. Hoshino, H., & Kubota, M. (2014). Canavan disease: clinical features and recent advances in research. Pediatrics International, 56(4), 477-483.

194. Kaul, R., Casanova, J., Johnson, A. B., Tang, P., & Matalon, R. (1991). Purification, characterization, and localization of aspartoacylase from bovine brain. Journal of neurochemistry, 56(1), 129-135.

195. Mattan, N. S., Ghiani, C. A., Lloyd, M., Matalon, R., Bok, D., Casaccia, P., & de Vellis, J. (2010). Aspartoacylase deficiency affects early postnatal development of oligodendrocytes and myelination. Neurobiology of disease, 40(2), 432-443.

196. Sturrock, R. R. (1980). Myelination of the mouse corpus callosum. Neuropathology and applied neurobiology, 6(6), 415-420.

197. Choi, I. Y., & Gruetter, R. (2004). Dynamic or inert metabolism? Turnover of N-acetyl aspartate and glutathione from d-[1-13C] glucose in the rat brain in vivo. Journal of neurochemistry, 91(4), 778-787.

198. Pessentheiner, A. R., Pelzmann, H. J., Walenta, E., Schweiger, M., Groschner, L. N., Graier, W. F., ... & Rieder, D. (2013). NAT8L (N-acetyltransferase 8-like) accelerates lipid turnover and increases energy expenditure in brown adipocytes. Journal of Biological Chemistry, 288(50), 36040-36051.

199. Francis, J. S., Strande, L., Markov, V., & Leone, P. (2012). Aspartoacylase supports oxidative energy metabolism during myelination. Journal of Cerebral Blood Flow & Metabolism, 32(9), 1725-1736.

200. Keil, U., Bonert, A., Marques, C. A., Scherping, I., Weyermann, J., Strosznajder, J. B., ... & Müller, W. E. (2004). Amyloid β-induced changes in nitric oxide production and mitochondrial activity lead to apoptosis. Journal of Biological Chemistry, 279(48), 50310-50320.

201. Cantó C, Auwerx J (2010) AMP-activated protein kinase and its downstream transcriptional pathways. Cell. Mol. Life Sci. 67(20), 3407–23.
Carling D, Mayer FV, Sanders MJ, Gamblin SJ

Abbreviations List

NAA: N-Acetylaspartate

NAAG: N-Acetylaspartylglutamate

Nat8L: N-acetyl-transferase-8-Like

ASPA: Aspartoacylase

AcCoA: Acetyl Coenzyme A

TCA: Tricarboxyllic Acid cycle

CNS: Central Nervous System

NaDC3: sodium-dependent dicarboxylate transporter

VGLUT: vesicular glutamate transporter

EAAT 1or 2 excitatory amino acid transporters

Glc: Glucose

Pyr Pyruvate

αKG: alpha-ketoglutamate

Glu: Glutamate

Gln: Glutamine

Ace: Acetate

Asp: Aspartate

FA: Fatty acids

QRT-PCR: Quantitative Real Time-Polymerase Chain Reaction

IHC: Immunohistochemistry

MalCoA: Malonyl Coenzyme A

IACUC: Institutional Animal Care and Use Committee

CD: Canavan's Disease

ISH: In Situ Hybridization

DNA: Deoxyribonucelic acid

RNA: Ribonucelic acid

cDNA: complimentary DNA

GAPDH: Glyceraldehyde-3-phosphate dehydrogenase

NeuN: A60 neuron-specific nuclear protein

DAB: diaminobenzidine

DIG: digoxigenin

WT: Wild-type

HPLC: High Performance Liquid Chromatography

AAV: Adeno-associated Virus

MBP: Myelin Basic Protein

MRS: Magnetic Resonance Spectroscopy

AD: Alzheimers Disease

PTSD: Post-Traumatic Stress Disorder

TBI: Traumatic Brain Injury

ALS: Amyotrophic Lateral Sclerosis

MMS: Mini Mental State Exam

APP: Amyloid Precursor Protein

PS1/2: Presenilin-1/2

$A\beta_{42}$: Amyloid Beta 42

FAD: Familial Alzheimers Disease

APP: Amyloid Precursor Protein

PS1/2: Presinillin ½

5XFAD: 5 mutation Familial Alzheimers Disease Mouse Model

5’ UTR: 5 prime untranslated region

ALS: Amyotrophic Lateral Sclerosis

ETC: Electron Transport Chain

ROS: Reactive Oxygenated Species

GSH: Glutathione

RNS: Reactive Nitrogen Species

DIG: Digoxin

DMEM: Dulbecco's Modified Eagle Medium

FBS: Fetal Bovine Serum

HeBs: Hepes Buffered Saline

GlnK: Ammonia transport signaling protein from *Methanococcus jannaschi*

cpmVenus: region circularly permuted monomeric GFP inserted into the T-Loop of GlnK

AGT: Aspartate/glutamate transporter

3-NPA: 3-nitroproprionic acid

Attributes

Figure 1.1: Samantha Zaroff designed the model, no experiment involved.

Figure 1.2: Samantha Zaroff designed the model, no experiment involved.

Figure 1.3: Jeremy Francis designed the model, no experiment involved.

Figure 1.4: Samantha Zaroff designed the model, no experiment involved.

Figure 1.5: Samantha Zaroff and Jeremy Francis designed the model, no experiment involved.

Table 1: Samantha Zaroff designed the model, no experiment involved.

Figure 1.6: Samantha Zaroff designed the model, no experiment involved.

Figure 1.7: Experimental Design, performance, and analysis by Jeremy Francis and Samantha Zaroff,

Figure 1.8: Experimental Design, performance, and analysis by Jeremy Francis and Samantha Zaroff,

Figure 2.1: Figure adapted from reference 84

Figure 2.2: Samantha Zaroff designed the model, no experiment involved.

Figure 2.3: Experimental Design, performance, and analysis by Samantha Zaroff,

Figure 2.4: Experimental Design, performance, and analysis by Jeremy Francis and Samantha Zaroff,

Figure 2.5: Experimental Design, performance, and analysis by Jeremy Francis, Vladamir Markov, and Samantha Zaroff,

Figure 2.6: Experimental Design, performance, and analysis by Samantha Zaroff

Figure 2.7: Experimental Design, performance, and analysis by Jeremy Francis and Samantha Zaroff,

Figure 2.8: Experimental Design, performance, and analysis by Samantha Zaroff

Figure 2.9: Experimental Design, performance, and analysis by Samantha Zaroff

Figure 2.10: Experimental Design, performance, and analysis by Jeremy Francis and Samantha Zaroff

Figure 3.1: Figure adapted from reference 125

Figure 3.2: Experimental Design, performance, and analysis by Samantha Zaroff

Figure 3.3: Experimental Design, performance, and analysis by Jeremy Francis, Vladamir Markov, and Samantha Zaroff

Figure 3.4: Experimental Design, performance, and analysis by Jeremy Francis and Samantha Zaroff

Figure 4.1: Samantha Zaroff designed the model, no experiment involved.